Master's thesis

NTNU
Norwegian University of Science and Technology
Faculty of Natural Sciences
Department of Materials Science and Engineering

Safia Hassan

Distribution of Aluminum and Calcium between Silicon and CaO-Al_2O_3-SiO_2 Slags at 1650 °C

Master's thesis in Materials Science and Engineering

Supervisor: Gabriella Tranell

July 2020

NTNU
Norwegian University of
Science and Technology

Safia Hassan

Distribution of Aluminum and Calcium between Silicon and CaO-Al_2O_3-SiO_2 Slags at 1650 °C

Master's thesis in Materials Science and Engineering
Supervisor: Gabriella Tranell
July 2020

Norwegian University of Science and Technology
Faculty of Natural Sciences
Department of Materials Science and Engineering

NTNU
Norwegian University of
Science and Technology

Preface

This thesis with the title ”Distribution of Aluminum and Calcium between Silicon and CaO-Al_2O_3-SiO_2 Slags at 1650 °C” is written for the course TMT4920 and has been carried out at the Departement of Materials Science and Engineering at Faculty for Natural Sciences at Norwegian University of Science and Technology (NTNU) during the spring of 2020. This work is funded by the SisAl EU project.

First of all, I would like to thank my supervisor, professor Gabriella Tranell for plenty of guidance, motivation and feedback throughout the semester and for arranging weekly meetings. Also, I would like to thank my co-supervisor, Dr. Ing. Mertol Gökelma for helpful insights and feedback on the work.

A big thanks to Dmitry Slizovskiy and Ivar Andre Ødegard for help during all the experiments performed for various reasons at short notices. I would also like to thank Morten Peder Raanes for performing EPMA analysis.

I am very thankful for the FactSage calculations performed by Kai Erik Ekstrøm, and the helpful insights regarding them.

I would also like to thank Torill Sørløkk for doing the XRF-analysis of the slag samples.

Finally, I would like to thank Inger Fygle for being huge support during this work. Thank you for the good conversations and helpful discussions.

Trondheim, 2020-07-08

Safia Hassan

Abstract

The main aim of this work was to investigate the equilibrium between silicon (Si) and calcia-alumina (CaO-Al_2O_3) slags and to determine the distribution of aluminum (Al) and calcium (Ca) in the silicon after equilibrium. By varying the metal/slag ratio in this system, ideally, a line will form across slag compositions in the lower parts of the CaO-Al_2O_3-SiO_2 phase diagram, where the SiO_2 concentration increases with increasing ratio. The motivation for investigating this area of the phase diagram came from the SisAl process, which is a novel, patented industrial process for producing silicon. A CaO-Al_2O_3 slag forms as a by-product of this process, and due to very little data in the CaO-Al_2O_3-rich region of the CaO-Al_2O_3-SiO_2 slag system, as most published work focuses on the SiO_2-rich area of the system, the present work was conducted to investigate that area.

Two different slags were prepared for equilibration with Si; a 35-65 in weight% (wt%) and a 45-55 wt% CaO-Al_2O_3 slag. Five metal/slag ratios were investigated; a metal slag ratio of 1/1, 2.5/1, 5/1, 7.5/1, and 10/1, where the mass of the slag was kept constant at 24 g. Equilibrium experiments were conducted in a closed induction furnace, and the slag and metal were charged in a graphite crucible. All experiments were conducted at 1650 °C, with one-hour holding time in an argon atmosphere. After equilibration, the furnace was shut off, and the samples were cooled down to room temperature without outer influence. After all experiments, the crucibles were cut, and slag and metal samples were cast in epoxy for analysis with EPMA (electron probe microanalyzer) and imaged with BSE (backscatter electrons). ICP-MS (inductively coupled plasma mass spectrometry) was also conducted on the metal samples.

The results show that the concentration of Al and Ca in Si in equilibrium with 35-65 wt% and 45-55 wt% CaO-Al_2O_3 slags decreases with increasing metal/slag ratio. For the 35-65 wt% CaO-Al_2O_3 slag series, the Al concentrations were 2.19 ± 0.23-9.74 ± 0.14 wt% and the Ca concentrations were between 1.08 ± 0.10-6.13 ± 0.05 wt%. For the 45-55 wt% CaO-Al_2O_3 slag series, the Al concentrations were 0.38 ± 0.20- 4.57 ± 0.02, and the Ca concentrations were between 2.35 ± 0.02-11.39 ± 0.10 wt%.

Experiments also showed an increase of Ca concentration with increasing CaO/Al_2O_3 ra-

tio, while the Al concentration decreases. The SiO_2 concentration in the slag increases with increasing metal/slag ratio, and the obtained SiO_2 concentrations after the equilibria experiments with 35-65 wt% and 45-55 wt% CaO-Al_2O_3 slags were between 9.83-27.08 wt% and 13.52-26.05 wt%, respectively. The activity coefficients of Al and Ca in Si has been calculated, and were determined to be in the range γ^0_{Al} = 0.32-1.16 and γ^0_{Ca} = 0.002-0.056 for the 35-65 wt% slag series and γ^0_{Al} = 1.43-3.14 and γ^0_{Ca} = 0.001-0.093 for the 45-55 wt% CaO-Al_2O_3 slag series.

The microstructure and intermetallic phases in the Si metal and the slag after equilibration were also investigated. In the Si metal equilibrated with 35-65 wt% CaO-Al_2O_3 slag, three prominent phases were present, which was determined to be Si_2Al_2Ca, the Si matrix and fcc Al. In the Si metal equilibrated with 45-55 wt% CaO-Al_2O_3 slag, three phases were present which was determined to be Si_2Ca, Si_2Al_2Ca, and the Si-matrix. The fractions of the phases, determined by image analysis and the chemical composition of the phases, decreased with increasing metal/slag ratio, which is in good agreement with the modeled results from FACTSAGE. In the slags, two phases were present. In the 35-65 wt% slag, a melilite phase, and a $CaAl_{12}O_{19}$ phase was observed, with fractions of 36.85-68.01 wt% and 31.94-63.15 wt%, respectively. In the 45-55 wt% slag, two phases were present, which was determined to be melilite and $CaAl_2Si_2O_8$, with fractions of 64.84-74.69 wt% and 25.31-35.16 wt%, respectively. Solidification calculations from FACTSAGE showed the presence of three to four phases in the slags. However, with respect to the experimentally observed phases, the results were in reasonable agreement.

Sammendrag

Hovedformålet med oppgaven var å undersøke likevekten mellom silisium (Si) og calcia-alumina (CaO-Al_2O_3) slagger. Ved å variere forholdet mellom metall og slagg i dette systemet vil det ideelt sett bli en linje på i den nedre delen på tvers av ulike slaggkomposisjoner av CaO-Al_2O_3-SiO_2 fasediagrammet der SiO_2 innholdet vil øke med økende forhold. Motivasjonen for å undersøke dette området av fasediagrammet har en grobunn fra SisAl prosessen, som er en ny, patentert industriell prosess for å produsere silisium, som danner biproduktet CaO-Al_2O_3 slagg. Ettersom artikler som publiseres som oftest fokuserer på det SiO_2-rike området av fasediagrammet, er dataene i den CaO-Al_2O_3-rike delen av CaO-Al_2O_3-SiO_2 slaggsystemet svært begrenset. På grunnlag av den begrensede tilgjengeligheten av informasjon ble oppgaven om å utforske denne delen av fasediagrammet utformet.

To ulike slagger ble preparert for likevektseksperimenter med silisum; et 35-65 vekt% og et 45-55 vekt% CaO-Al_2O_3 slagg. Fem ulike forhold mellom metall/slagg ble undersøkt med en konstant masse på 24 g; 1/1, 2.5/1, 5/1, 7.5/1 og 10/1. Likevektseksperimentene ble utført i en lukket induksjonsovn, der slagget og metallet ble tilsatt i en grafittdigel. Alle eksperimenter ble utført i en argonatmosfære ved 1650 °C og en time holdetid. Etter likevektseksperimentene, ble ovnen avslått og prøvene avkjølt til romtempereatur, uten ytre påvirkning. Da alle eksperimentene var blitt utført ble diglene kuttet. Deretter ble metall- og slaggprøver støpt i epoksy for videre analyser med elektronmikrosonde-analysator (EPMA) og avbildning med tilbakespredte elektroner (BSE). Induktivt koblet massespektrometri (ICP-MS) ble også utført på metallprøvene.

Resultatene viser at konsentratsjonen av Al og Ca, i likevekt med 35-65 vekt% og 45-55 vekt% CaO-Al_2O_3 slagger, avtar med økende metall/slaggforhold. For slaggserien med 35-65 vekt% CaO-Al_2O_3, var Al-konsentrasjonene 2.19 ± 0.23-9.74 ± 0.14 vekt% og Ca-konsentrasjonenene var 1.08 ± 0.10-6.13 ± 0.05 vekt%. For slaggserien med 45-55 vekt% CaO-Al_2O_3, var Al-konsentrasjonene 0.38 ± 0.20- 4.57 ± 0.02 og Ca-konsentrasjonene 2.35 ± 0.02-11.39 ± 0.10 vekt%.

Eksperimentene viste også at Ca-konsentrasjonen øker når forholdet mellom CaO/Al_2O_3

øker, samtidig som Al-konsentrasjonen avtar. SiO_2-konsentrasjonen i slagget øker når metall/slagg forholdet økes, der SiO_2-konsentrasjonen etter likevektseksperimenter etter 35-65 vekt% CaO-Al_2O_3 serien var mellom 9.83-27.08 vekt%. Etter 45-55 vekt% CaO-Al_2O_3 serien var SiO_2-konsentrasjonen mellom 13.52-26.06 vekt%. Aktivitetskoeffisientene til Al og Ca i Si er også beregnet, og ble bestemt til å være i området γ^0_{Al} = 0.32-1.16 og γ^0_{Ca} = 0.002-0.056 for 35-65 vekt% slaggserien og γ^0_{Al} = 1.43-3.14 og γ^0_{Ca} = 0.001-0.093 for 45-55 vekt% slaggserien.

Videre ble det gjort undersøkelser av mikrostrukturen og de intermetalliske fasene i Si-metallet, etter likevekt med slaggene. I Si-metallet ekvilibrert med 35-65 vekt% CaO-Al_2O_3 slagg, var tre faser tilstede og disse ble bestemt til å være Si_2Al_2Ca, Si-matrise og fcc Al. I Si-metallet ekvilibrert med 45-55 vekt% CaO-Al_2O_3 var også tre faser tilstede og disse tre ble bestemt til å være Si_2Ca, Si_2Al_2Ca og Si-matrisen. Fraksjonene av alle fasene ble fastslått med bildeanalyse, og kjemisk sammensetning, og resultatene fra dette viser at fraksjonen av alle fasene avtar når metall/slagg forholdet økes. Dette viser seg å være i god overenstemmelse med de modellerte resultatene fra FACTSAGE.

I slaggene var to faser observert. I 35-65 vekt% slaggen, var en melilitt og en $CaAl_{12}O_{19}$ fase observert, med fraksjoner på henholdsvis 36.85-68.01 vekt% og 31.94-63.15 vekt%. Også i 45-55 vekt% slaggen ble det observert to faser. De ble bestemt til å være henholdsvis melilitt og $CaAl_2SiO_8$, med fraksjoner på henholdsvis 64.84-74.69 vekt% og 25.31-35.16 vekt%. Størkningsberegninger fra FACTSAGE viste at det var 3-4 faser i slaggene. Ved å kun ta hensyn til de fasene som ble bestemt eksperimentelt, var resultatene i rimelig enighet.

Table of Contents

List of Tables

List of Figures

Chapter 1

Introduction

This thesis aimed to investigate the equilibrium between silicon metal and CaO-Al_2O_3 slags. In the SisAl process, which is a novel, patented industrial process for producing silicon, a CaO-Al_2O_3 slag is formed as a byproduct of this process. This slag may be utilized in different applications. However, the data in the CaO-Al_2O_3 rich region of the CaO-Al_2O_3-SiO_2 phase diagram are limited.

1.1 Background and Motivation

The development of clean and renewable energy is urgent due to the environmental deterioration and the energy crisis the world is facing. In 2018, an installation mark of 100 GW per year for photovoltaics was reached for the first time. Photovoltaics still has a small share in the global power market, but the European solar market is growing and is expected to continue to grow for years to come, and The Compound Annual Growth Rate (CAGR) of photovoltaics installations was 35 % between 2010-2019. [1] [2]

In the traditional carbothermic reduction of silicon, for every tonne produced silicon, 3.1 tonnes of CO_2 is emitted. "The SisAl project represents an environmental and economically sustainable alternative to today's carbothermic reduction process in the submerged arc furnace (SAF), allowing silicon production in an increasingly carbon-lean Europe." [3]

In the SisAl process, silicon dioxide (as fines or lumps) and calcium oxide are combined in a vessel at temperatures 1600-1700 °C. An aluminum source (Al scrap, dross, etc.) are introduced to reduce the calcium silicate (CaO-SiO_2) slag to silicon metal, which forms

a high-purity (99.9 %) calcium aluminate ($CaO\text{-}Al_2O_3$) slag. Further, the silicon metal and $CaO\text{-}Al_2O_3$ slag get separated. The $CaO\text{-}Al_2O_3$ slag can be separated into CaO, and Al_2O_3 as individual compounds through a hydrometallurgical process, where the Al_2O_3 can be utilized to produce high-purity aluminum, or the $CaO\text{-}Al_2O_3$ slag can be sold to the market for use in the refractory industry. However, the thermodynamic properties of this $CaO\text{-}Al_2O_3$ slag are limited as the studies in the $CaO\text{-}Al_2O_3$-rich region in the $CaO\text{-}Al_2O_3\text{-}SiO_2$ ternary phase diagram are very limited, as most studies focus on the SiO_2 rich area of the phase diagram. The aim of this thesis is thus to possibly utilize this slag from the SisAl process and to gain more knowledge about the $CaO\text{-}Al_2O_3$ system. A profound understanding of this system's thermodynamic properties is of great importance in several applications such as metallurgical slags, ceramic materials, geology, and cement.

By equilibrating the $CaO\text{-}Al_2O_3$ slag with silicon metal with different metal/slag ratios, some of the silicon will oxidize to SiO_2, and the slag will be more SiO_2-rich, and we will move upwards in the $CaO\text{-}Al_2O_3\text{-}SiO_2$ phase diagram in the area where the data is inadequate, as shown in figure. 1.1.

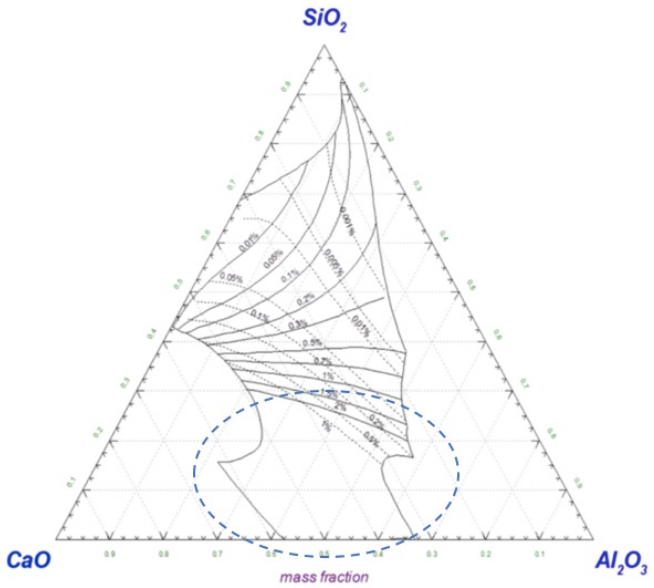

Figure 1.1: The $CaO\text{-}Al_2O_3\text{-}SiO_2$ phase diagram at 1600 °C, with isoconcentration lines for Al (full lines) and Ca (dashed lines), marked with the area of interest in this thesis. [4]

Also, by equilibrating silicon with $CaO\text{-}Al_2O_3$ slags, some calcium and aluminum will

dissolve into the silicon. By understanding the distribution of calcium and aluminum in silicon after equilibrating with $CaO\text{-}Al_2O_3$ slags, it may also open up for making different Si-Al-Ca alloys, in a cost-effective and environmentally friendly way. By navigating different metal/slag ratios in this system, the alloy produced can be directly customized.

1.2 Objectives

The main objective of this thesis is to investigate the equilibrium between solar grade silicon (SoG-Si) and $CaO\text{-}Al_2O_3$ slags, and the distribution of Ca and Al in the silicon after equilibrium. Two different $CaO\text{-}Al_2O_3$ slags were prepared; 35-65 wt% $CaO\text{-}Al_2O_3$ and 45-55 wt% $CaO\text{-}Al_2O_3$. Five experiments with five different metal/slag ratios were conducted for each slag; 1/1, 2.5/1, 5/1, 7.5/1, and 10/1, where the amount of slag was kept constant at 24 g, and the amount of silicon metal was varied between 24-240 grams. Two parallels of each experiment were performed, except for the metal/slag ratios 2.5/1, 5/1 and 7.5/1 for the 45-55 wt% $CaO\text{-}Al_2O_3$ slags due to time limitations caused by the COVID-19 situation. In all, 17 experiments were conducted. All metal- and slag samples were characterized with EPMA (Electron Probe Micro Analysis), where the overall composition of the phases in the metal and the slag was investigated after equilibrium. Thermodynamic modeling of all experiments was also conducted in FACTSAGE, and compared with the experimental data obtained.

Chapter 2

Theory and Literature Review

2.1 The Element Silicon

In Europe, a substantial amount of silicon (Si) is produced for many applications. In the crust of the earth, large amounts of silicon are found in the form of silicon dioxide (SiO_2) and silicates. The earth's crust contains about 25 wt% silicon, which makes it the second most abundant element on earth after oxygen. [5] Despite this, silicon was added on the European Commission's list of Critical Raw Materials in 2014 with the definition of a critical raw material being: "raw materials with a high supply-risk and high economic importance." The recycling rate and substitutability of silicon are low, and therefore it is listed as critical raw material. China accounts for 56 % of the global silicon production, while Europe only produces 10-12 % silicon of the 2.9 million tonnes produced while using 25 % of the world production of silicon. [6] [7] In addition to this, the production of the silicon industry faces another challenge; carbon leakage. [8]

The consumption of silicon is mainly divided between additives for aluminum alloys (50 %), silicones (30 %), and solar photovoltaics (PV) (17 %), and these markets show strong growth. [7] Whereas, the global silicone market is expected to reach USD 28.6 billion by 2024 at 7.0 % CAGR (compound annual growth rate) between 2019-2024. [9] Also, the solar photovoltaic market is growing by more than 40 % annually [10], while the Al-Si casting alloys are growing by 3.4 % CAGR. [11]

2.2 Overview of the Solar Silicon Production

In the 1940s, with the development of aluminum alloys, silicone, and high-purity polysilicon for electronics, metallurgical grade silicon with at least 96 % silicon content became an essential raw material.

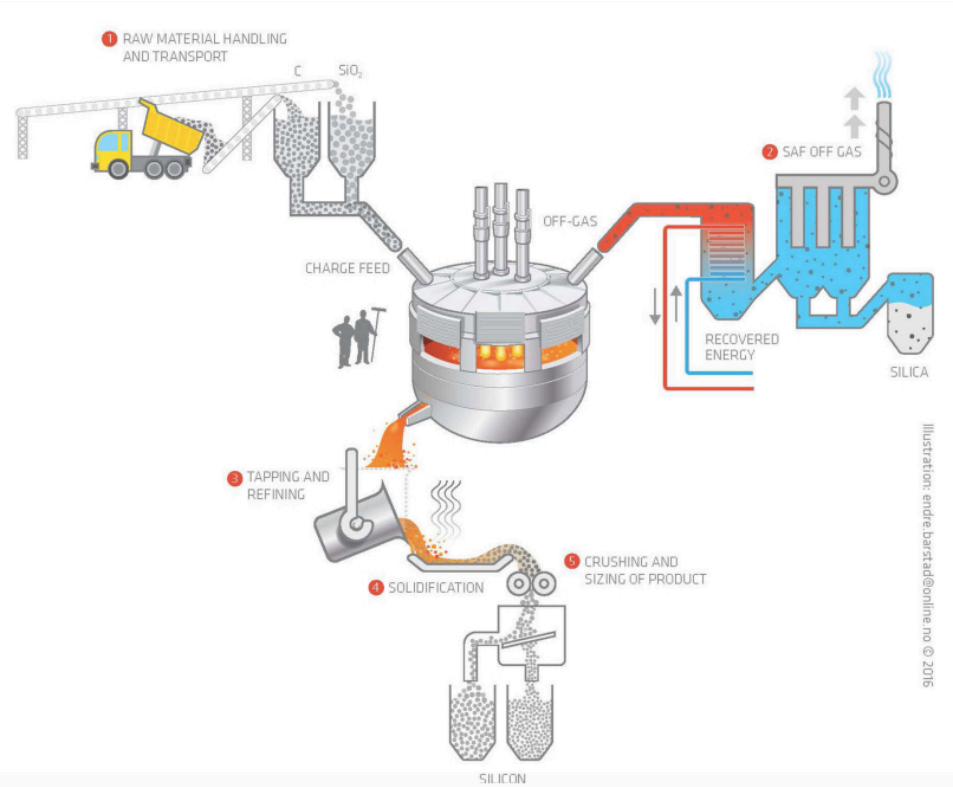

Figure 2.1: A schematic of the submerged arc furnace (SAF) used for the carbothermic production of silicon. [12]

The raw materials required for silicon production are pure quartz, with more than 97 % SiO_2 with a carbon source of either coal, charcoal, or wood chips. MG-Si is prepared by carbothermic reduction of SiO_2 at temperatures up to 1900-2000 °C, with the main reaction showed in eq. (2.1) [13]:

$$\mathrm{SiO_2(s) + 2\,C(s) \longrightarrow Si(l) + 2\,CO(g)} \tag{2.1}$$

Theoretically, when producing silicon from carbothermic reduction if assuming 100 %

yield, it is seen from the ideal reaction (2.1), that 0.85 tonnes of carbon are required to produce 1 tonne of silicon. However, practically, a yield of 100 % silicon is rarely the case as there will be some silicon loss to gas-phase reactions, mainly SiO(g). The real reaction in the carbothermic reduction is more complex, and some carbon will be consumed to other reactions [5]:

$$(1+\mathrm{x})\mathrm{SiO_2} + (2+\mathrm{x})\mathrm{C} \rightleftharpoons \mathrm{Si} + \mathrm{xSiO} + (2+\mathrm{x})\,\mathrm{CO} \tag{2.2}$$

$$(1+\mathrm{x})\mathrm{SiO_2} + (2+\mathrm{x})\mathrm{C} + (1+\mathrm{x})\mathrm{O_2} \rightleftharpoons \mathrm{Si} + \mathrm{xSiO_2\,(silica\,fume)} + (2+\mathrm{x})\,\mathrm{CO_2} + \mathrm{heat} \tag{2.3}$$

$$\mathrm{CO\,(g)} + \frac{1}{2}\mathrm{O_2\,(g)} \rightleftharpoons \mathrm{CO_2(g)} \tag{2.4}$$

The total reactions in the carbothermic reduction of silicon are showed in (2.2) and (2.3). A typical yield of silicon metal is about 80-90 %, which means that about 10-20 % of the silicon is lost as fumed silica. This yield means that for every 1-tonne silicon produced, 1.03 tonnes of carbon is consumed, which corresponds to 2 tonnes of CO(g) according to eq. (2.2). In the furnace outlet, the CO(g) will react with oxygen in the air and produce CO_2(g), as shown in eq. (2.4). To summarize: 2 tonnes of CO(g) will produce approximately 3.1 tonnes of CO_2(g), which results in 1 tonne of silicon, which again results in 3.1 tonnes of CO_2(g). [5]

There are also other challenges from the airborne emissions from silicon production, such as [12]:

- Nitrogen oxides (NO and NO_2), which are often referred to as NO_x, are important because they create fine particles and build up in the ozone layer. NO_x-gasses are formed by direct oxidation of the nitrogen at temperatures above 1400 °C, which are frequently observed in the SAF. The average NO_x concentrations in the furnace off-gas is typically 11 kg gas/per ton product alloy (semi-continuous process) and 22 kg gas/per ton product alloy (batch process).
- Polycyclic aromatic hydrocarbons (PAH) consists of two or more joined aromatic (benzene) rings, and they are often formed by incomplete combustion of organic materials. Some PAH-forms are linked to various forms of cancer and several detri-

mental health and environmental effects. In silicon production, the primary source of PAH is the reductants in the furnace and the baking of carbon electrodes. In Norway, typical PAH values range from 10-70 kg per site and year. PAH emissions are linked to furnace design, and by increasing the off-gas temperature, the PAHs will be destroyed.

- Methane (CH_4) and other volatile hydrocarbons are primarily generated in the combustion of the coke and coal, but the carbon-based electrodes will also contribute to the greenhouse gas emission. The number of hydrocarbon emissions is highly dependant on the furnace operation conditions and the alloy type produced. Lindstad et al. [14] estimated the typical CH_4 emissions for different alloys and furnace operations in the 1990s, but the values obtained vary of a magnitude of 10 when comparing to the reported values from Norwegian Si and FeSi smelters.

Ozturk and Fruehan [15] studied the gasification of SiO_2 in a CO(g) atmosphere at 1650 °C. They monitored the weight loss in the reaction between the SiO_2 spheres and the CO(g), according to eq. (2.5):

$$\mathrm{SiO_2(s) + CO\,(g) \rightleftharpoons SiO\,(g) + CO_2(g)} \tag{2.5}$$

Their results shows (plotted by Schei et al. [5]) that eq. (2.5) in the formation of SiO(g) is highly dependant on the size of the SiO_2 particles, as seen in figure 2.2. In practice, this means that SiO_2 particles with smaller size are not of use as a raw material in the carbothermic reduction process, due to reduced gas permeability in the furnace, which can lead to unstable operation such as the gas build-up and blow-outs.

As opposed to the aluminothermic reduction of silicon and, more specifically, the SisAl process, where small SiO_2 fines can be utilized instead of using SiO_2 lumps, using fines will enable the possibility of utilizing low-cost raw materials which are unsuitable for the carbothermic reduction process for silicon production. [3]

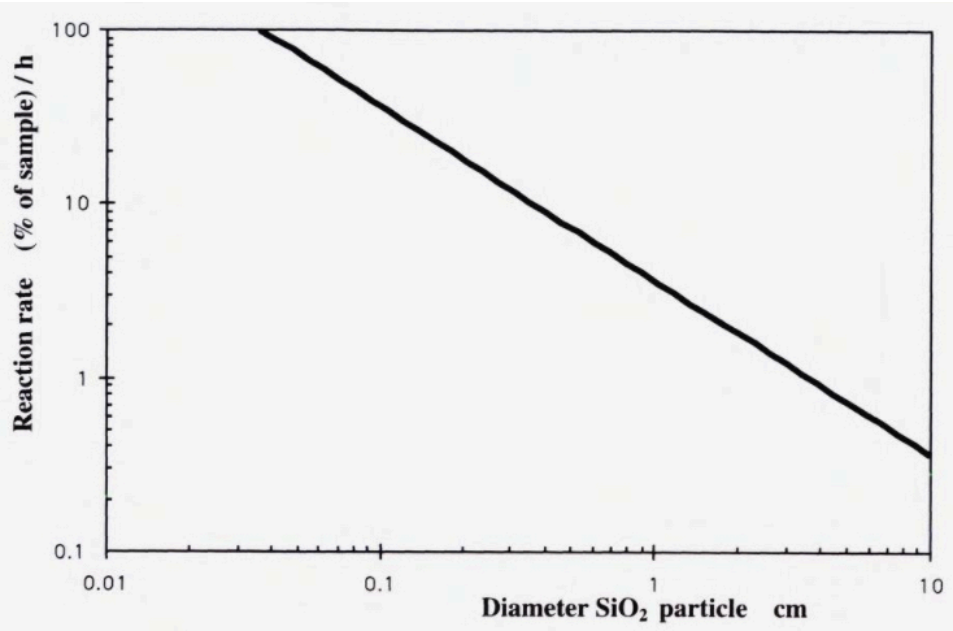

Figure 2.2: The reaction rate of SiO_2 particles as a function of the diameter of the SiO_2 particles at 1650 °C. The graph is produced by Schei et al. [5], from estimations of measurements by Ozturk and Fruehan. [15]

2.3 Alternatives to the Carbothermic Process

2.3.1 Metallothermic Reduction

Advanced materials have been prepared using reactive metals as reducing agents since 1808 when Humphry Davy isolated alkali metals. [16] In 1826, the technique was expanded after the discovery and isolation of aluminum by Hans Christian Ørsted and Friedrich Wöhler in 1827-1845. [17]

Metallothermic reduction reactions are displacive reactions that utilize reactive metals to reduce compounds. This method can produce compounds like metals, alloys, nonmetal elementary substances, and composites, often in a scalable manner. Reactive metals such as lithium, magnesium, aluminum, sodium, potassium, calcium, ferrosilicon, and intermetallics are used to reduce oxides, sulfides, or halides into metals, alloys, or nonmetals. [17] [18] The selection of reducing metal is affected by several factors:

- The affinity for the reducing compound

- The price of the reducing material
- The boiling point of the reducing material, which should be low
- The vapor pressure, which should be low
- The produced slag should be easily melted
- Intermetallic compounds should not be formed with the produced metal

A displacive reaction can in general be described as:

$$\mathrm{AB} + \mathrm{C} \longrightarrow \mathrm{A} + \mathrm{CB} \tag{2.6}$$

Where AB and CB denote oxides, halides, or other compounds, C denotes reactive metals or intermetallics, while A represents more electronegative metals, alloys, or nonmetals. [17] [18]

Metallothermic reduction to produce silicon was first performed by Gay-Lussac and Thenard, by heating silicon tetrafluoride (SiF_4) with metallic potassium, which resulted in impure, amorphous silicon. This was also the first discovery of silicon in general, but the product was not purified or characterized. [17]

Magnesiothermic Reduction

Silicon produced by magnesiothermic reduction has several application areas such as gas sensors, optical devices, optoelectronic devices, biomedical applications, and Li-ion batteries. The magnesiothermic reduction reaction of SiO_2 can be written as [19]:

$$2\,\mathrm{Mg\,(g)} + \mathrm{SiO_2(s)} \longrightarrow 2\,\mathrm{MgO\,(s)} + \mathrm{Si\,(s)} \qquad \Delta H_{650^\circ C} = -564.42 kJmol^{-1} \tag{2.7}$$

As all alkaline earth metals, magnesium will generate silicides or result in unreacted silica when reacted with SiO_2 [19]:

$$2\,\mathrm{Mg\,(g)} + \mathrm{Si\,(s)} \longrightarrow 2\,\mathrm{Mg_2Si} \qquad \Delta H_{650^\circ C} = -318.92 kJmol^{-1} \tag{2.8}$$

The formation of magnesium silicide is due to the magnesium being supplied in the vapor phase to the silicon surface. The finished product on the silicon particle surface will

prevent further reaction and thus hinder the access of magnesium to the silica interior. As a result, the unreacted silica will cause a mismatch of the stoichiometric ratio of magnesium and silica, which will lead to an unfavorable side reaction that produces magnesium silicide (Mg_2Si) as shown in eq. (2.8), and removal of this compound is necessary. Often, the magnesium silicide is removed by etching using hydrofluoric acid (HF). This etching step has a disadvantage itself due to deterioration and changing of the morphology and structure of the surface. However, the purity of silica can be improved by controlling the magnesium to the silica ratio to some extent or ramping the heating temperature. [19]

A higher degree of control over the magnesiothermic reduction reaction is necessary when producing high-quality silicon nanostructures. [20] Kim et al., [19] developed a new approach for complete conversion of silica. They used vertically oriented mesoporous silica channels presented in a two-dimensional material, reduced graphene oxide (rGO) sheets. The big advantage of this system is that the gaseous magnesium can access the thin film silica through channels. By this approach, about 10 nm scale silicon nanoparticles were produced with no unreacted silica or magnesium silicide. To demonstrate how good this new technique is, they used the powder to fabricate silicon electrodes in a lithium-ion battery with good cycling stability.

Aluminothermic Reduction of Silicon

Aluminothermic reduction of silicon is an alternative to the carbothermic reduction of silica (SiO_2) or $SiCl_4$. [21] Several researchers have widely investigated the aluminothermic reduction process. One substantial advantage of the aluminothermic reduction of silicon versus carbothermically produced silicon is the degree of impurities in the metal. For example, carbothermically produced silicon is characterized by boron and carbon concentrations above 20 ppma and some hundred ppma, respectively. On the other hand, pure raw materials can be utilized with the aluminothermic reduction, thus yielding silicon with sufficiently low boron and carbon levels. [22]

It is possible to reduce either utilize $SiCl_4$ or SiO_2 with aluminum metal, and a high-purity silicon metal will be produced. The aluminum metal is supplied in solid or liquid form, due to the low vapor pressure of aluminum metal, which is 10^{-7} atm at 1300 K, and the reaction goes as follows [21]:

$$3\,\mathrm{SiO_2\,(l)} + 4\,\mathrm{Al(s,l)} \longrightarrow 3\,\mathrm{Si\,(s)} + 2\,\mathrm{Al_2O_3} \qquad \Delta G^{\circ}_{1600^{\circ}C} = -423.33 kJmol^{-1} \tag{2.9}$$

This reaction is exothermic, which means it will generate heat. The silica will be reduced, while the aluminum will oxidize.

When reducing $SiCl_2$, the main reaction can be written as:

$$3\,\mathrm{SiCl_4\,(g)} + 4\,\mathrm{Al(s,l)} \longrightarrow 3\,\mathrm{Si\,(s)} + 4\,\mathrm{AlCl_3} \qquad \Delta G^\circ = XkJmol^{-1} \tag{2.10}$$

The byproduct $AlCl_3$ is removed as a vapor.

Different sources of silicon can be utilized, as shown in eq. (2.9) and eq. (2.10) Quartz, as for the carbothermic reduction, can be used as a reducing agent. However, since there is no carbon present, the large SiO generation when using small quartz particles is not present. Hence, fine quartz (fines) can be exploited in the process. [3] The availability of high-purity quartz sand is big since it cannot be utilized in the traditional silicon plants.

Slag systems containing SiO_2 (for example, CaO-SiO_2 slags) can also be used as an oxidizing agent. Using a slag containing SiO_2 will also serve the purpose as a silicon source, and the CaO will act as a solvent for Al_2O_3. [22] When utilizing slags as oxidizing materials, the oxides must have a higher Gibbs free energy value than Al_2O_3, as shown in the Ellingham diagram in fig. 2.8. A new process, applying this slag system, will be discussed in the next section, 2.3.1.

In the traditional aluminothermic reduction process, an equilibrium will be established between the silicon and aluminum. The composition of the Al-Si alloy depends on the amounts of silica and aluminum present in the system. Furthermore, a theoretical composition of the resulting metal can be calculated using the Al-Si phase diagram (fig. 2.3). If assuming an operating temperature of 1600 °C (1873 K) and an over-eutectic composition of silicon, at room temperature and assuming that the solidification follows the liquidus line, the resulting phases will be one silicon phase and one eutectic Si-Al alloy will be present. Fig. 2.3 shows the solidification path from 1600 °C to room temperature.

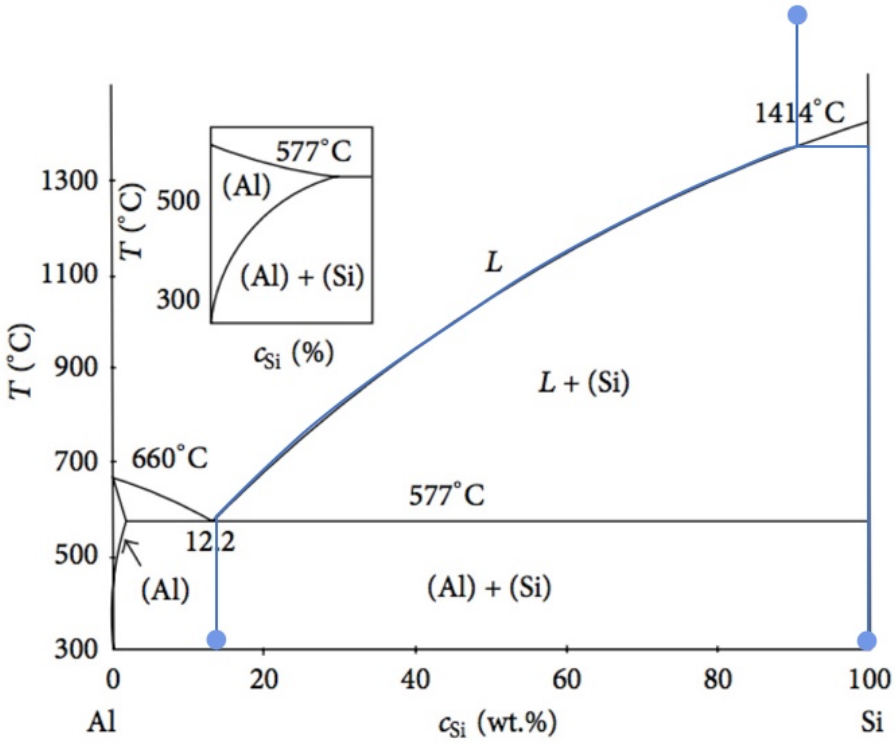

Figure 2.3: The Al-Si phase diagram. The blue lines shows the solidification path from an operation temperature of 1600 °C to room temperature, assuming an over-eutectic composition of silicon. [23]

The SisAl Process

The SisAl Process is a novel, industrial process for producing silicon, patented by Gabriella Tranell and Jafar Safarian, and coordinated by Gabriella Tranell. And in the following section, information is taken from the SisAl project pilot. [3]

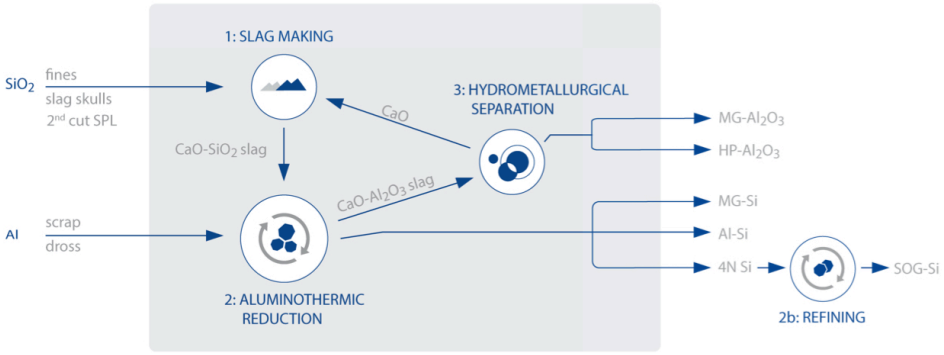

Figure 2.4: A schematic flow chart of the SisAl process. [3]

In the SisAl pilot, Al scrap and dross are used to metallothermically reduce quartz to silicon. Fig. 2.4 shows the integrated SisAl process.

The SisAl process is divided into several steps (as shown in fig. 2.4), and a summary of those steps will be presented in the following paragraph.

1. A CaO-SiO_2 slag is made, preferably of SiO_2 fines, which are less expensive than lumps in a vessel at temperatures 1600-1700 °C with a CaO:SiO_2 mass ratio of approximately 1.

2. An aluminum metal source (Al scrap or dross) is introduced to the CaO-SiO_2 to reduce the CaO-SiO_2 slag to Si-metal, forming a CaO-Al_2O_3 slag. Further, the Si-metal gets separated from the CaO-Al_2O_3 slag. The overall chemical reaction from the main process can be written as:

$$\mathrm{SiO_2\,(in\,CaO{-}SiO_2\,slag)} + \frac{4}{3}\,\mathrm{Al} \rightleftharpoons \mathrm{Si\,(l)} + \frac{2}{3}\,\mathrm{Al_2O_3\,(in\,CaO{-}Al_2O_3\,slag)}$$
$$\Delta H_{1550^\circ C} = -174.8 kJmol^{-1} \tag{2.11}$$

As seen from the reaction mentioned above, $\frac{4}{3}$ moles of Al_2O_3 is present for every mole of Si. To attain a slag with as low as possible SiO_2 content, and hence minimize Si-losses to the slag, it is expedient to keep the Al addition non-stoichiometric. By utilizing slags as oxidizing materials, the process can be performed at 1500-1600 °C as opposed to the traditional carbothermic reduction where the operating temperature is around 2000 °C. Due to the exothermic nature of this reaction, the energy supply required to run the reaction is low, as the heat formation from the reaction melts the Al. Thus, the heat formation can be controlled by the speed of the Al addition of the process.

3. Separation of the CaO-Al_2O_3 slag is necessary. Separation can be accomplished by hydrometallurgical processes. The advantage here is that this process is known (as a modification of the hydrometallurgical process in the "Pedersen-Process") for the production of alumina from calcium aluminate slags of modeled composition from a prior reduction of bauxite ores.

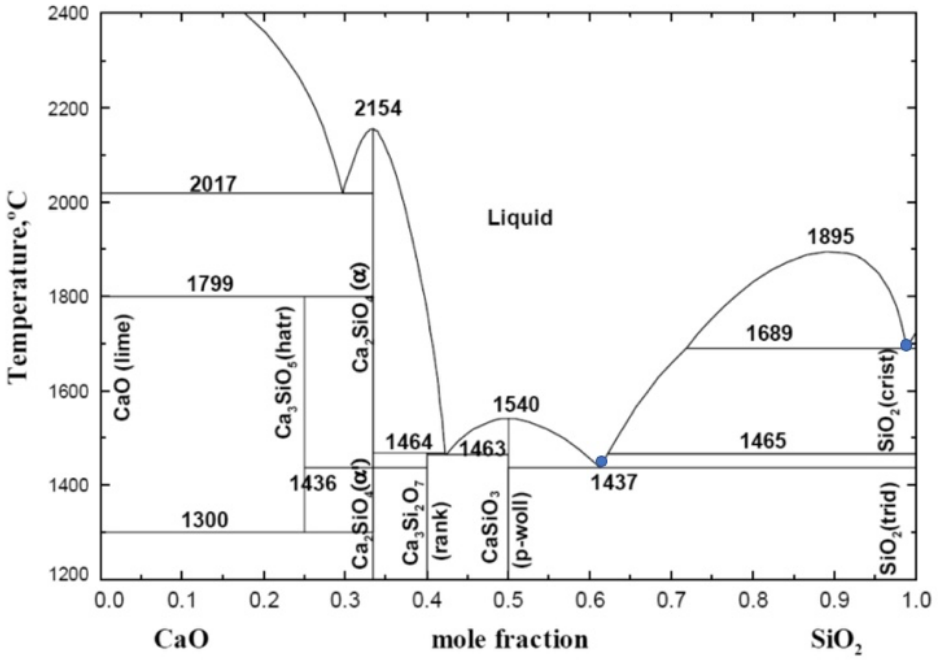

Figure 2.5: The CaO-SiO_2 phase diagram, with points marking the eutectic and the melting temperature of SiO_2. Taken from Jung et al. [24]

Figure 2.5 shows the CaO-SiO_2 phase diagram, with marked points for the eutectic and melting point of SiO_2. As mentioned in point 1., by utilizing a CaO-SiO_2 slag as an oxidizing material, the operating temperature can be lowered from 2000 °C as in the carbothermic reduction in SAF, to 1500-1700 °C in the SisAl process, as showed in figure 2.5 by choosing a slag with approximately 60 mol% CaO (37 wt%) and 40 mol% (63 wt%) SiO_2.

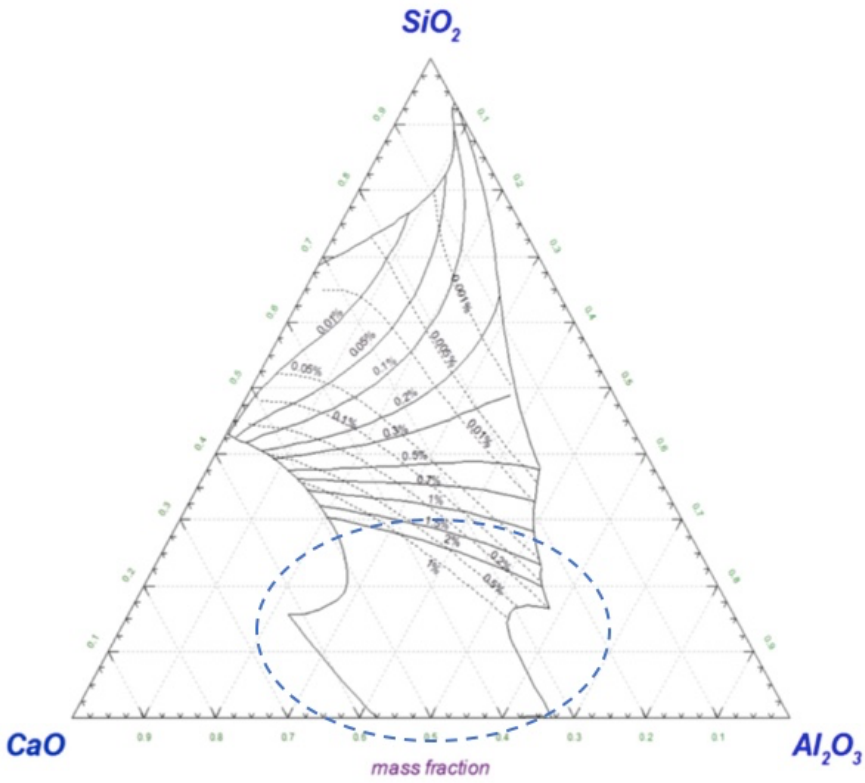

Figure 2.6: The CaO-Al_2O_3-SiO_2 phase diagram at 1600 °C with isoconcentration lines for Ca and Al, marked in blue with the area of interest for this thesis.

Figure 2.6 shows the CaO-Al_2O_3-SiO_2 phase diagram at 1600 °C with isoconcentration lines for Al and Ca. This diagram can be utilized to find the slag composition at equilibrium with silicon metal, and this can be obtained from plotting a specific metal composition in the phase diagram, where the full and dashed lines represent the isoconcentration lines for Al and Ca, respectively. Which brings the motivation behind this thesis; to possi-

bly utilize the CaO-Al_2O_3 slag from the SisAl process, and also to gain more knowledge about the slag which is a byproduct from the this process as the studies about the CaO-Al_2O_3 rich region in the CaO-Al_2O_3-SiO_2 ternary phase diagram is limited because most studies focus on the SiO_2-rich region.

2.4 The $CaO\text{-}Al_2O_3(\text{-}SiO_2)$ Slag Systems

A profound understanding of the thermodynamic properties of the $CaO\text{-}Al_2O_3$ system is of great importance in several applications such as metallurgical slags, ceramic materials, geology, and cement. Due to the high temperatures in the system, accurate experimental measurements are generally challenging to achieve. Therefore, some parts of the phase diagram and some thermodynamic properties are still not unambiguously determined. [25]

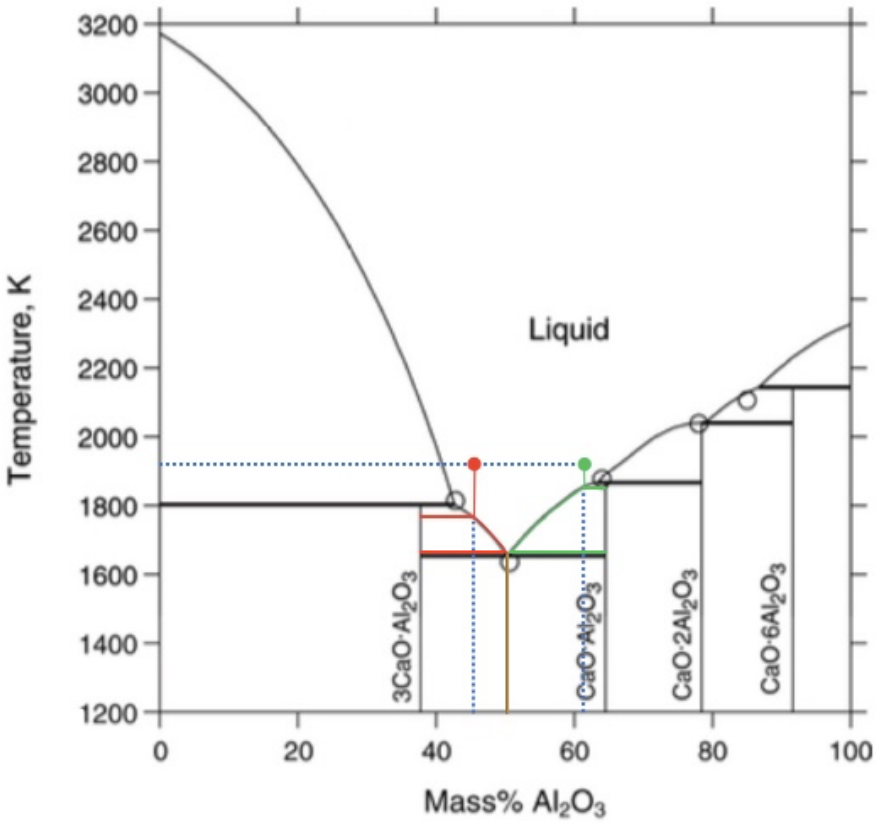

Figure 2.7: The $CaO\text{-}Al_2O_3$ phase diagram. The dashed red and green lines show the starting compositions of the slags used for this project. The full red and green lines show the solidification paths of both the compositions from 1923 K (1650 °C) to room temperature. [26]

Fig. 2.7 shows the solidification path of the two slag compositions relevant for this project from 1650 °C. A slag initially containing 45-55 wt% $CaO\text{-}Al_2O_3$ (red line) and 35-65 wt% (green line) will have the same total composition at room temperature with a theoret-

ical composition of 58.7 wt% Al_2O_3 and 41.3 wt% CaO, however, with different phases present. The 45-55 wt% CaO-Al_2O_3 slag will have two phases with more $3\,CaO \cdot Al_2O_3$ and some $CaO \cdot Al_2O_3$, while the 35-65 wt% CaO-Al_2O_3 slag will have more $CaO \cdot Al_2O_3$ and some $3\,CaO \cdot Al_2O_3$.

2.4.1 Formation of Oxides

Using the Ellingham diagram, the formation of elements in the slag phase can be predicted, as seen from figure 2.8, where the Gibbs energy of formation of oxides from elements is shown as a function of temperature.

For a given reaction to occur, the thermodynamic energy barrier ΔG° has to be overcome with barrier $\Delta G^\circ \leq 0$. The driving force for the reaction increases with more negative ΔG° values. Based on this, the more negative the ΔG° value, the bigger the likelihood for the element to form an oxide. At chemical equilibrium, in silicon, this means that any metal oxide with a lower ΔG° value, will be reduced and absorbed into the molten silicon, and metal oxides with much higher ΔG° values will be distributed in the slag, while a small amount will be in the silicon.

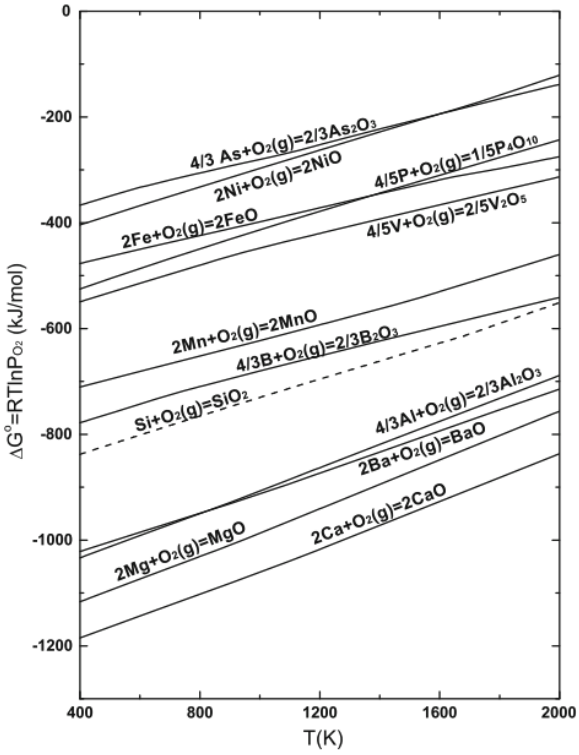

Figure 2.8: Ellingham diagram for oxides. [27]

As can be seen from figure 2.8, both Al_2O_3, and CaO are less stable than SiO_2, which means that silicon should not be oxidized into the slag if both the slag and silicon is considered ideal solutions. However, several studies show that some silicon will be oxidized into the slag phase.

2.4.2 Slag Properties

Properties such as composition, viscosity, the interfacial tension between silicon melt and slag, and the diffusion coefficient of the impurities will determine the slag's behavior in equilibrium. To predict and understand how a slag will perform when equilibrated with silicon, the before-mentioned properties of a slag is significantly important. [5] In the following sections, some important slag properties will be discussed more in detail.

Bacicity and Slag Structures

A pure oxide system can be considered ionic crystals, and one way to categorize these oxides is as Lewis acids, bases, or amphoterics, where they can receive or donate electrons. Metals in high oxidation states, or non-metals with a coordination number of 3 or 4 form primarily acidic oxides. [5] [28]

Properties such as viscosity and density will be affected by the composition of the slag. Different oxides can be used in the slag; basic oxides, acid oxides, and amphoteric oxides. The ratio between basic and acidic oxides will determine the properties, as mentioned earlier. Acidic oxides are oxygen acceptors and form chemical bonds with other oxides, thereby increasing the slag's viscosity. [28]

The term basicity is usually described as the mass ratio between the basic oxides (network modifiers) and acidic oxides (network formers). In the CaO-Al_2O_3 system, Al_2O_3 will most likely have an acidic nature, and the basicity is:

$$B = \frac{wt\%CaO}{wt\%Al_2O_3} \tag{2.12}$$

and the same goes for the CaO-Al_2O_3-SiO_2 slag system, where the basicity can be expressed as

$$B = \frac{wt\%CaO}{wt\%Al_2O_3 + wt\%SiO_2} \tag{2.13}$$

An acid oxide such as SiO_2 with a coordination number of 4 and tetrahedral structure will when going from solid to liquid loose its covalent structured network of ${SiO_2}^{-4}$ tetrahedrons and degrade into a random orientation of ${SiO_2}^{-4}$ tetrahedrons. In the tetrahedra structure, each oxygen atom is shared once with its nearby tetrahedra, resulting in two oxygen atoms for every silicon atom. In a pure silicate melt, the tetrahedrons will form bridges between each other, resulting in polymeric network structures [28]. This is characterized by this equation [5]:

$$\mathrm{SiO_2} + 2\,{\mathrm{O_2}}^{-} \rightleftharpoons {\mathrm{SiO_4}}^{4-} \tag{2.14}$$

The same goes for Al_2O_3 when assuming network breaking properties:

$$\mathrm{Al_2O_3} + 2\,{\mathrm{O_2}}^{-} \rightleftharpoons 2\,{\mathrm{AlO_4}}^{5-} \tag{2.15}$$

The network breaking leads to a decrease in the viscosity of the slag. Eq. (2.16) shows the

oxygen donor behaviour of the basic oxide CaO [5]:

$$\mathrm{CaO} \rightleftharpoons \mathrm{Ca_2}^{+} + \mathrm{O_2}^{-} \tag{2.16}$$

Networks are formed between cations and oxygen anions. The coulombic interaction between the cation and oxygen anion is defined as:

$$I = \frac{2z_c}{(r_c + r_o)^2} \tag{2.17}$$

A large I value will result in relatively strong interaction between the cation and the oxygen, and smaller values in weaker interactions when $I > 1.7$, the oxide will work as a network former, where SiO_2 is a good example. Oxides with $I < 0.7$ will break the network structure when mixed to a network former. CaO is an example of an oxide which works as a network modifier. However, when $0.7 < I < 1.7$, the oxide can act as a network former or a network modifier, depending on the system, and these oxides are called amphoteric oxides. Al_2O_3, an amphoteric oxide, will act as a network former when the degree of polymerization is low or as a network modifier when the degree of polymerization is high. More in-depth of the viscosity behaviors of slags will be discussed in the following section. [5]

When adding a basic oxide like CaO in a mixture with SiO_2, it will have network breaking properties because they work as oxygen donors. Therefore will chemical bonds between the basic oxide and other oxides form and break up bonds between other oxides, resulting in a decreased polymerization level. With CaO concentrations above 10 mol%, complex silicate anions will form in the mixture. This will result in an ionic liquid configuration with some distinct silicate anions or slags. [28] [29] However, an undulating trend of viscosity as a function of composition has been found from several researchers. Lee et al. [30] studied the viscosity of the CaO-MgO-Al_2O_3-SiO_2(-FeO) slag system, and they observed a decrease in viscosity with increasing CaO/SiO_2 mass ratio, up to a critical point of 1.3, then, the viscosity increased with increasing CaO/SiO_2 mass ratio. In a study by Xu et al. [31], they investigated the viscosity a low SiO_2 CaO-4MgO-Al_2O_3-SiO_2 slag, with the CaO/Al_2O_3 ratio varying from 0.66-1.95, and the Al_2O_3 was considered to be a network former. Their results are similar to the ones obtained from Lee et al. [30] They found that the viscosity of the system decreased with increasing temperature and decreased with increasing mass ratio of CaO/Al_2O_3 to minimum values. However, increasing the

mass ratio of CaO/Al_2O_3 even further, the viscosity increased from the minimum point, in a V shape, as shown in figure 2.9 a). The highest viscosity values were obtained at the highest and lowest CaO/Al_2O_3 values. This is due to the high-melting phases formed, such as magnesium olivine and spinel; on the other hand, the lowest viscosity values were obtained when the slag formed low-melting-point phases like $12\,CaO \cdot 7\,Al_2O_3$. Figure 2.9 b) also shows that the viscosity of the slag decreases with increasing temperature according to Arrhenius equation (see section 2.4.2) and eq. (2.18).

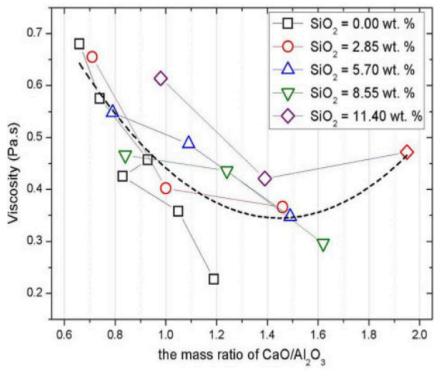

(a) The relation between viscosity and the CaO/Al_2O_3 mass ratio at 1550 °C.

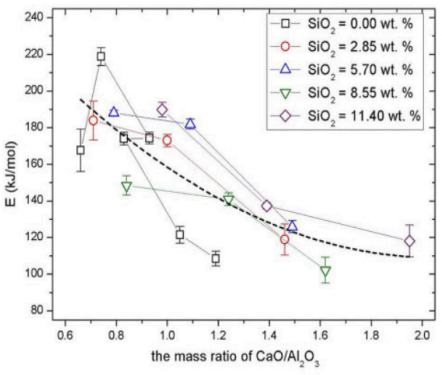

(b) The relation between the activation energy and the CaO/Al_2O_3 mass ratio at 1550 °C.

Figure 2.9: The relation between the mass ratio of CaO/Al_2O_3, viscosity and activation energy. [31]

This means, for this system, the initial slag basicity will be 0.54 and 0.82 for the 35-65 wt% CaO-Al_2O_3 and the 45-55 wt% CaO-Al_2O_3 slag, respectively. Incorporating the data from the study by Xu et al. [31], the slag with basicity of 0.54 may form high-melting-point material. However, it is worth mentioning that the high-melting-point material obtained from low CaO/Al_2O_3 mass ratio was magnesium olivine, and there is little to none MgO in the system of this study.

Viscosity of CaO-Al_2O_3-SiO_2 Slags

Viscosity is an important parameter for flow and mass transfer properties in the slag and the metal. In a slag/metal system, the slag will have a higher viscosity. Therefore, the mass transfer in the metal will be higher than in the slag (approximately two orders of magnitude). For liquid metals and simple ionic melts, the temperature dependence can be

represented by an Arrhenius type equation [5]:

$$\eta = \eta_0 \exp(\frac{E_\eta}{RT}) \tag{2.18}$$

Where η_0 is the viscosity at a given temperature, E_η is the activation energy for viscous flow. With increasing temperature, the viscosity decreases, as seen in eq. (2.18). For slags with a high degree of polymerization (low basicity), the relation seen from eq. (2.18) is usually not obeyed due to their large E_η values and their network forming properties, as mentioned in section 2.4.2. [5]

However, the Arrhenius equation (2.18) is still valid if the Eyring's expression (eq. (2.19)) is inserted as a pre-exponential factor.

$$\eta_0 = \frac{N_A \hbar}{V_M} \tag{2.19}$$

The presence of solid particles in the slag melt also strongly affects the viscosity. An estimate of the effective viscosity, η_e is given by the expression [32]:

$$\eta_e = \eta(1 - 1.35\phi)^{-2.5} \tag{2.20}$$

Where η is the viscosity of the liquid fraction of the suspension, ϕ is the volume of solid particles (assumed uniform and spherical). [32]

The time required for a system to reach equilibrium depends on the diffusivity of species, for example, Al or Ca, which can be expressed from the Stokes-Einstein equation:

$$D = \frac{k_B T}{6\pi\eta r} \tag{2.21}$$

Where k_B is the Boltzmann's constant, T is absolute temperature, η is the viscosity, and r is the radius of a spherical particle in a fluid. However, Jakobsson [33] states that there is no diffusion of spherical particles in the Si-slag system; therefore, the equation will not be accurate. Aside from that, the equation gives the general relation between diffusivity and viscosity in liquids.

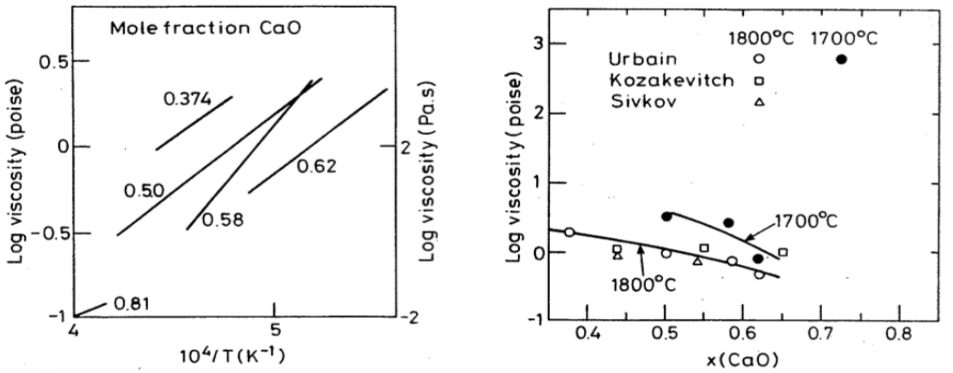

(a) Viscosities in the CaO-Al_2O_3 melt system as function of reciprocal temperature

(b) Viscosities in the CaO-Al_2O_3 melt system as a function of the mole fraction of CaO at 1700 °C and 1800 °C

Figure 2.10: Viscosities in the binary CaO-Al_2O_3 system, taken from Schlackenatlas. [34] The data points are from several researches.

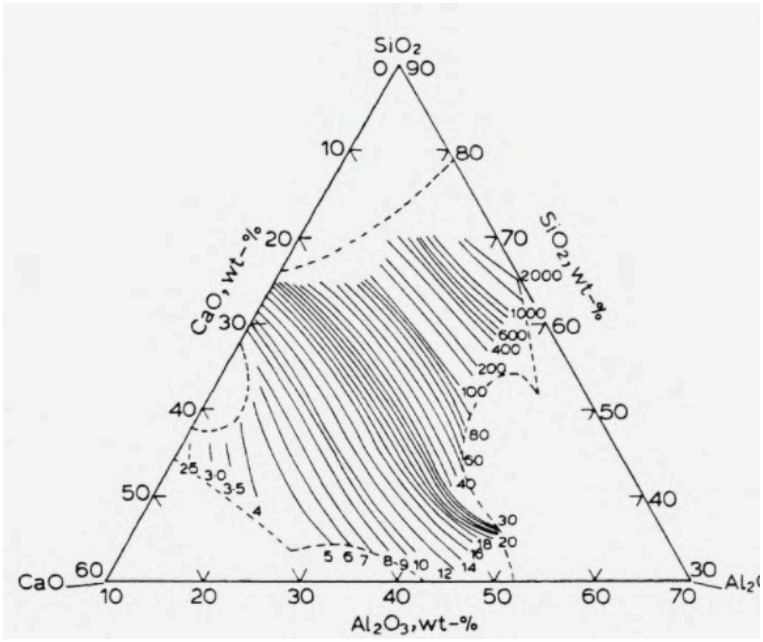

Figure 2.11: Iso-viscosity lines (given in poise), for the ternary CaO-Al_2O_3-SiO_2 slag melts at 1500 °C. Image taken from Schei et al. [5], reproduced with data from Turkdogan. [35] According to more recent data, the recommended values should be 20 % lower.

In figure 2.10, the viscosity of the CaO-Al_2O_3 the liquid slag system is shown, as a function of reciprocal temperature (a) and as a function of the mole fraction of CaO (b). It is seen from a) that the viscosity of the binary CaO-Al_2O_3 slag system is very temperature dependant, as shown in eq. (2.18). From b), it is seen that the viscosity of the CaO-Al_2O_3 slag system decreases with increasing CaO content.

From figure 2.11, the iso-viscosity lines for the CaO-Al_2O_3-SiO_2 liquid system at 1500 °C are shown. The iso-viscosity lines are parallel with the iso-concentration lines of CaO, due to the network breaking properties of CaO, as mentioned in 2.4.2. From the figure, it is seen that when the concentration of CaO decreases, and the concentration of Al_2O_3 increases, there is a shift in the iso-viscosity lines, and they become more parallel to the isoconcenration lines of SiO_2. This is a clear indication of the amphoteric behavior of Al_2O_3 in the silicate melt, where it behaves like a network former (4-oxygen-coordinated-ion) in the region where $CaO/Al_2O_3 > 1$ and as a network modifier (Al-coordinated-6-oxygen) when $CaO/Al_2O_3 < 1$. [28]

Siafakas et al. [36] measured the viscosity in the CaO-Al_2O_3-SiO_2 slag system in a wide temperature range (1350-2527 °C). In their study, it was concluded that the SiO_2/Al_2O_3 ratio had no impact on the degree of polymerization of the aluminosilicate network in the composition range with basicity of 0.85-1.50. However, abnormal behavior of the viscosity at a SiO_2/CaO mass ratio of 1.57 was observed due to the formation of $12\,CaO \cdot 7\,Al_2O_3$-like clusters. It was also found that the viscosity of slags with constant SiO_2 content decreased with increasing CaO/Al_2O_3 mass ratio due to the depolarization of the aluminosilicate network. They finally concluded that the total influence of the viscosity both attain from the influence of the network depolymerization and the cluster formation of primary solid phases.

Interfacial Properties

The interfacial properties of slags have a great influence on the reaction kinetics, nucleation, and formation of suspensions of solid particles or liquid droplets in molten slags. All interfacial properties are recorded at equilibrium conditions, if nothing else is stated, and the interface is defined as a surface if the second phase is a gas. The surface energy is defined as ”the work required to increase the area of a surface by a unit area.” [5]

For liquids, the surface tension decreases when the temperature increases and the relation can be shown by the following equation over a limited temperature range [5]:

$$\sigma = \sigma_0 + \left(\frac{d\sigma}{dT}\right) T \tag{2.22}$$

The value of slag/metal interfacial tension is most likely not affected by the slag composition, but rather by the surface-active elements in the metal phase. Matsushita et al. [37] did a comprehensive literature review regarding the interfacial tension of molten slag systems. Furthermore, they write that when Sun et al. [38] investigated the interfacial tension between liquid Fe-Si and CaO-Al_2O_3-SiO_2 system, the interfacial tension increased with increasing Si concentrations. El Gammal et al. [39] measured the interfacial tension between CaO-Al_2O_3-SiO_2 slags and Armco iron, and studied the influence of Si on interfacial tension. They found that the interfacial tension decreased with increasing Si content. However, they state that the influence of Si on the interfacial tension has been reported from several researchers to either 1) decrease, 2) increase or 3) increase and decrease with Si addition, which emphasizes the lack of agreement between researchers and the need of further work on this matter. A clear relation between the surface tension and temperature for CaO-Al_2O_3-SiO_2 liquid slag system is not reported. Sun et al. [40] also investigated the interfacial tension for CaO-SiO_2-FeO slags with 30 wt% FeO and varying compositions of CaO and SiO_2. They found that the interfacial tension varies from 0.393-0.536 N/m, and there is shown a slight increase of the interfacial tension with increasing CaO/SiO_2 mass ratio.

2.4.3 Consideration of Equilibrium Time in the CaO-Al_2O_3(-SiO_2) system

The main reactions to consider in the system relevant for this thesis are:

The silicon metal will react with the oxygen from the CaO and Al_2O_3 and form SiO_2.

$$[\mathrm{Si}] + \mathrm{O_2} \rightleftharpoons (\mathrm{SiO_2}) \tag{2.23}$$

At high temperatures/pressures, the silicon metal may form SiO(g), which is considered a loss.

$$[\mathrm{Si}] + \frac{1}{2}\mathrm{O_2} \rightleftharpoons \mathrm{SiO} \tag{2.24}$$

The Si from the melt will reduce some of the CaO and Al_2O_3, and simultaneously some Si

will get oxidized to SiO_2, and some Ca metal, and Al metal will dissolve into the Si metal:

$$[\mathrm{Si}] + 2\,(\mathrm{CaO}) \rightleftharpoons 2\,[\mathrm{Ca}] + (\mathrm{SiO_2}) \tag{2.25}$$

$$3\,[\mathrm{Si}] + 2\,(\mathrm{Al_2O_3}) \rightleftharpoons 4\,[\mathrm{Al}] + 3\,(\mathrm{SiO_2}) \tag{2.26}$$

With the total reaction between Ca and Al being:

$$2\,[\mathrm{Al}] + 3\,(\mathrm{CaO}) \rightleftharpoons 3\,[\mathrm{Ca}] + (\mathrm{Al_2O_3}) \tag{2.27}$$

In a study by Ahn et al. [41], they measured the change of concentration as a function of reaction time to investigate the time to approach equilibrium. Silica-rich master slag (22-9-69 wt% CaO-Al_2O_3-SiO_2 slag) and a silica crucible were used at 1550 °C, and the reaction time varied from 6-24 hours. The concentrations of Ca and Al in Si asymptotically reached a constant value within 6 hours.

Dumay et al. [42] determined the equilibrium time between ferrosilicon liquid alloys (65 wt% Si, FeSi65) with CaO-Al_2O_3-SiO_2 liquid slags with a composition of (15.1-9.84-51.7 wt% CaO-Al_2O_3-SiO_2) at 1450 °C. The first set of experiments were carried out with excess or low Al contents in the FeSi65 alloy. The second set of experiments was carried out with the FeSi65 alloy containing various Ca and Al concentrations. They discovered that when the initial amount of Al in the FeSi65 alloy was too far from the equilibrium concentration, equilibrium was never reached. Also, findings by studying the metal/slag interface after experiments showed that the metal/slag interface was covered by anorthite for the highest initial Al concentrations in the FeSi65 alloy, and covered by silica when the FeSi65 alloy was Al depleted. These blockages in the metal/slag interface are most likely due to the initial conditions. In the Al-rich alloys, the Al oxidation was rapid at first because the system was far from equilibrium. The alumina was produced by the reduction of silica and accumulated at the metal/slag interface because the diffusion of alumina was slower than the pace it was produced. This lead to the formation of an anorthite layer, which acted as a diffusion barrier. When it comes to Ca, on the other hand, the same behavior was not observed. This is most likely due to the ease of diffusion of Ca ions in the silicate slag, as well as Ca-rich solid phases are unstable as aluminosilicates.

To summaries, depending on the viscosity of the slag, Dumay et al. [42] found that the

necessary time for their system to reach equilibrium was 12-48 h, and they concluded with that the primary phenomenon impeding the kinetics of the system, is the formation of an alumina layer on the metal that after some time leads to the formation of an anorthite layer, which slowly dissolves in the slag. They also found that with higher initial concentrations of Al in the FeSi65 alloy, the accumulation of the anorthite was so high, that even 48 hours is not enough to reach equilibrium.

In the present study, at first, the slag will have high CaO-Al_2O_3 content, as this is the starting composition, where the 45-55 wt% CaO-Al_2O_3 slag will have the lowest viscosity (see section 2.4.2), and the 35-65 wt% CaO-Al_2O_3 will have a higher viscosity. As time proceeds, some of the Si will oxidize, and the slag composition will change to be more SiO_2 rich. Nevertheless, both slag systems will have relatively low viscosities.

There will always be a driving force to approach equilibrium between the slag and the metal, which will result in mass transport from the slag and to the silicon metal, and the dissolution of Ca and Al in the silicon have five potential rate-limiting steps [43]:

1. Transport of Ca and Al from the bulk slag melt to the bulk silicon melt.
2. Ca, and Al diffuses through the boundary layer.
3. Oxidation of the species Ca and Al at the silicon bulk melt-slag interface.
4. Diffusion of Ca and Al through the slag boundary layer.
5. Ca and Al in oxide form is transported from the slag boundary layer to the bulk melt of the slag.

If local equilibrium in the chemical oxidation reactions in eq. (2.23)-(2.26) is assumed, the equilibrium will be reached relatively fast. To determine the rate-limiting step in this process, some assumptions have to be made. If local equilibrium is assumed in the metal/slag interface, the driving force for dissolution of Ca and Al in Si will be the difference of concentration of Ca and Al between the metal and the slag, due to the much higher CaO and Al_2O_3 content in the slag than the concentration of Ca and Al in the Si-melt. Therefore, it is reasonable to assume that the mass transfer between the slag and Si will be relatively fast initially.

The transport of [Ca] and [Al] in Si and the slag boundary layers are dependant on convection and diffusion. As seen in reaction (2.25) and (2.26), reduction of [Ca] and [Al] are linked with reaction (2.23). From this, it is clear that all three before-mentioned reactions

have the same rate-limiting step; transport of the species [Ca] and [Al] from the slag bulk melt, to the silicon bulk melt.

2.4.4 Thermodynamic Evaluation

In aluminothermic reduction of silicon, the slag phase is present as an ionic melt, where the molten slag and metal are immiscible. To illustrate the formation of oxides, the reaction $x[El]$ + $\frac{y}{2}$ $\{O_2\} \rightarrow (El_xO_y)$ can be considered, where x and y are integers. The main reactions when equilibrating silicon and the formation of CaO-Al_2O_3 slags are given eq. (2.23)-(2.27).

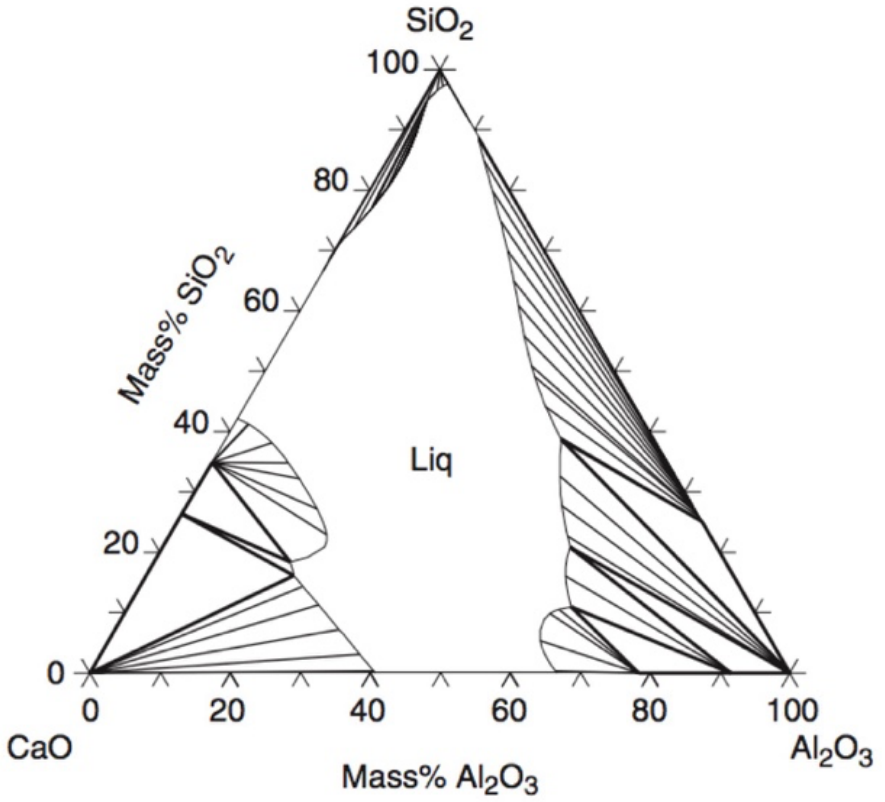

Figure 2.12: The CaO-Al_2O_3-SiO_2 phase diagram at 1650 °C, showing the isothermal section. The thick straight lines represent the three-phase equilibrium fields. The liquid phase equilibrates with various solid phases, while the thin straight lines show the tie lines. [29]

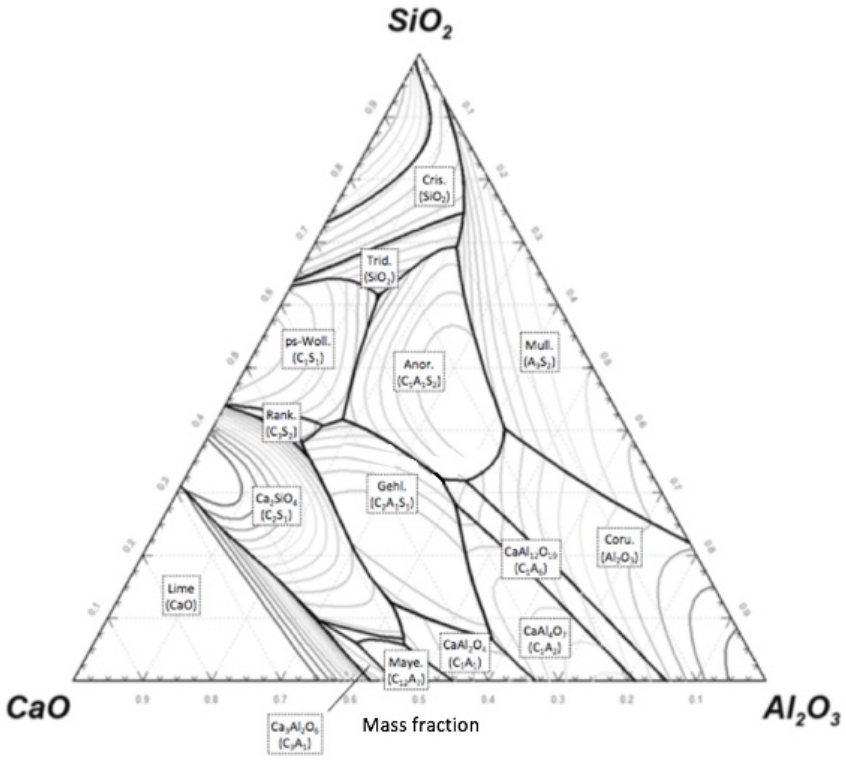

Figure 2.13: The CaO-Al_2O_3-SiO_2 phase diagram, showing the possible phases in the ternary system. [4]

Figure 2.12 shows the CaO-Al_2O_3-SiO_2 phase diagram at 1650 °C, showing the isothermal section, and figure 2.13 shows the general CaO-Al_2O_3-SiO_2 phase diagram, obtained from FactSage.

As seen in reaction (2.27), the concentration of (Al_2O_3) and (CaO) depends on the equilibrium between the species [Al] and [Ca] in the silicon melt. The concentrations of [Al] and [Ca] in silicon at equilibrium are determined by the activity- and interaction coefficients, which vary with their respective concentrations. The equations for the activity coefficients of [Al] and [Ca] are shown in eq. (2.33) and (2.32), and will be discussed further in section 2.4.5 and 2.4.6.

In the Si-CaO-Al_2O_3 system, the oxygen from the oxides will react with the silicon and form some SiO_2 and SiO, as shown in eq. (2.23) and eq. (2.24). Further, the Si will react

with Al_2O_3 and CaO and form SiO_2 in the slag, and some Al_2O_3 and CaO will reduce to Al Ca and dissolve in the Si metal:

$$2\,(\mathrm{Al_2O_3})(\mathrm{l}) + [\mathrm{Si}]\,(\mathrm{l}) \rightleftharpoons 3\,(\mathrm{SiO_2})(\mathrm{s,l}) + 4\,[\mathrm{Al}] \tag{2.28}$$

With the equilibrium constant:

$$K = \frac{a_{Al}^4 \cdot a_{SiO_2}^3}{a_{Si}^3 \cdot a_{Al2O3}^2} \tag{2.29}$$

$$2\,(\mathrm{CaO})\,(\mathrm{l}) + [\mathrm{Si}]\,(\mathrm{l}) \rightleftharpoons (\mathrm{SiO_2})(\mathrm{s,l}) + 2\,[\mathrm{Ca}] \tag{2.30}$$

With the equilibrium constant:

$$K = \frac{a_{SiO_2} \cdot a_{Ca}^2}{a_{Si} \cdot a_{CaO}^2} \tag{2.31}$$

Where the species with brackets designates elemental presence in the liquid silicon metal phase. The distribution of Ca and Al between the molten silicon metal and the slag phase at equilibrium for a given temperature is important. [41] From eq. (2.29) and (2.31) it is seen that the equilibrium will be displaced towards the right if Al and Ca have a negative deviation from ideal behavior in the liquid silicon melt or a positive deviation from ideal behavior in the liquid slag. Also, if Al_2O_3 and CaO have a positive deviation from ideality, the reaction will be displaced towards the right and towards the left if they have a negative deviation from ideality. Goncharov et al. [44] established that both CaO and Al_2O_3 show great negative deviations from the thermodynamic properties of perfect solutions, as shown in figure 2.14.

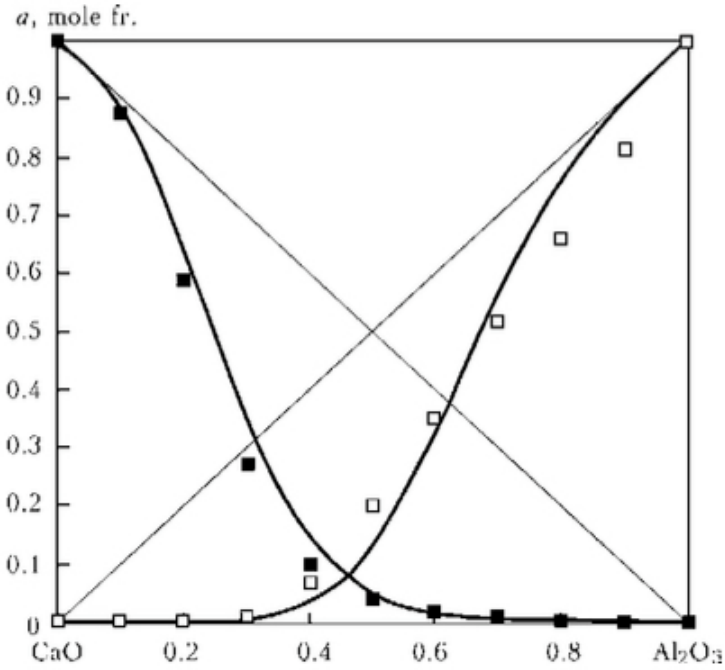

Figure 2.14: The activities of CaO and Al_2O_3 in the CaO-Al_2O_3 system melts at 1827-2027 °C. Taken from Goncharov et al. [44]

The activity of the species Ca, and Al in the Si metal will be as follows:

$$\mathrm{a_{Ca}} = \gamma_{\mathrm{Ca}} \cdot \mathrm{X_{Ca}} \tag{2.32}$$

$$\mathrm{a_{Al}} = \gamma_{\mathrm{Al}} \cdot \mathrm{X_{Al}} \tag{2.33}$$

The reactions at the interface between the slag and Si metal will be [45]:

$$\mathrm{Ca\,(s) + O\,(g) \rightleftharpoons CaO\,(l)} \tag{2.34}$$

$$\mathrm{2\,Al\,(s) + 3\,O\,(g) \rightleftharpoons Al_2O_3(l)} \tag{2.35}$$

The reactions between the species and oxygen can be thermodynamically discussed based

on Gibbs free energy for reaction (2.34) and (2.35) [45]:

$$\Delta G_{2.34} = \Delta G^{\circ}_{2.34} + RTln\left(\frac{a_{CaO}}{a_{Ca} \times p_{O_2}}\right) = \Delta G^{\circ}_{2.34} + RTln\left(\frac{a_{CaO}}{\gamma_{Ca} \times X_{Ca} \times p_{O_2}}\right) \tag{2.36}$$

$$\Delta G_{2.35} = \Delta G^{\circ}_{2.35} + RTln\left(\frac{a_{Al_2O_3}}{a_{Al} \times p_{O_2}}\right) = \Delta G^{\circ}_{2.35} + RTln\left(\frac{a_{\mathrm{Al_2O_3}}}{\gamma_{Al} \times X_{Al} \times p_{O_2}}\right) \tag{2.37}$$

Where ΔG° is the change of standard Gibbs free energy for reaction (2.34) and (2.35), p_{O_2} is the normalized oxygen partial pressure at the slag-silicon interface, a_{Ca} and a_{Al} are the Raoultian activities of Ca and Al, respectively. γ_{Ca} and γ_{Al} are the Raoultian activity coefficients and X_{Ca} and and X_{Al} are the molar fraction of the species Ca and Al in silicon, respectively. [45]

When the metal-slag system reaches equilibrium, $\Delta G_{2.34}$ and $\Delta G_{2.35}$ = 0. Then, eq. (2.36) and eq. (2.37) be rewritten as [45]:

$$\Delta G^{\circ}_{2.34} = -RTln\left(\frac{a_{CaO}}{\gamma_{Ca} \times X_{Ca} \times p_{O_2}}\right)_e \tag{2.38}$$

$$\Delta G^{\circ}_{2.35} = -RTln\left(\frac{a_{Al_2O_3}}{\gamma_{Al} \times X_{Al} \times p_{O_2}}\right)_e \tag{2.39}$$

where the subscript e expresses equilibrium values for all the parameters in the parenthesis. [45] After the reaction between Si the slags, some of the oxygen from the oxides will dissolve into the molten Si and form some SiO_2:

$$\frac{1}{2}\,\mathrm{O_2(g)} \rightleftharpoons \underline{\mathrm{O}}\,(\mathrm{wt\%\,in\,Si\,melt}) \tag{2.40}$$

When both the partial pressure of oxygen and the oxygen in the molten silicon are in equilibrium, it can be written as:

$$p_{O_2}^{1/2} = \gamma_O \times X_O \tag{2.41}$$

$$\Delta G^{\circ}_{1.17} = RTln\left(\frac{\gamma^{\circ}_{O} \times M_{Si}}{100 \times M_{O}}\right) \tag{2.42}$$

Where γ_O and γ°_{O} are the activity coefficient of oxygen in molten silicon and at infinite dilution, respectively. M_{Si} and M_O are the atomic weights of silicon and oxygen, respectively.

Tanashi et al. [45] report that the self-interaction, second- and the higher-order interactions related to oxygen, can be neglected due to the dissolution of oxygen in the molten silicon in equilibrium with silica or silica-containing slags is very diluted. If the silicon in the system is very pure, it is expected to follow Raoult's law. This means that the activity of silicon is equal to the molar fraction of silicon. Silicon will, therefore, follow Raoult's law when an impurity element follows Henry's law, due to the relation of the beforementioned law through the Gibbs-Duhem equation. [46] A problem with this approach is to determine the activity coefficients γ_i for all the equations mentioned above. However, in the system relevant for this thesis, the silicon will not be very pure and will be relatively highly alloyed with both Ca and Al, and the interaction coefficients need to be considered, which will be more discussed in section 2.4.6.

2.4.5 Acticity Coefficients at Infinite Dilute Solutions

Lu et al. [47] did an extensive literature review regarding the activity coefficients of Al and Ca at infinite dilute solutions and found that the γ°_{Al} = 0.773 at 1700 K from experiments conducted by Desai et al. [48] In 1998, Miki et al. [49], on the other hand, determined the activity coefficient of aluminum in dilute liquid silicon (0.992 $<x_{Si}<1$) as the expression at temperatures between 1723-1848 K γ°_{Al} = -1570T^{-1} + 0.236. In the following year, 1999, Miki et al. [50] found that γ°_{Al} = -3610T^{-1} + 0.452 at temperatures between 1723-1823 K. Another way to calculate the γ°_{Al} in the liquid Al-Si system is based on the CALPHAD method, the CALculation of PHAse Diagram. The method is based on the determined thermochemical properties and a phase diagram. [51] In 2003, Iwata et al. [52] predicted the γ°_{Al}(l) in infinite dilute solutions using first-principle calculations based on density functional theory, assuming the regular solution model. They found that log(γ°_{Al})(l) = 3.91 at 1723 K when ignoring atomic relaxation and log(γ°_{Al})(l) = 3.30 when considering atomic relaxation. In 2015, using the molecular interaction model, Liu et al. [53] predicted the activities and activity coefficients of aluminum in Al-Si melt based on experimental data from the literature. They found that the activity coefficient of aluminum in infinite dilution silicon solution at 1673-2273 K to be log(γ°_{Al})(l) = 7.6698 $\times$ 10^{-5}T -

0.4356. In 2012, Safarian et al. [54] calculated γ°_{Al}(l) at the melting point of silicon (1687 K) to be 0.370 from the activity curve using a simple formula utilizing liquidus constant functions. Lu et al. [47] conclude that at infinite dilute silicon melts, the activity coefficient of Al reveals a slight negative deviation from ideality.

Lu et al. [47] also did an extensive literature review on the activity coefficient of calcium (γ°_{Ca}). And in the following section, the results they found will be presented. As for the γ°_{Al}(l) value, the γ°_{Ca} (l) in the Ca-Si system can also be found with the CALPHAD method. [55] In 1971, Wynnyckyj and Pidgeon [56] determined the γ°_{Ca} (l) in molten Ca-Si alloys with 50-76 mol% Si at 930-1220 °C by directly measuring the vapor pressure. This revealed a large negative deviation from Raoult's law. In 1998, Miki et al. [49], predicted the activity coefficient of Ca by equilibrating molten Ca-Si alloys with SiO_2-saturated CaO-SiO_2 melts at 1723-1823 K. They presented their results as γ°_{Ca} (l) = -7670T^{-1} + 1.53 using the least-squares method. By using a chemical equilibration technique for silicon alloys with lead (Pb), Miki et al. [50] also further investigated the thermodynamic properties of the Ca-Si system. By utilizing the Knudsen Cell method, the γ°_{Ca} (l) in molten silicon for infinitely dilute solution relative to pure liquid standard state was determined to follow the equation log(γ°_{Ca}) (l) = -14300T^{-1} + 1.55 at temperatures between 1723-1823 K. Oliveira Pinto and Takano [57] measured the γ°_{Ca} (l) in dilute silicon solutions. This was done by equilibrating a silica-saturated CaO-SiO_2 slag in an induction furnace under an argon atmosphere, with electronic-grade silicon (9N) in a silica crucible. They presented their results as log(γ°_{Ca}) (l) = -15427T^{-1}+1.02 at 1823 K. Their results were in good agreement with Ahn et al. [41] at 1823 K in 2017. The consistent results between the activities of CaO in the slag, which are based on the γ°_{Ca} (l) value and the measured concentrations of the CaO in the slag, is a strong indication that the values found for γ°_{Ca} (l) are sensible. Lu et al. [47] conclude that at infinite dilute silicon melts, the activity coefficient of Ca reveals a strong negative deviation from ideality.

2.4.6 Interaction Coefficients at Non-Dilute Solutions

Several species in silicon may affect their respective activities, and these changes may be characterized as interaction coefficients. They derive from a Taylor series expansion of the excess free energy of the solution and are defined by considering the activity coefficient at infinite dilution from the first order formalism of Wagner for infinite dilute solutions of components 1-2-3,...-N. Where component 1 is the solvent and these expressions can be written as (the following equations are taken from Pelton [58] which originates from

Wagner [59]):

$$ln\gamma_i = ln\gamma_i^0 + \sum_{j=2}^{n} \epsilon_i^j x_j + X_j) \tag{2.43}$$

where the activity coefficient of solute *i* is defined as

$$\gamma_i = \frac{a_i}{X_i} \tag{2.44}$$

where a_i and X_i is the activity and mole fraction of *i*, respectively, where the mole fraction is defined as:

$$X_i = \frac{n_i}{n_1 + n_2 + ... + n_N} \tag{2.45}$$

where n_i is the number of moles in the solution. The activity coefficient γ_i^0 is the activity coefficient at an infinitely dilute solution, defined as when $X_1 \rightarrow 1$. The parameters ϵ_i and ϵ_j are "first-order parameters." Taken the Gibbs-Duhem equation into account, where:

$$\sum X_i dln\gamma_i = 0 \tag{2.46}$$

the limit at infinite dilution can be shown as:

$$\epsilon_{ij} = \epsilon_{ji} \tag{2.47}$$

and

$$ln\gamma_i = -\frac{1}{2} \sum_{i=2}^{n} \sum_{j=2}^{n} \epsilon_{ij} X_i X_j \tag{2.48}$$

However, eq. (2.43) and (2.48) only obey the Gibbs Duhem equation when infinite dilute solutions are considered.

For two- or three-component systems, a modified first-order formalism must be considered, a quadratic order of formalism. Many simple binary systems agree relatively closely to the quadratic order formalism, up to relatively large values of X_2. This was resolved by Darken [60], as read in [58] When considering a binary system 1-2 where 1 is the solvent, the "quadratic formalism" goes as follows:

$$\frac{g^E}{RT} = a_{12}X_1X_2 + C_2X_2 \tag{2.49}$$

where g^E is the excess molar Gibbs energy, and:

$$\frac{g^E}{RT} = \sum_{i=1}^{N} ln\gamma_i \tag{2.50}$$

where C_2 and a_{ij} are constants. When differentiating:

$$ln\gamma_2 = a_{12}X_1^2 + C_2 = (a_{12} + C_2 - 2a_{12}X_2 + a_{12}X_2^2) \tag{2.51}$$

and finally:

$$ln\gamma_1 = a_{12}X_2^2 \tag{2.52}$$

When $C_2 = 0$, the second-order formalism reduces to regular solution equations. When considering ternary systems, the second-order formalism can be extended to:

$$\frac{g^E}{RT} = (a_{12}X_1X_2 + a_{23}X_2X_3 + a_{31}X_3X_1) + (C_2X_2 + C_3X_3) \tag{2.53}$$

which can be differentiated in the same matter as eq. (2.51), for a deeper embroidment of eq. (2.53), see the article written by Pelton. [58]

2.4.7 Distribution of Al and Ca between Si and CaO-Al_2O_3-SiO_2 Slags

Knowledge about the distribution of Ca and Al between the slag and the silicon melt is essential, and several researchers have studied the equilibrium between silicon and CaO-Al_2O_3-SiO_2 slags. However, the data in the low SiO_2 region is inadequate. In the following sections, the most relevant litterateur will be presented. Details from the findings of relevant studies are given in table 2.1.

Morita et al. [61] studied the distribution of slag forming elements between the CaO-Al_2O_3-SiO_2 slag system at 1550 °C and 1600 °C. They performed two experiments with CaO-Al_2O_3-SiO_2 slags with high CaO and Al_2O_3 contents, with some of the most relevant slag compositions being X_{SiO_2} = 0.094, X_{CaO} = 0.432, $X_{Al_2O_3}$ = 0.474 and X_{SiO_2} = 0.071, X_{CaO} = 0.367, $X_{Al_2O_3}$ = 0.562. They found that when the alloys are equilibrated with slags in the lower SiO_2 region, the Ca and Al contents of the alloys will be high, with the highest obtained Ca and Al concentrations being 10.4 wt% Ca and 6.46 wt% Al, and for the second experiment, 14.9 wt% Ca and 4.46 wt% Al were obtained. Considering the Al content, this study is in good agreement with the study obtained from Weiss and Schwerdtfeger [62] even though the temperature difference of 50 K in regards to the aluminum content of the SiO_2 saturated slags. This is a strong suggestion that the aluminum content in SiO_2 saturated slags is relatively independent of temperature.

Ahn et al. [41] measured the distribution of Ca and Al between molten silicon and SiO_2-rich CaO-Al_2O_3-SiO_2 at 1550 °C (1823 K) they found that the concentrations of Al in Si follow an exponential trend along the liquidus line when the slag is saturated with SiO_2. The results from their extrapolated work are also in good agreement with the results obtained from Morita et al. [61] concerning the Al content. However, the Ca concentration was significantly higher for both studies than the ones obtained from Weiss and Scherdtfeger [62] at 1500 °C, which is an indication of that the calcium content increases with increasing temperatures. When comparing with the work of Fujiwara et al. [63], the obtained values for Al is lower, but Fujiwara et al. [63] had higher Al_2O_3 content initially, and the experiments were run at 50 K higher.

The study conducted by Morita et al. (2000) [61] is also in good agreement with the study by Fujiwara et al. [63] which equilibrated silicon with Al_2O_3 and $CaAl_{12}O_{19}$ and $CaAl_{12}O_{19}$ saturated CaO-Al_2O_3-SiO_2 slags. The results from the studies obtained from Morita et al. (2000) [61] and Fujiwara et al. [63] are plotted together in fig. 2.15 and fig. 2.16 showing the results for the slag composition alongside with the liquidus saturated with the aluminate compounds.

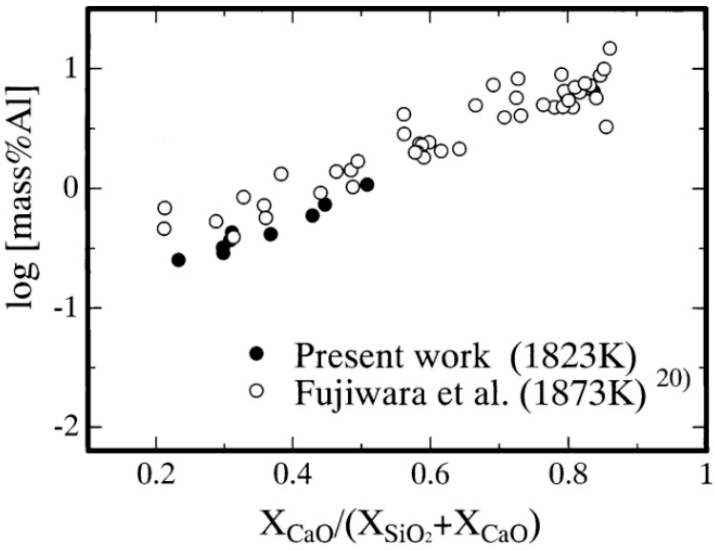

Figure 2.15: The relation between $X_{CaO}/X_{SiO_2}+X_{CaO}$ and log [mass% Ca] in Si based alloys in equilibrium with the CaO-$AlO_{1.5}SiO_2$ slags saturated with $AlO_{1.5}$, $CaO \cdot 12\,AlO_{1.5}$ or $CaO \cdot 4\,AlO_{1.5}$, taken from Morita et al. [61]

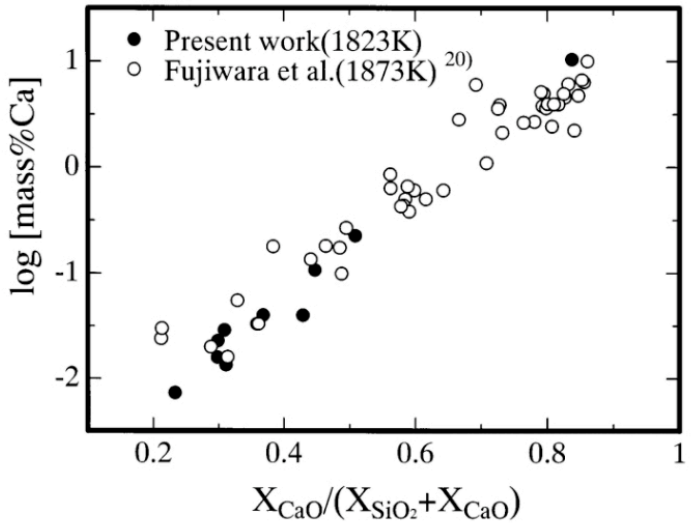

Figure 2.16: The relation between $X_{CaO}/X_{SiO_2}+X_{CaO}$ and log [mass% Ca] in Si based alloys in equilibrium with the CaO-$AlO_{1.5}SiO_2$ slags saturated with $AlO_{1.5}$, $CaO \cdot 12\,AlO_{1.5}$ or $CaO \cdot 4\,AlO_{1.5}$, taken from Morita et al. [61]

Table 2.1: Experimental details and results from different researchers, with important parameters as equilibrium time, the activity coefficients of Ca And Al, initial and final Ca and Al concentration, etc.

Reference	T(°C)	Equilibrium time (h)	Atmosphere	Slag	lnγ_{Ca}	lnγ_{Al}
Morita et al. [61]	1550 and 1600	18	Ar	CaO-Al_2O_3-SiO_2 (CaO-Al_2O_3-rich)	-$\frac{14300}{T}$ + 1.55	-$\frac{3610}{T}$ + 0.425
Ahn et al. [41]	1550	6	Ar	CaO-Al_2O_3-SiO_2 (SiO_2-rich)	-7.25	-0.77 and -0.68
Dumay et al. [42] (Experiment 20)	1450 and 1550	12-48	Ar-10%He	CaO-Al_2O_3-SiO_2	-5.81	-0.43
Weiss et al. [62]	1500 and 1600	1/2-48	Ar	CaO-Al_2O_3-SiO_2 (SiO_2-rich)	NA	-0.60
Fujiwara et al. [63]	1600	3-5	Ar	CaO-Al_2O_3-SiO_2 (CaO-Al_2O_3-rich)	NA	NA

Reference	Si mass	Slag mass	Initial Ca	Final Ca	Initial Al	Final Al
Morita et al. [61]	8 g	16 g	NA	0.3-15.9 wt%	NA	0.22-5.7 wt%
Ahn et al. [41]	5 g	10 g	NA	0.025-0.073 wt%	NA	0.015-0.032 wt%
Dumay et al. [42] (Experiment 20)	60 g (FeSi65)	60 g	0.001-0.19 wt%	0.019-0.074 wt%	0.015-0.26 wt%	0.23-0.52 wt%
Weiss et al. [62]	2 g	5 g	NA	0.0003-0.023	NA	0.0016-0.18 wt%
Fujiwara et al. [63]	2.0-3.5 g	4-6 g	0.02 wt%	8 wt%	0.4 wt%	10 wt%

2.5 Activities in the CaO-Al_2O_3-SiO_2 Slag System

Rein and Chipman [64] determined the activity of $AlO_{1.5}$ and CaO, SiO_2 in the ternary system CaO-Al_2O_3-SiO_2 at 1500-1600 °C (1773-1873 K) by measuring the distribution of silicon between the slag and Fe-Si-C alloys saturated with graphite or silicon carbide under a CO atmosphere. Their plotted isoactivity diagram for CaO, $AlO_{1.5}$ and SiO_2 are shown in figure 2.17 and 2.18, respectively.

Morita et al. (2000) [61] determined the activity of SiO_2 by equilibrating the CaO-Al_2O_3-SiO_2 slag with Si at 1550 and 1600 °C and used the equilibrium distribution of the Ca and Al between the ternary slag and silicon a Gibbs-Duhem integration. In a later study, Morita et al. (2002) [65] determined the activities of CaO and Al_2O_3, and also here, their work fits well with the values obtained from Rein and Chipman [64], however, at activities above 30 mol% Al_2O_3, their activities are lower.

Kang et al. [66] determined the activity of SiO_2 in $CaO-Al_2O_3-SiO_2$ melts with low SiO_2 content ($<$10 wt%) at 1600 °C, and compared the results with the study by Morita et al. (2000) [61] By equilibrating the melts with copper as the reference metal at controlled partial pressures, the isoactivity of SiO_2 were drawn from the measured values. They found that SiO_2 shows a positive deviation from their previous data, as well as a relation between the CaO and SiO_2 content where the SiO_2 activity decreases with increasing CaO content. Their results also showed a higher activity of SiO_2 than the ones obtained from Rein and Chipman [64], as well as a more drastic decrease in the activity of SiO_2 with increasing CaO-content. Their obtained isoactivity values are plotted together with the ones obtained from Rein and Chipman [64] in figure 2.19

Mao et al. [26] did a thermodynamic assessment of the CaO-Al_2O_3-SiO_2 system, and the activities they obtained fit relatively well with the ones obtained from Rein and Chipman.

As a summary, the work by Morita et al. (2000) [61] at 1550 °C is in close agreement with the work by Rein and Chipman [64]. Therefore, Rein and Chipman's work is considered the most representative for the $CaO-Al_2O_3-SiO_2$ system at 1600 °C.

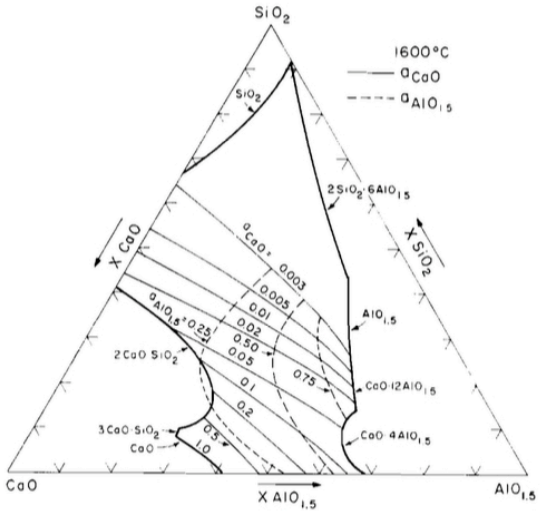

Figure 2.17: The isoactivity diagram for CaO and $AlO_{1.5}$ at 1600 °C, by Rein and Chipman. [64]

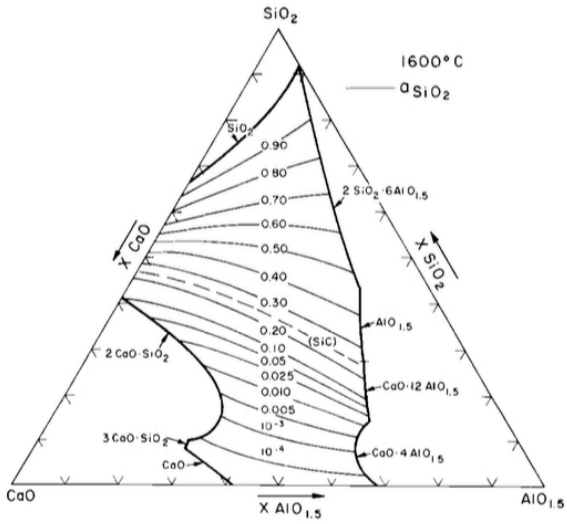

Figure 2.18: The isoactivity diagram for SiO_2 at 1600 °C, by Rein and Chipman. [64]

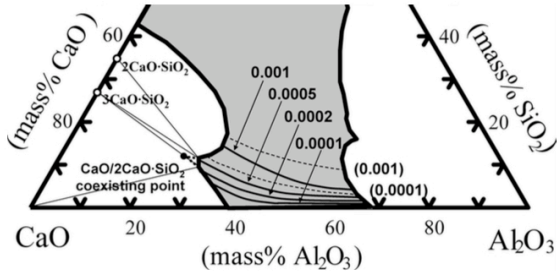

Figure 2.19: The isoactivity diagram for SiO_2 at 1600 °C, by Kang et al. compared with the results obtained from Rein and Chipman (dotted lines) in the isothermal region. [66]

2.6 Thermodynamic Modeling

All experiments performed in this study were modeled with the thermochemical software FACTSAGE. FACTSAGE was introduced in 2001, and is a fusion of FACT-Win-F*A*C*T and ChemSage/SOLGASMIX thermochemical packages which was founded in the 1970s. In the FACTSAGE software modules for information, databases, calculation, and manipulation can be found, which enables the possibility to access and manipulate pure substances and solution databases. [67]

2.7 Microstructure and Phases of Si-Al-Ca Alloys

The studies on Si-Al-Ca alloys are minimal. However, in figure 2.21, the phases present at different silicon, aluminum, and calcium concentrations can be found. It is also known that the type of intermetallic phases present is dependent on the chemistry of the metal. As seen from figure 2.21, depending on the initial composition and solidification conditions, different phases of silicon will form, in addition to phases containing aluminum, calcium, and silicon when assumed that silicon is the main element.

Anglezio et al. (1990) [68] investigated cast metallurgical grade silicon with the concentrations of the impurities of interest being Al= 0.18 wt% and Ca = 0.22 wt%, with natural cooling to room temperature. They found that calcium is tied up in two main phases; Si_2Ca and Si_2Al_2Ca, which agrees well with the findings from Margaria et al. [69].

Margaria et al. [69] also found two Si-Al-Ca rich phases when studying the intermetallic phases in metallurgical grade silicon; Si_2Ca and Si_2Al_2Ca. They identified the phases with imaging with backscatter electrons, and the chemical composition was measured with X-ray images. Table 2.2 shows the composition of the two phases found.

Table 2.2: Mean chemical composition of the major intermetallic elements from the study obtained from Margaria et al. [69] All values are given in mol%.

Compound	Si	Al	Ca
Si_2Ca	66.8	0.6	32.2
Si_2Al_2Ca	40.2	39.0	19.80

In a later study, Anglezio et al. (1994) [55] did a thermodynamic assessment of the Si-Al-Ca system, and they analyzed Si-Al-Ca samples to determine the chemical composition of the ternary eutectic. They found that the microstructure presented in figure 2.20 reveals the main phase Si_2Al_2Ca and that the light and dark areas resemble a eutectic, and table 2.3 shows the composition of the phases.

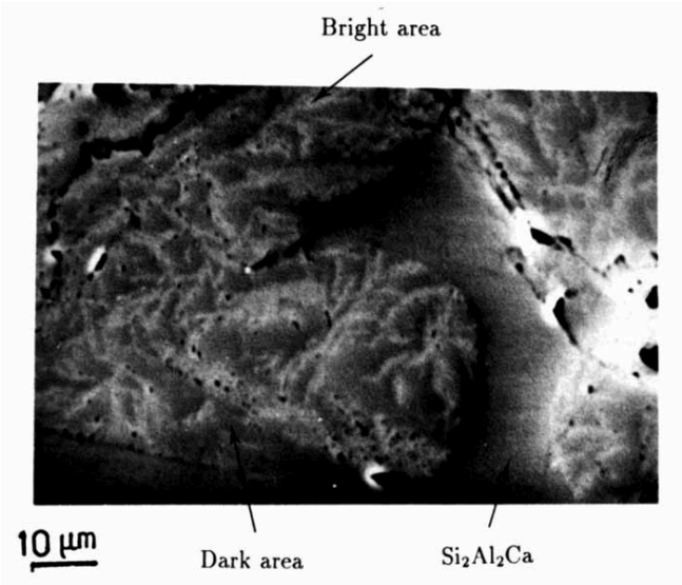

Figure 2.20: Micrography taken with electron microprobe analysis (EPMA), which reveals the phase Si_2Al_2Ca and showing eutectic light and dark areas. [55]

Table 2.3: Results from EPMA-analysis showing the chemical composition of the ternary eutectic Si-Al-Ca system.

	Wt%			mol%		
	Si	**Al**	**Ca**	**Si**	**Al**	**Ca**
Bright area	37.9	20.5	41.6	42.9	24.1	33.0
Dark area	32.3	25.7	42.0	36.6	30.2	33.2
Mean value	41.8	23.8	41.8	38.9	28.0	33.1

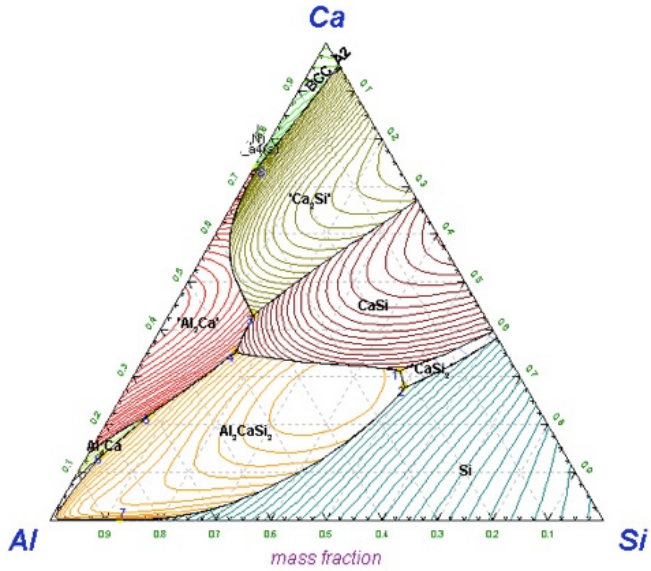

Figure 2.21: The Si-Al-Ca phase diagram, in the temperature range 540.51-1413.84 °C. [4]

Maria Møll [70] remelted metallurgical grade silicon to investigate the solidification behavior of silicon (macro- and microstructure) after casting. She found the presence of Si_2Al_2Ca as both a major and minor phase, depending on the alloy. Also, it was found that the distribution of intermetallic phases changed with the cooling rate and affected the cast silicon, and she states that a faster cooling results in a more homogeneous distribution of the intermetallic phases. And her results also agree well with both Anglezio et al. [55] [68] and Margaria et al. [69]

Chapter 3

Experimental

This chapter will present the materials used, and the methodology behind the experiments performed. The equilibria experiments between silicon in CaO-Al_2O_3 slags were carried out to investigate the low-SiO_2 part in the CaO-Al_2O_3-SiO_2 slag system which is rarely studied, and several characterization methods were performed to gain information about this system.

3.1 Preparation of Slags

Two compositions of CaO-Al_2O_3 slags were prepared; 45-55 wt% CaO-Al_2O_3 and 55-45 wt% CaO-Al_2O_3. The slags were made from commercial oxides, with a purity of the α-Al_2O_3 powder being 99.9 %, and the CaO-powder was of reagent grade. For the 45-55 wt% (69-31 mol%) CaO-Al_2O_3 slags, 1100 grams of Al_2O_3 and 900 grams of CaO were mixed, and for the 55-45 wt% (59.8-40.2 mol%) CaO-Al_2O_3, 900 grams of Al_2O_3 and 1100 grams of CaO were mixed.

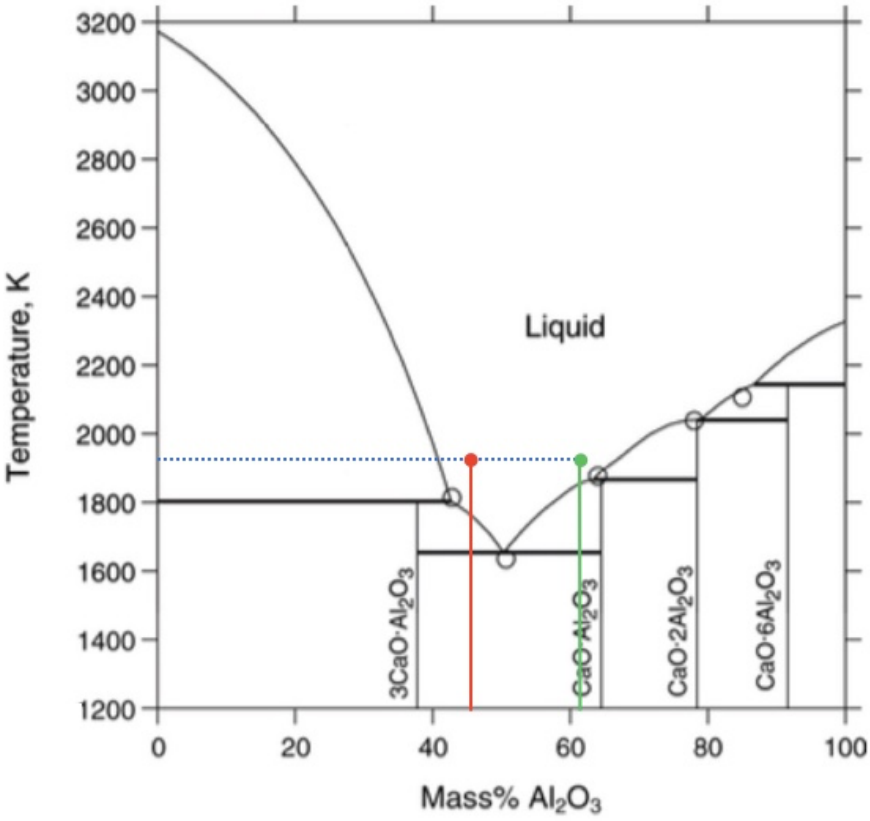

Figure 3.1: The $CaO\text{-}Al_2O_3$ phase diagram, with the chosen compositions for this work marked. Taken from [26]

The powders were weighed and mixed manually, then poured in a graphite crucible and placed in a 75-kVA induction furnace and heated with a rate of approximately 1 °C/s up to approximately 2300 °C (45-55 wt% $CaO\text{-}Al_2O_3$) and 1800 °C (55-45 wt% $CaO\text{-}Al_2O_3$). Further, the powder mixture was cast in a graphite mold and cooled down to room temperature for three hours. This process was repeated two times, with grinding of the slag in between with an agate mortar. The first slag was heated up to 2300 °C because it was the first slag that was made, and to make sure that the temperature was well above the melting temperature. A severe dusting of the CaO powder was observed, and the targeted compositions were not reached. Therefore, the new slag compositions will be named 35-65 wt% $CaO\text{-}Al_2O_3$ (old 45-55 wt% $CaO\text{-}Al_2O_3$) and 45-55 wt% $CaO\text{-}Al_2O_3$ (old 55-45 wt% $CaO\text{-}Al_2O_3$).

Table 3.1: Oxides detected from XRF-analysis on the start slags.

Compound (wt%)	**Slag 1**	**Slag 2**
SiO_2	0.31	0.37
CaO	34.16	45.61
Al_2O_3	64.55	52.68
Na_2O	ND	ND
P_2O_5	0.02	0.02
SO_3	0.01	0.01
K_2O	ND	ND
MgO	0.37	0.42
TiO_2	0.01	0.01
Cr_2O_3	0.03	0.02
Fe_2O_3	0.21	0.12
ZnO	ND	ND
SrO	0.01	0.02
Mn_2O_3	0.01	0.01
LOI (%) 1000°C	-0.04	-1.10
Sum (%)	99.66	98.18

Table 3.1 shows the compositions of the slags used in this thesis. The total sum of the components CaO and Al_2O_3 in slag 1 and slag 2 is 98.72 wt% and 98.29 wt%, and as the sum is 99.66 wt% and 98.18 wt% respectively, the total amount of other oxides are 0.94 wt% and 0.11 wt%, respectively. One important thing to note is the ”LOI” value, which is the weight loss/weight gain of the sample after melting in the test. As seen in the row ”sum,” the total amount of compounds detected are less than 100 %, indicating that there are some elements the analysis did not detect.

3.2 Apparatus

For all of the equilibria experiments, the heat is applied electrically by induction of the material. The electromagnetic forces in the furnace help with the melt's stirring, which is an advantage. The temperature was measured with a c-type thermocouple, and fig. 3.2 shows a schematic of the furnace used.

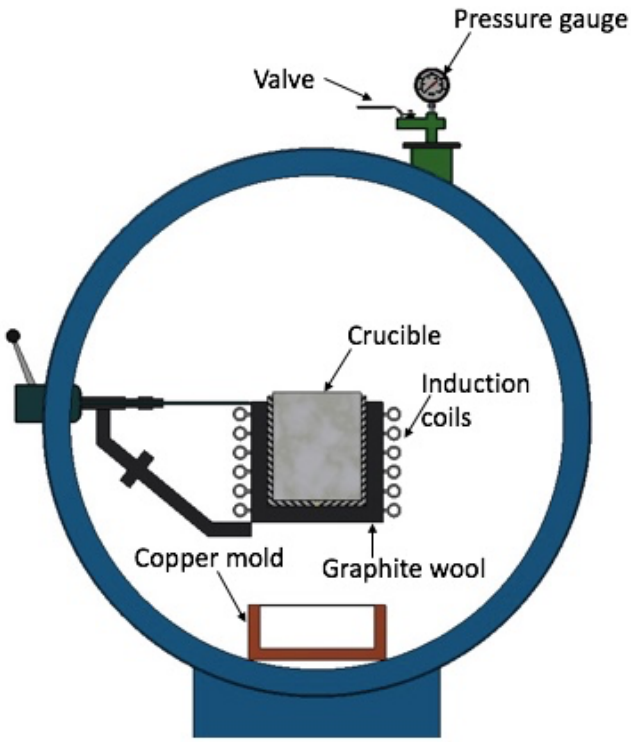

Figure 3.2: Schematic of the induction furnace used for the equilibria experiments.

3.3 Procedure

Equilibria experiments were conducted to study the equilibrium distribution of aluminum and calcium between CaO-Al_2O_3 slags and silicon. Silicon with at least 8N purity was used for all the equilibrium experiments. The metal/slag ratio varied for each experiment, and the ratios were 1/1, 2.5/1, 5/1, 7.5/1, and 10/1. Giving a series of 5 different experiments for each slag composition. The weight of the slag was kept constant at 24 grams, as well as the holding temperature. A temperature well above the melting temperature of the two slag compositions was chosen and was set to be 1650 °C. High-purity graphite crucibles were used for all experiments with an inner diameter of 70 mm and an inner height of 150 mm and were filled with slag and metal before the crucible was placed inside the furnace. The furnace was evacuated to 3 millibars or lower and then filled with 5N or 6N pure argon gas three times. This was done to minimize the oxygen in the system as much as possible, and the experiments were run at slightly overpressure, at around 1020-1030

millibars. Heating was started after the last evacuation, and the target temperature, 1650 °C, was reached after 15-30 minutes, and all the samples were held at this temperature for 1 hour to reach equilibrium between the slag and the metal. Two parallels of almost every experiment were performed. After the holding time was reached, the furnace was turned off, and the sample cooled down and taken out of the furnace.

To name the samples, the following methodology was used: 45-55-240-1, which means that the slag composition for the experiment were 45-55 wt% CaO-Al_2O_3, the weight of the silicon is 240 grams, which means that the metal/slag ratio is 10/1, and it is the first parallel in the series. The same methodology will sometimes be used when referring to experiments in the following sections.

For the 7.5/1 experiments, 180 grams of silicon was used. 5/1, 120 grams, 2.5/1, 60 grams, and 1/1, 24 grams of silicon were used, respectively.

A total of 17 experiments were performed. One parallel was only performed for the experiments 45-55-60-1, 45-55-120-1, and 45-55-180-1, due to time constraints because of the COVID-19 situation.

Table 3.2: Experimental matrix for all slag experiments, all carried out at 1650 °C, with one hour holding time.

Exp. #	Slag composition	Metal/slag ratio	$m_{silicon}$	Parallel
1	35-65 CaO-Al_2O_3	1/1	24 g	1
2	35-65 CaO-Al_2O_3	1/1	24 g	2
3	35-65 CaO-Al_2O_3	2.5/1	60 g	1
4	35-65 CaO-Al_2O_3	2.5/1	60 g	2
5	35-65 CaO-Al_2O_3	5/1	120 g	1
6	35-65 CaO-Al_2O_3	5/1	120 g	2
7	35-65 CaO-Al_2O_3	7.5/1	180 g	1
8	35-65 CaO-Al_2O_3	7.5/1	180 g	2
9	35-65 CaO-Al_2O_3	10/1	240 g	1
10	35-65 CaO-Al_2O_3	10/1	240 g	2
11	45-55 CaO-Al_2O_3	1/1	24 g	1
12	45-55 CaO-Al_2O_3	1/1	24 g	2
13	45-55 CaO-Al_2O_3	2.5/1	60 g	1
14	45-55 CaO-Al_2O_3	5/1	120 g	1
15	45-55 CaO-Al_2O_3	7.5/1	180 g	1
16	45-55 CaO-Al_2O_3	10/1	240 g	1
17	45-55 CaO-Al_2O_3	10/1	240 g	2

3.4 Characterization Methods

3.4.1 Sample Preparation

All the crucibles were cut with a diamond blade. Metal and slag samples were then cold mounted in epoxy resin. Further, the cold mounted samples were polished as preparation for EPMA. The polishing steps were as follows:

1. MD-Piano 220, with water as the lubricant. The speed was 300 rpm, and the force was set to 35 N. This step was essentially set to 1 minute, but this step was repeated a few times until all the epoxy was polished away.

2. MD-Piano 1200, with water as the lubricant. The speed was set to 150 rpm, and the force was set to 35 N. This step was run 2 minutes.

3. MD-Largo, with the abrasive type DiaPro Allegro/Largo 9 µm, The speed was 150

rpm, and the force was set to 35 N. This step was run in 8 minutes.

4. MD-Dac, with the abrasive type DiaPro Dac 3 µm. The speed was 150 rpm, and the force was set to 35 N. This step was run for 8 minutes.

5. MD-Nap, with the abrasive type DiaPro Nap B 1 µm. The speed was 150 rpm, and the force was set to 35 N. This step was run for 1 minute.

3.4.2 Electron Probe Microanalysis (EPMA)

To investigate the phases and interactions in the samples, an analysis with Electron Probe Microanalyzer (EPMA) was conducted of all metal and some of the slag samples. The analysis was performed by Senior Engineer Morten Peder Raanes (NTNU) using the JXA-8500F Field Emission Electron Probe Microanalyzer at NTNU, Trondheim. EPMA uses wavelength dispersive X-ray spectrometer (WDS), a high probe current and small probe diameter, to perform elemental analysis of the samples. This gives an indication of the different phases present in the samples. The analysis was done at metal and slag pieces that were representative of the whole sample.

All samples were also imaged with a backscatter detector with this instrument. With backscatter imaging, the darker the contrast, the lower the mean atomic number is.

3.4.3 X-Ray Fluoresence (XRF)

A small amount of the starting slags were crushed to fine powders in a ring mill in a tungsten carbide chamber. A BRUKER S8 Tiger 4 kW X-ray spectrometer was used to examine the compositions of the slags used for the reduction experiments. 0.5 grams of sample is mixed with 5.0 grams of lithium tetraborate ($Li_2B_4O_7$)/lithium metaborate ($LiBO_2$) (66/34) and then melted. The sample material is preheated at 1000 °C before melting, and the results from the analysis are calculated back to the sample before preheating. The concentrations of the main elements were calculated semi-quantitatively using the software package GEO-QUANT.

3.4.4 Inductively Coupled Plasma Mass Spectrometry (ICP-MS)

Chemical analysis was performed by ALS Scandinavia to find out the impurity content in the silicon metal. The metal and slag were separated carefully to ensure that there was no slag present in the metal samples. This analysis method was performed on the starting silicon metal and the silicon metal after equilibria experiments. The method proceeds as follows:

1. The samples were first prepared in paint steel barrels.
2. ICP-MS was performed according to ASTM D3682: 2013 and ASTM D4502: 2008, by melting lithium metaborate ($LiBO_2$) and dissolving with HNO_3.
3. Dissolution has taken place with HNO_3/HCl/HF, according to SS-EN 13656: 2003.
4. Analysis with ICP-SFMS has been done according to SS-EN ISO 17294-2: 2016 and the EPA method 200.8: 1994.

It is worth noting that the results obtained from the analysis can be affected if, for example, there is a need for extra dilution due to the sample matrix, but also if the amount of sample is limited.

3.5 Determination of Area Fraction of Phases Present

To determine the amount of each phase present in the metal and the slags, the BSE images taken were imported to the image analysis software ImageJ. [71] The threshold was fitted to each image to accurately depict the area fraction of each phase before the image was converted to a binary image (minor white phases and black background).

However, it is worth mentioning that the aluminum-rich phase in the metal from the 35-65 wt% CaO-Al_2O_3 slag series was too small to calculate a reasonable area fraction. This phase was therefore assumed to be about 0.5-1 % or less after studying all images.

3.6 Thermodynamic Modeling with FactSage

Thermodynamic modeling was implemented to have a comparative basis for the experiments performed. The modeling of all the equilibrium experiments performed was conducted by Kai Erik Ekstrøm. Thermodynamical data was acquired from the software FactSage 7.3.

The calculations of the system are done in FactSage with the FToxid (oxide/slag solutions) and FTlite (metal solutions) databases. The temperature was set to 1650°C.

Chapter 4

Results

This chapter aims to give an overview of the results obtained from the experiments carried out this spring, where the objective is to determine the equilibrium composition in the Si metal when the metal/slag ratio is varied, as well as investigating how the distribution of Al and Ca, and the slag composition influences the phases obtained in the metal. Solidification calculations for the slag will also be presented, but it is not the main focus and will only be discussed briefly. All experiments performed are also modeled in the FactSage thermochemical software 7.1, and the results from this are also included.

Error bars in the graphs presented in this section represents the uncertainty calculated through a student t-distribution with a confidence interval of 95 % and a sample size of two, as deviations to the average values. An example of such calculation can be found in appendix D.

All concentrations presented are calculated from result obtained from EPMA when taking the mean of the composition of all phases measured, and taking the area fraction into account (assuming area fraction = volume fraction).

4.1 Visual Inspection

This section will present the most important visual observations. All crucibles were cut with a diamond blade to look at the cross-section after the experiments. The cross-sectional views and a general overview of the solidified slag and silicon in the crucible after smelting trials will be displayed here. Only the crucibles from 1/1 and 10/1 experiments will be shown here, as most of the images look very similar.

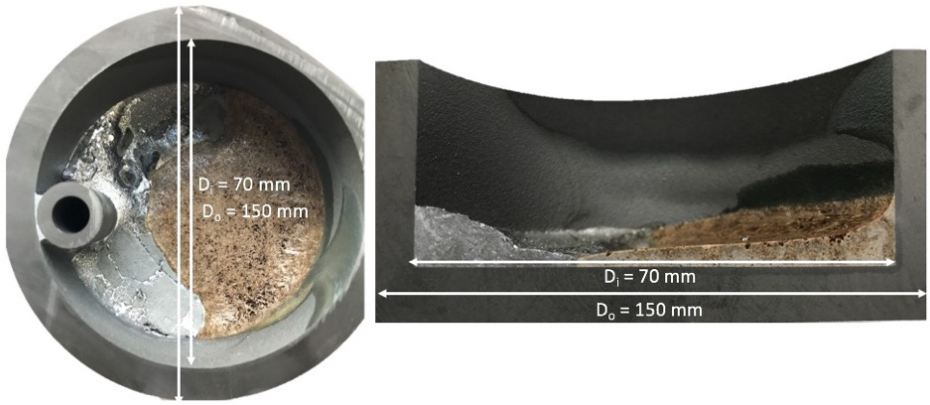

Figure 4.1: Illustrative images, showing the dimensions of all crucibles used for the experiments conducted in this thesis. Brown area: slag, silver area: metal.

Figure 4.1 shows the dimensions of crucibles used for all experiments. The crucible has an inner diameter of 70 mm and an outer diameter of 150 mm.

(a) Top of crucible for sample 35-65-24-2.

(b) Top of crucible for sample 45-55-240-2

Figure 4.2: Top of crucibles after experiments with biggest difference with the 35-65 wt% CaO-Al_2O_3 slag series, with a metal/slag ratio of (a) 1/1 and (b) 10/1.

In figure 4.2, the top of crucibles are shown, where (a) is from sample 35-65-24-2 and (b) is from sample 35-65-240-2. The difference in visible slag is clear, as it is almost impossible to see the slag from a top overview with a large amount of metal.

(a) Cross-section of the crucible from sample 35-65-24-2.

(b) Cross-section of the crucible from sample 35-65-240-2.

Figure 4.3: Cross-section of crucibles with the biggest difference, a metal/slag ratio of (a) 1/1 and (b) 10/1.

In figure 4.3, the cross-section of the crucibles from sample 35-65-24-1 (a) and 35-65-240-1 (b) is shown. The slag in (b) is almost not visible, while in (a), more slag is clearly visible.

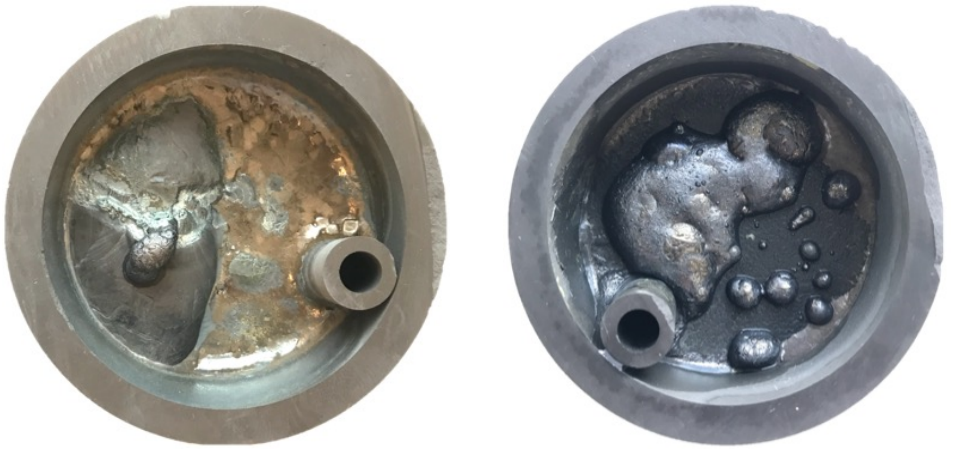

(a) Top of crucible for sample 45-55-24-1.

(b) Top of crucible for sample 45-55-240-1.

Figure 4.4: Top of crucibles after experiment conducted with 1/1 and 10/1 metal slag ratio, for the 45-55 wt% CaO-Al_2O_3 slag series.

Figure 4.4 shows the crucibles from the 45-55 wt% CaO-Al_2O_3 slag series, from the top after being cut. In (a), the slag is more visible, as opposed to in (b).

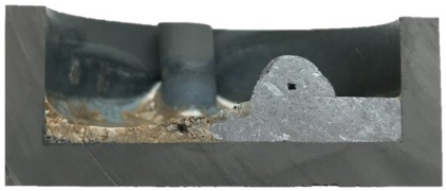

(a) Cross-section of the crucible from sample 45-55-24-1.

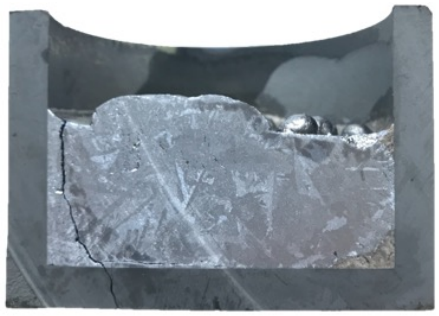

(b) Cross-section of the crucible from sample 45-55-240-1.

Figure 4.5: Cross-section of crucibles with the biggest difference, a metal/slag ratio of (a) 1/1 and (b) 10/1.

In figure 4.5, the cross-section of the crucibles from sample 45-55-24-1 (a) and 45-55-240-1 (b) is shown. The slag in (b) is almost not visible, while in (a), more slag is visible.

Comparing the two different slag-series, there are some differences, as in the colors of the slag. The 35-65 wt% slag was more brown-like, whereas the 45-55 wt% slag had a green tint. Looking at the cross-sections, the metal phases look fairly similar.

4.2 Distribution of Ca and Al Between Si and $CaO-Al_2O_3$ Slags

All values presented in the following graphical presentations are from the EPMA-analysis. All error bars indicate a 95 % confidence interval based on two replicate splits. It is worth mentioning that some of the error bars are small and barely visible.

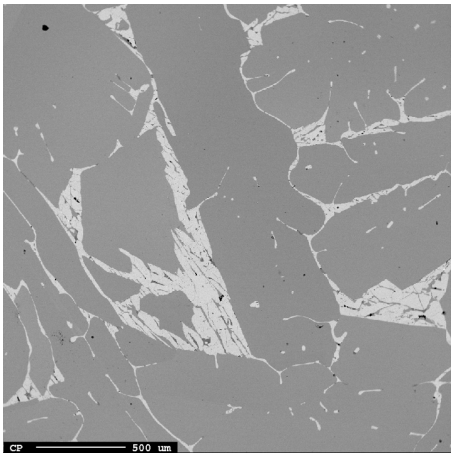

(a) Sample 35-65-24-2, imaged with 40x magnification, showing the phases present in the metal.

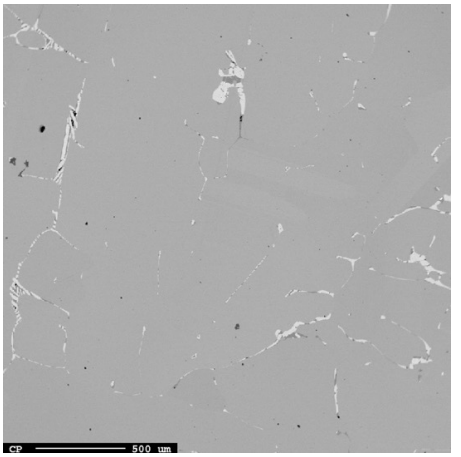

(b) Sample 35-65-240-1, imaged with 40x magnification, showing the phases present in the metal.

Figure 4.6: BSE images, showing the slag phases for the two extremes; metal/slag ratio 1/1 (a) and (b) 10/1.

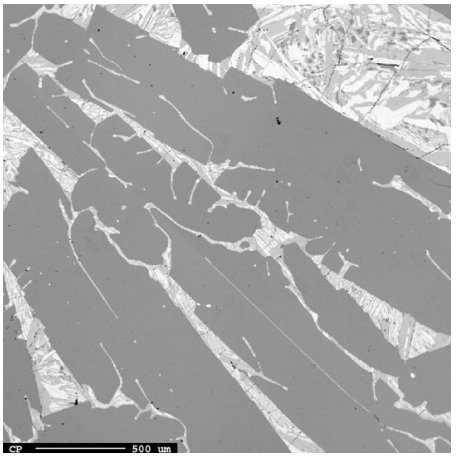

(a) Sample 45-55-24-2, imaged with 40x magnification, showing the phases present in the metal.

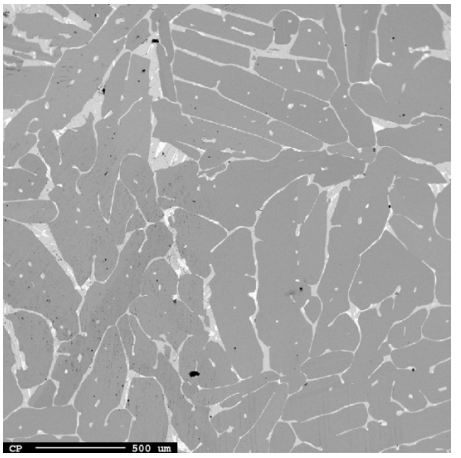

(b) Sample 45-55-240-2, imaged with 40x magnification, showing the phases present in the metal.

Figure 4.7: BSE images, showing the slag phases for the two extremes; metal/slag ratio 1/1 (a) and (b) 10/1.

As seen from figure 4.6 and 4.7, the amount of phases decreases when increasing the metal/slag ratio in the Si metal equilibrated with 35-65 and 45-55 wt% CaO-Al_2O_3 slag, in addition, the volume fraction of the phases are bigger in general, with lower metal/slag ratios.

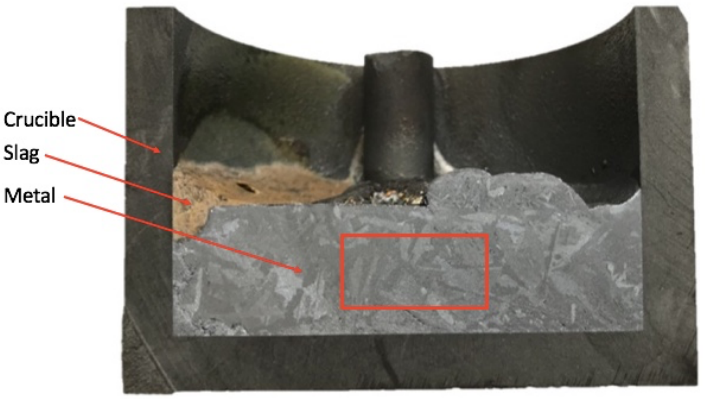

Figure 4.8: All samples for EPMA analysis were endeavored to be cut in the same area (approximately in the red square).

Figure 4.8 shows the area where the samples were cut for further analysis with EPMA.

Table 4.1: The composition of the metal and the slag from all experiments. The ± values are given where two replicate splits were performed, based on a 95% confidence interval.

	Metal (wt%)			Slag (wt%)		
Sample	**[Si]**	**[Al]**	**[Ca]**	**CaO**	**Al_2O_3**	**SiO_2**
35-65-24	84.12 ± 0.46	9.74 ± 0.14	6.13 ± 0.05	35.14	53.83	11.03
35-65-60	93.49 ± 0.17	4.33 ± 0.62	2.17 ± 0.03	29.89	60.28	9.82
35-65-120	95.81 ± 0.13	3.01 ± 0.15	1.18 ± 0.09	32.86	54.48	12.66
35-65-180	96.73 ± 0.07	2.19 ± 0.23	1.08 ± 0.10	32.82	46.78	20.40
35-65-240	94.27 ± 0.87	3.58 ± 0.13	2.15 ± 0.01	31.18	41.74	27.08
45-55-24	84.04 ± 0.76	4.57 ± 0.02	11.39 ± 0.10	39.52	46.06	13.52
45-55-60	93.79	1.42	4.79	38.95	45.13	17.22
45-55-120	94.48	1.07	4.45	37.37	38.37	24.26
45-55-180	95.48	0.61	3.91	37.44	42.86	20.48
45-55-240	97.27 ± 0.33	0.38 ± 0.20	2.35 ± 0.02	34.64	39.31	26.05

Table 4.1 shows the composition of all metal- and slag samples after the experiments. The values given are based on the mean from two parallels, except for the sample 45-55-60, 45-55-120 and 45-55-180, where only one parallel for each experiment were performed.

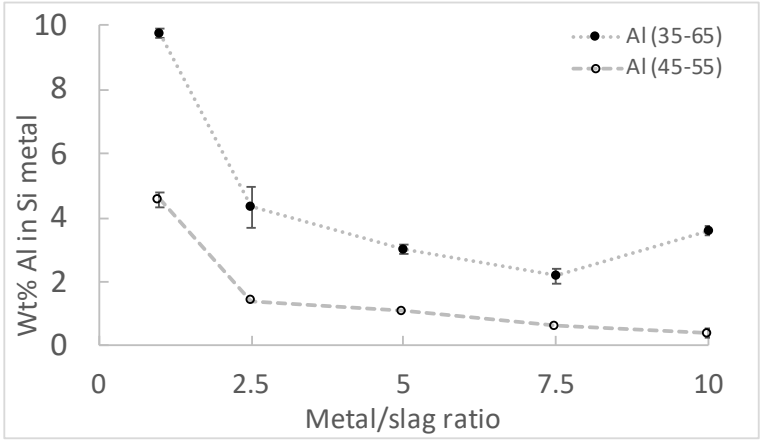

Figure 4.9: The concentration of Al in Si equilibrated with 35-65 wt% CaO-Al_2O_3 and 45-55 wt% CaO-Al_2O_3 slags at 1650 °C.

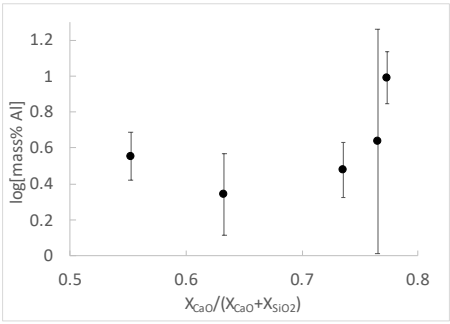

(a) The relation between $X_{CaO}/(X_{CaO}+X_{SiO_2})$ and log(mass% Al) in Si in equilibrium with 35-65 wt% CaO-Al_2O_3 slag.

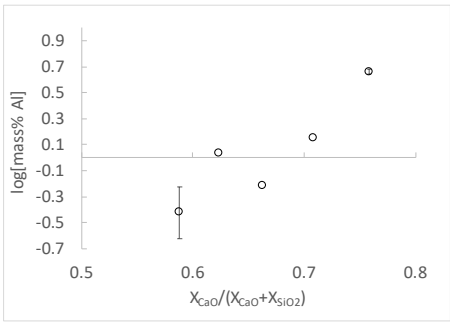

(b) The relation between $X_{CaO}/(X_{CaO}+X_{SiO_2})$ and log(mass% Al) in Si in equilibrium with 45-55 wt% CaO-Al_2O_3 slag.

Figure 4.10: The relation between the concentration of Al and $X_{CaO}/(X_{CaO}+X_{SiO_2})$ for all experiments.

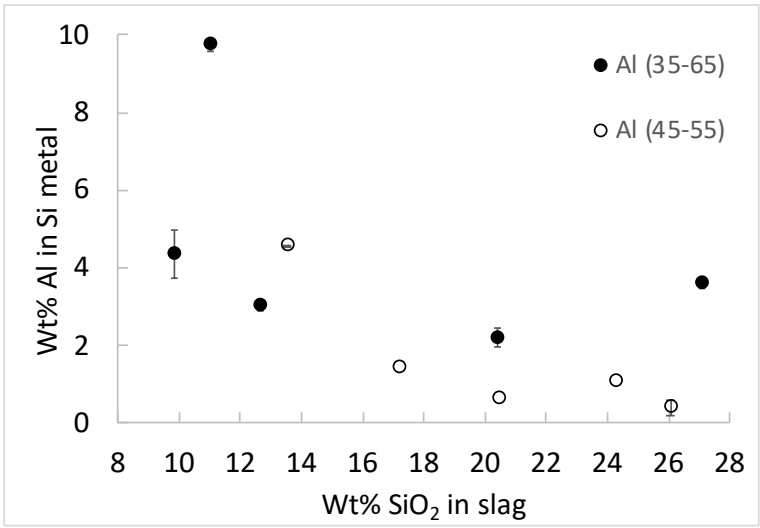

Figure 4.11: The concentration of Al in Si equilibrated with 35-65 wt% CaO-Al_2O_3 and 45-55 wt% CaO-Al_2O_3 slags as a function of the SiO_2 concentration in the slag.

Figure 4.9 shows the distribution of Al in the silicon metal equilibrated with 35-65 wt% slag and 45-55 CaO-Al_2O_3. It is seen that the Al content in the silicon generally decreases with increasing slag/metal ratio (9.74 ± 0.14-2.19 ± 0.23 and 4.57 ± 0.02 - 0.38 ± 0.20), as well as the Al content in the metal from 35-65 wt% CaO-Al_2O_3 slag is higher than in the metal from 45-55 wt% CaO-Al_2O_3 slag. It is worth mentioning that the measured value on

the 10/1 metal/slag ratio for the 35-65 wt% CaO-Al_2O_3 slag series is measured very near the slag, thus, giving higher values than the ones measured in the middle of the crucible (see figure 4.8). In figure 4.10, it is seen that the concentration of Al in Si increases with increasing $X_{CaO}/(X_{CaO} + X_{SiO_2})$ ratio in the slag after equilibration with 35-65 (a) and 45-55 (b) wt% CaO-Al_2O_3 slag. Simultaneously as the metal/slag ratio increases, the SiO_2 concentration in the slag increases, and the concentration of Al in the Si metal decreases, as seen in figure 4.11.

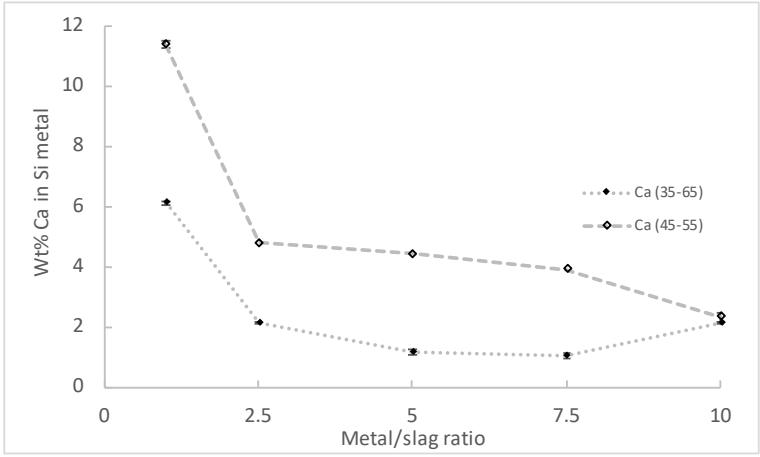

Figure 4.12: The concentration of Ca in Si equilibrated with 35-65 wt% CaO-Al_2O_3 and 45-55 wt% CaO-Al_2O_3 slags at 1650 °C.

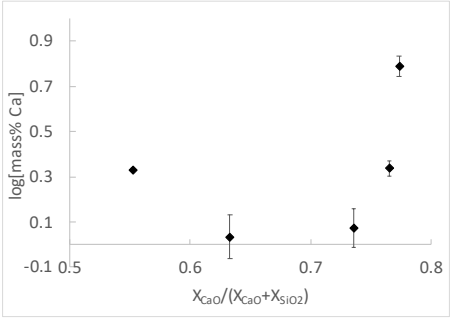

(a) The relation between $X_{CaO}/(X_{CaO} + X_{SiO_2})$ and log(mass% Ca) in Si in equilibrium with 35-65 wt% CaO-Al_2O_3 slag.

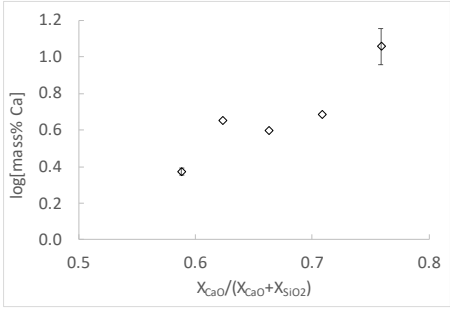

(b) The relation between $X_{CaO}/(X_{CaO} + X_{SiO_2})$ and log(mass% Ca) in Si in equilibrium with 45-55 wt% CaO-Al_2O_3 slag.

Figure 4.13: The relation between the concentration of Ca and $X_{CaO}/(X_{CaO} + X_{SiO_2})$ for all experiments.

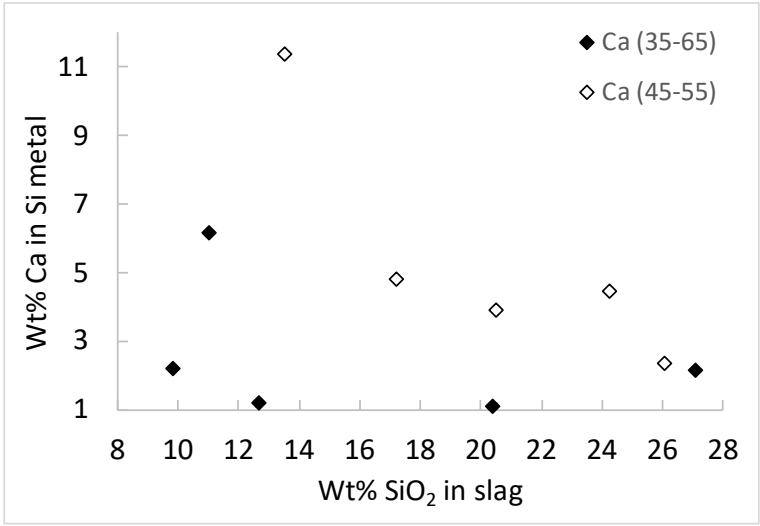

Figure 4.14: The concentration of Ca in Si equilibrated with 35-65 wt% $CaO\text{-}Al_2O_3$ and 45-55 wt% $CaO\text{-}Al_2O_3$ slags as a function of the SiO_2 concentration in the slag.

Figure 4.12 shows the distribution of Ca in the silicon metal equilibrated with 35-65 wt% slag and 45-55 $CaO\text{-}Al_2O_3$. It is seen that the Ca content in the silicon generally decreases with increasing slag/metal ratio (6.13 ± 0.05-1.08 ± 0.10 and 11.39 ± 0.10-2.35 ± 0.02), as well as the Ca content in the metal from 35-65 wt% $CaO\text{-}Al_2O_3$ slag is lower than in the metal from 45-55 wt% $CaO\text{-}Al_2O_3$ slag. Also, here, it is worth mentioning that the measured value on the 10/1 metal/slag ratio for the 35-65 wt% $CaO\text{-}Al_2O_3$ slag is measured very near the slag, thus, giving higher values than the ones measured in the middle of the crucible. In figure 4.13, it is seen that the concentration of Ca in Si increases when the relation $X_{CaO}/(X_{CaO} + X_{SiO_2})$ increases in the slag after equilibration with 35-65 (a) and 45-55 (b) wt% $CaO\text{-}Al_2O_3$ slag. However, the points are somewhat scattered. Simultaneously as the metal/slag ratio increases, the SiO_2 concentration in the slag increases, and the concentration of Ca in the Si metal decreases, as seen in figure 4.14.

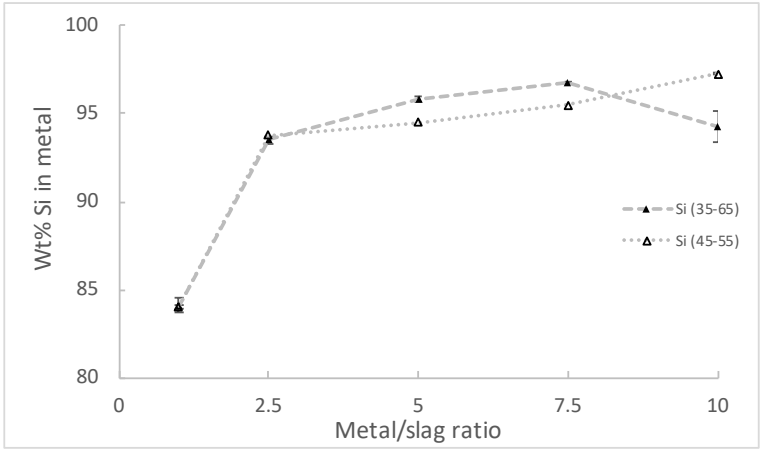

Figure 4.15: The concentration of Si in Si-metal equilibrated with 35-65 wt% CaO-Al_2O_3 and 45-55 wt% CaO-Al_2O_3 slags at 1650 °C.

Figure 4.15 shows the overall amount of Si in the silicon metal equilibrated with 35-65 wt% CaO-Al_2O_3 (CaO:Al_2O_3=0.54) and 45-55 wt% CaO-Al_2O_3 (CaO:Al_2O_3=0.82) as a function of the metal/slag ratio. The Si-content increases with increasing metal/slag ratio.

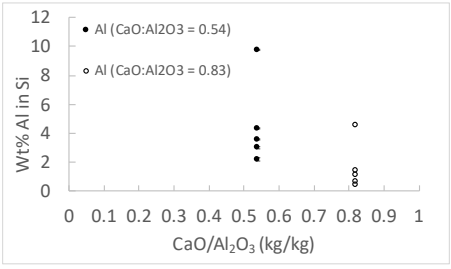

(a) The amount of Al as a function of CaO/Al_2O_3 ratio on start-slag.

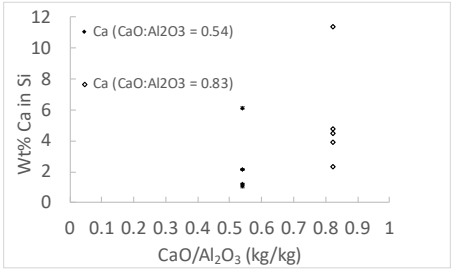

(b) The amount of Ca as a function of CaO/Al_2O_3 ratio on start-slag.

Figure 4.16: The concentrations of Al and Ca are plotted together with the CaO/Al_2O_3 ratio, to illustrate how the concentrations change with the ratio.

Figure 4.16 shows the concentrations of Al and Ca in silicon equilibrated with 35-65 wt% CaO-Al_2O_3 slags and 45-55 wt% CaO-Al_2O_3 slags as a function of the CaO/Al_2O_3 ratio in the starting slag. It is seen that the concentration of Al in the silicon decreases with increasing CaO/Al_2O_3 ratio, as opposed to the Ca concentration, which increases with increasing CaO/Al_2O_3 ratio. And figure 4.17 shows the CaO/Al_2O_3 ratio as a function of metal/slag ratio. The points in metal/slag ratio = 0 is the start compositions without metal.

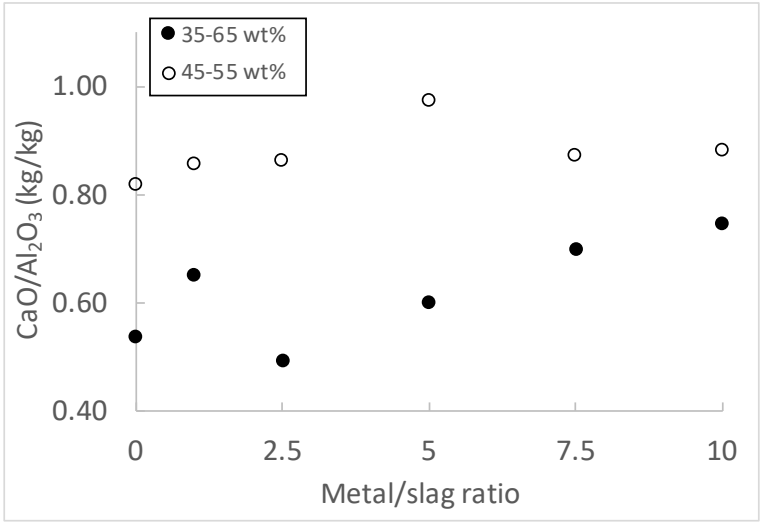

Figure 4.17: The CaO/Al_2O_3 ratio as a function of metal/slag ratio.

For the 35-65 wt% slag (full circle), higher reduction rates of Al_2O_3 to Al is observed, resulting in a higher CaO/Al_2O_3 ratio, which agrees well with the Al concentrations in the Si metal. For the 45-55 wt% slag, more CaO is reduced to Ca and dissolves into the Si metal, resulting in a lower CaO/Al_2O_3 ratio. After equilibration, the CaO/Al_2O_3 ratio remains relatively constant for all metal/slag ratios, with a slight increase for the 35-65 wt% slag.

Table 4.2: Compared concentrations of Si, Al, and Ca obtained concentrations from ICP-MS and calculated values from EPMA. All values are given in wt%.

	EPMA			**ICP-MS**		
Metal/slag ratio	**Si**	**Al**	**Ca**	**Si**	**Al**	**Ca**
35-65 wt%						
1/1	84.12	9.74	6.13	94.2	4.58	2.86
2.5/1	93.49	4.33	2.17	96.5	2.37	1.09
5/1	95.81	3.01	1.18	94.8	4.40	1.95
7.5/1	96.73	2.19	1.08	98.5	1.11	0.476
10/1	94.27	3.58	2.15	99.0	1.23	0.478
45-55 wt%						
1/1	84.04	4.57	11.39	91.0	4.44	6.05
2.5/1	93.79	1.42	4.79	89.1	4.35	5.84
5/1	94.48	1.07	4.45	96.0	1.71	1.52
7.5/1	95.48	0.61	3.91	97.0	0.893	0.967
10/1	97.27	0.38	2.35	98.1	1.33	1.22

Table 5.2 shows the ICP-MS results compared with the calculated concentrations from EPMA-analysis. For the Al and Ca concentrations in Si in equilibrium with 35-65 wt% CaO-Al_2O_3 slag, it is seen that the Ca and Al concentrations calculated from EPMA are somewhat higher, except for the Al concentration in the metal/slag ratio 5/1. However, the concentrations seem to be in relatively good agreement, besides from the concentrations in the metal/slag ratios of 1/1.

For the Al concentrations in Si in equilibrium with 45-55 wt% CaO-Al_2O_3 slag, the concentrations are in relatively good agreement, besides the higher Al concentration in the metal where the metal/slag ratio is 7.5/1 than 10/1 from ICP-MS, which is unexpected. The Ca concentrations calculated from EPMA are in general higher than the obtained concentrations from ICP-MS, besides from the concentration where the metal/slag ratio is 2.5/1, however, the concentrations at this point are close.

To summarise, the concentration of Al and Ca decreases with increasing metal/slag ratio and the SiO_2 concentration increases in the slag, while the concentration of Si increases. The concentration of Al decreases with increasing CaO/Al_2O_3 ratio, and the concentration of Ca increases with increasing CaO/Al_2O_3 ratio.

4.2.1 Composition of the Slags

The slag phases were analyzed with EPMA, and the values shown in the following graphs are mean values based on the EPMA- and image analysis.

Table 4.3: The initial and final compositions of the slags used in this thesis. The initial compositions are analyzed with XRF, while the final compositions are analyzed with EPMA, and together with image analysis, the overall composition is calculated. All values are given in wt%.

	Before			After		
Sample	**CaO**	**Al_2O_3**	**SiO_2**	**CaO**	**Al_2O_3**	**SiO_2**
35-65-24	34.16	64.55	0.31	35.14	53.83	11.03
35-65-60	34.16	64.55	0.31	29.90	60.28	9.83
35-65-120	34.16	64.55	0.31	32.86	54.48	12.66
35-65-180	34.16	64.55	0.31	32.83	46.78	20.40
35-65-240	34.16	64.55	0.31	31.18	41.74	27.08
45-55-24	45.61	52.68	0.37	39.52	46.06	13.52
45-55-60	45.61	52.68	0.37	38.95	45.13	17.22
45-55-120	45.61	52.68	0.37	37.37	38.37	24.26
45-55-180	45.61	52.68	0.37	37.44	42.86	20.48
45-55-240	45.61	52.68	0.37	34.64	39.31	26.05

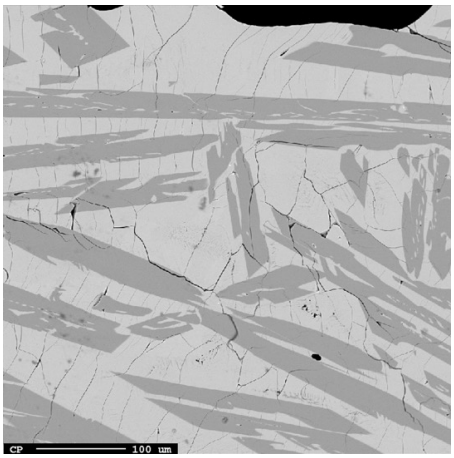

(a) Sample 35-65-24-2, imaged with 200x magnification, showing the phases present in the slag.

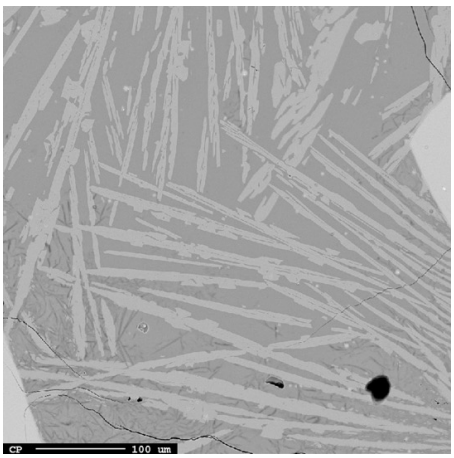

(b) Sample 35-65-24-2, imaged with 200x magnification, showing the phases present in the slag.

Figure 4.18: BSE images, showing the slag phases for the two extremes; metal/slag ratio 1/1 (a) and (b) 10/1.

Table 4.3 shows the initial and final slag compositions of the slags after all equilibrium experiments. The values are based on a mean value between two replicate splits and the mean value and area fraction between the light and dark phases present, as shown in figure 4.18. Figure 4.18 illustrates the representative phases present in the majority of slags. Where the phases where above $\sim$ 30 µm, the light and dark phase were measured individually with EPMA. Some slag phases were more fine in structure, and then, a defocused beam was used to analyze the composition of the slag, which gives and averaged composition.

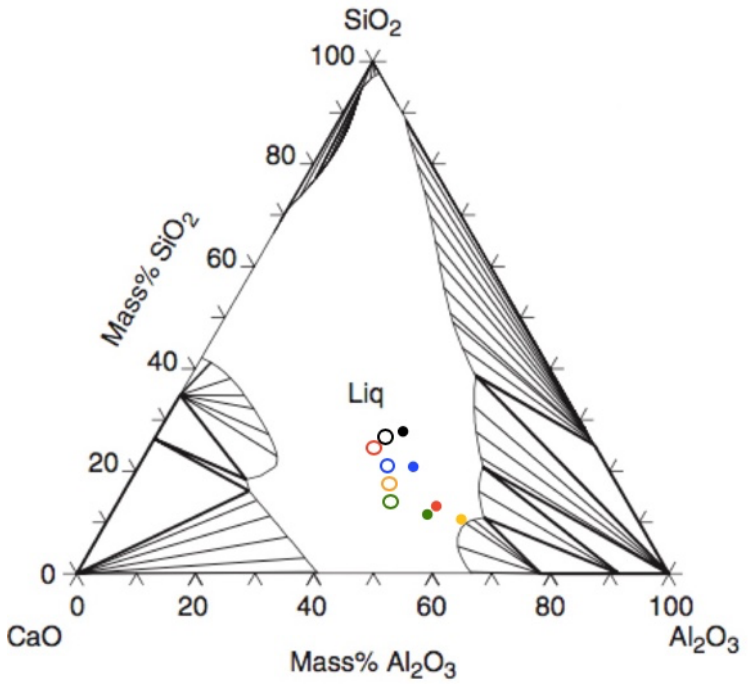

Figure 4.19: CaO-Al_2O_3-SiO_2 phase diagram at 1650 °C. [29] The composition of the 35-65 (open circle) and 45-55 (filled circle) wt% CaO-Al_2O_3 slag after the experiments, plotted in a ternary phase diagram for all metal/slag ratios. Green: 1/1, orange: 2.5/1, red: 5/1, blue: 7.5/1, black: 10/1. All values are given in wt%.

From figure 4.19, it is seen that the SiO_2 content in the slag increases with increasing metal/slag ratio in general, aside from the metal/slag ratio of 2.5/1 which have a lower SiO_2 concentration than 1/1. The Al_2O_3 concentration decreases with increasing metal/slag ratio and thus, increasing SiO_2 concentration, as well as the CaO concentration which also decreases with increasing metal/slag ratio and increasing SiO_2 concentration.

Almost the same goes for the slag compositions after equilibration with 45-55 wt% CaO-Al_2O_3 where it is seen that the SiO_2 content in the slag increases with increasing metal/slag ratio, except for the metal/slag ratio 7.5/1, which has lower SiO_2 concentration than 5/1. The Al_2O_3 and CaO concentration decreases with increasing metal/slag ratio and increasing SiO_2 concentration.

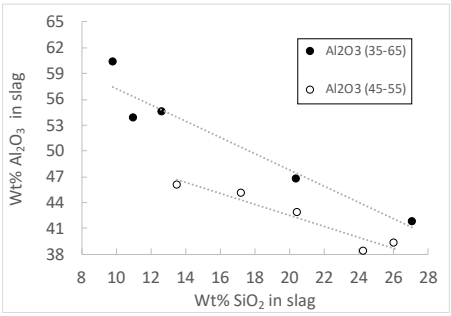

(a) Concentration of Al_2O_3 as a function of the concentration of the SiO_2 concentration after equilibrium with Si from both slag compositions.

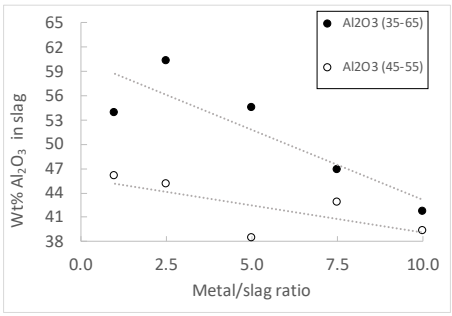

(b) Concentration of Al_2O_3 as a function of metal/slag ratio.

Figure 4.20: An illustration of the relation between the Al_2O_3 concentration, the SiO_2 concentration and the metal/slag ratio.

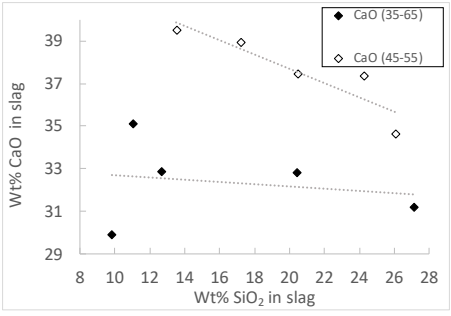

(a) Concentration of CaO as a function of the concentration of the SiO_2 concentration after equilibrium with Si from both slag compositions.

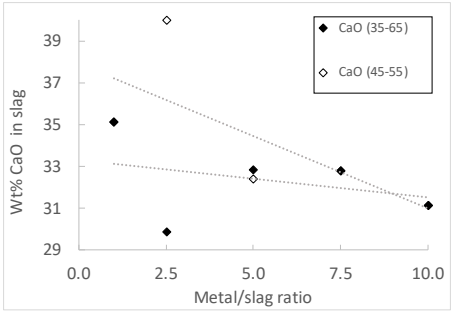

(b) Concentration of CaO as a function of metal/slag ratio.

Figure 4.21: An illustration of the relation between the CaO concentration, the SiO_2 concentration and the metal/slag ratio.

Figures 4.20 and 4.21 are included to emphasize the relation between the concentration of Al_2O_3, CaO and the metal/slag ratio and SiO_2. From these figures, it is clear that both the Al_2O_3 and CaO concentration both decreases with increasing metal/slag ratio and increasing SiO_2 concentration.

4.2.2 Phases Present in the Metal Equilibrated with 35-65 wt% and 45-55 wt% $CaO\text{-}Al_2O_3$ Slags

The metals from the experiments with the 35-65 $CaO\text{-}Al_2O_3$ slag had three prominent phases: a Si_2Al_2Ca phase, one Al-rich phase, and one Si-rich phase, which was the matrix. For the metal from the experiments with 45-55 $CaO\text{-}Al_2O_3$ slags, three phases were also present; a Si_2Ca phase, a Si_2Al_2Ca phase and a Si-rich phase, which was the matrix. Samples from all experiments were imaged with backscatter electrons. Only some of the images will be presented here, and the rest can be found in appendix B.1 and appendix B.2. Also, all values presented in the following figures are from the EPMA-analysis. All error bars indicate a 95 % confidence interval based on two replicate splits.

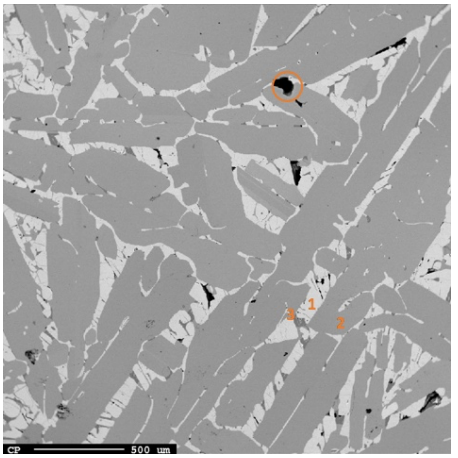

(a) Sample 35-65-2, imaged with 40x magnification, marked with 1, 2, 3 showing the phases present. The orange circle denotes a pore.

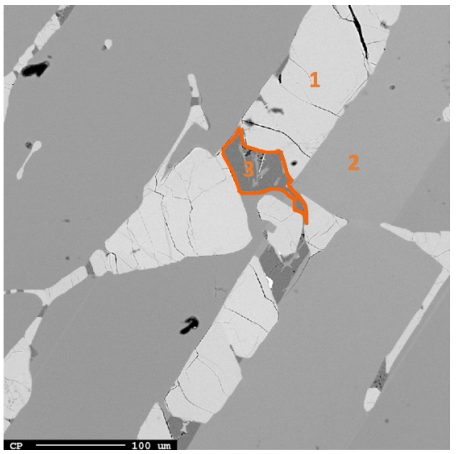

(b) Sample 35-65-24-2, imaged with 200x magnification, showing the present phases more clearly.

Figure 4.22: BSE images, showing an overview of the phases present at 40x and 200x for the sample 35-65-24-2, where the Al-rich phase has a red outline.

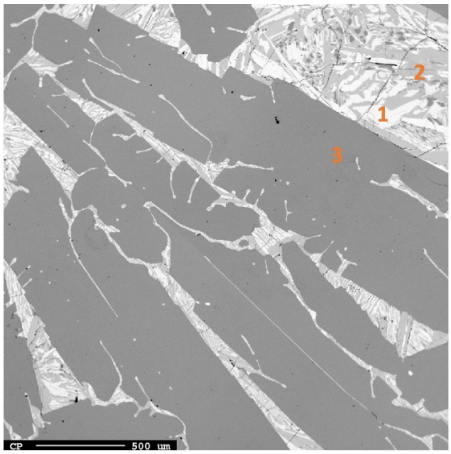

(a) Sample 45-55-24-2, imaged with 40x magnification, marked with points for the present phases.

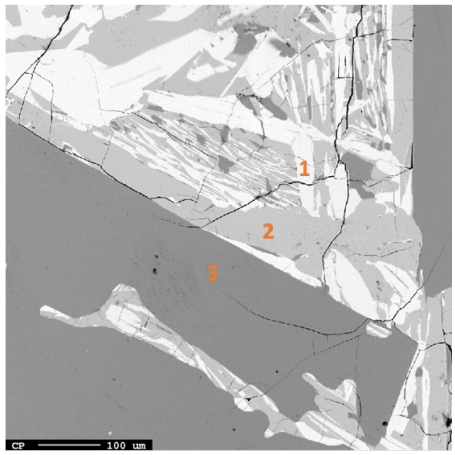

(b) Sample 45-55-24-2, imaged with 200x magnification, showing the present phases more clearly.

Figure 4.23: BSE images, showing an overview of the phases present at 40x and 200x for the samples 45-55-24-2.

Figure 4.22 and 4.23 shows the phases present in the metal from sample 35-65-24-2 and 45-55-24-2 (metal/slag ratio 1/1), and is an illustration of all phases present in the metal from both slag experiments. In figure 4.22, the points 1, 2, and 3 denotes the Si_2Al_2Ca phase, the Si-matrix and the Al-rich phase, respectively. In 4.23, the points 1, 2, and 3 denotes the Si_2Ca phase, the Si_2Al_2Ca phase and the Si-matrix.

Table 4.4: Composition of the Al-rich phase in the Si-metal equilibrated with 35-65 wt% CaO-Al_2O_3 slag.

Sample	Si	Al	Ca
35-65-24	1.95	97.70 ± 0.08	0.40
35-65-60	2.79	96.31 ± 0.22	0.23
35-65-120	2.63	97.23 ± 0.88	0.19
35-65-180	3.04	97.06 ± 0.14	0.14
35-65-240	2.04	98.27 ± 0.24	0.19

Table 4.4 shows the composition of the Al-rich phase in the Si-metal equilibrated with 35-65 wt% CaO-Al_2O_3 slag. The concentration of Al in this phase is relatively constant at 96-98 wt% Al, with traces of Si and Ca.

Table 4.5: Composition of the mixed phase (Si_2Al_2Ca) in the metal from the experiments performed with 35-65 CaO-Al_2O_3 slag (point 1 in figure 4.22).

Sample	Si	Al	Ca
35-65-24	37.78 ± 0.13	36.30 ± 0.16	26.57 ± 0.21
35-65-60	38.59 ± 0.04	36.28 ± 0.08	26.90 ± 0.05
35-65-120	38.27 ± 0.20	36.40 ± 0.04	26.96 ± 0.18
35-65-180	38.38 ± 0.29	36.26 ± 0.23	26.55 ±0.13
35-65-240	38.49 ± 0.21	36.04 ± 0.25	26.81 ± 0.25

Table 4.6: Composition of the mixed phase (Si_2Al_2Ca) in the metal from the experiments performed with 45-55 CaO-Al_2O_3 slag (point 2 in figure 4.23).

Sample	Si	Al	Ca
45-55-24	37.08 ± 0.50	35.91 ± 0.22	27.02 ± 0.14
45-55-60	37.79	36.16	26.79
45-55-120	38.66	35.99	27.24
45-55-180	39.23	35.61	27.21
45-55-240	38.50 ± 0.35	35.92 ± 0.15	26.85 ± 0.15

Table 4.7: Composition of the Si_2Ca phase in the metal from the experiments performed with 45-55 CaO-Al_2O_3 slag (point 1 in figure 4.23).

Sample	Si	Al	Ca
45-55-24	57.99 ± 0.30	0.88 ± 0.09	41.92 ± 0.30
45-55-60	57.16	0.97	41.90
45-55-120	58.17	1.03	42.13
45-55-180	58.44	1.04	41.89
45-55-240	57.83 ±0.23	1.13 ± 0.23	41.48 ± 0.28

Table 4.5 and table 4.6 shows the composition of the Si_2Al_2Ca phase present in the metals from 35-65 wt% CaO-Al_2O_3 and the 45-55 wt% CaO-Al_2O_3 experiments. It is clear that the composition of the Si_2Al_2Ca phase is independent of metal/slag ratio for both slag compositions. Also, the same goes for the Si_2Ca phase in the metal from 45-55 wt% slag series; the composition of the phase is relatively independent of the metal/slag ratio.

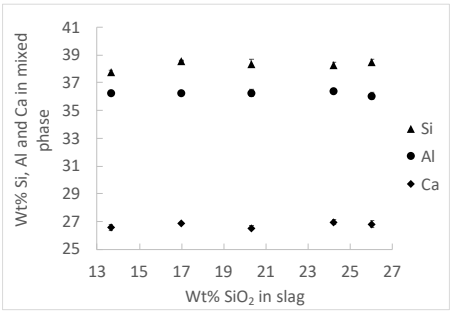

(a) The concentration of Si, Al and Ca in Si_2Al_2Ca phase in the metal equilibrated with 35-65 wt% CaO-Al_2O_3 slag as a function of the SiO_2 concentration in the equilibrated slag.

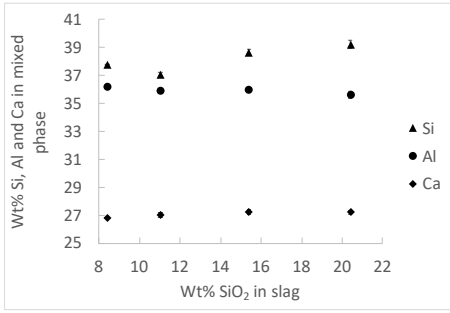

(b) The concentration of Si, Al and Ca in the Si_2Al_2Ca phase in the metal equilibrated with 45-55 wt% CaO-Al_2O_3 slag as a function of the SiO_2 concentration in the equilibrated slag.

Figure 4.24: Comparison of the mixed phases in both metal series as a function of the SiO_2 concentration in both equilibrated slags.

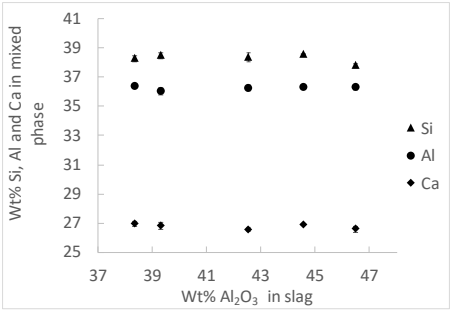

(a) The concentration of Si, Al and Ca in the Si_2Al_2Ca phase in the metal equilibrated with 35-65 wt% CaO-Al_2O_3 slag as a function of the Al_2O_3 concentration in the equilibrated slag.

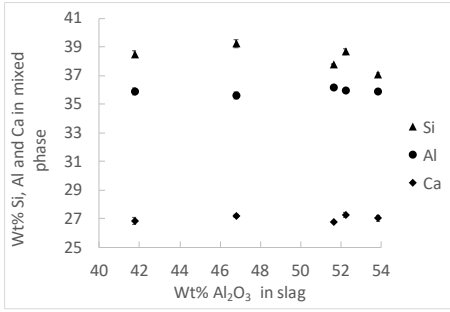

(b) The concentration of Si, Al and Ca in the Si_2Al_2Ca phase in the metal equilibrated with 45-55 wt% CaO-Al_2O_3 slag as a function of the Al_2O_3 concentration in the equilibrated slag.

Figure 4.25: Comparison of the Si_2Al_2Ca phase in both metal series as a function of the Al_2O_3 concentration in both equilibrated slags.

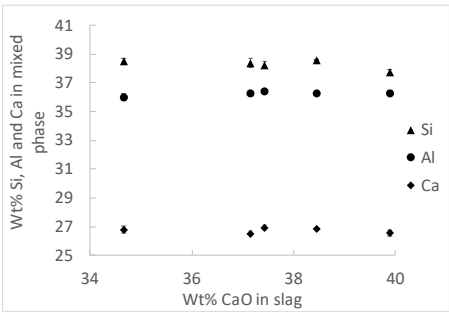

(a) The concentration of Si, Al and Ca in the Si_2Al_2Ca phase in the metal equilibrated with 35-65 wt% CaO-Al_2O_3 slag as a function of the CaO concentration in the equilibrated slag.

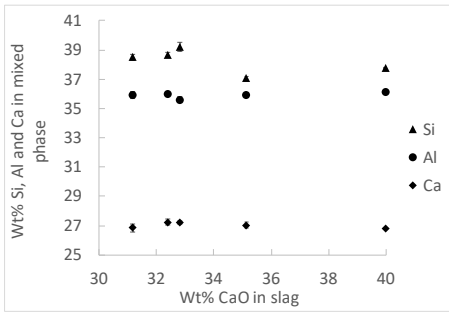

(b) The concentration of Si, Al and Ca in the Si_2Al_2Ca phase in the metal equilibrated with 45-55 wt% CaO-Al_2O_3 slag as a function of the CaO concentration in the equilibrated slag.

Figure 4.26: Comparison of the mixed phases (Si_2Al_2Ca) in both metal series as a function of the CaO concentration in both equilibrated slags.

As seen from figure 4.24, 4.25 and 4.26, the amount of Si, Al and Ca in the Si-Al-Ca-rich phase in the metal from both series does not change significantly with increasing SiO_2, Al_2O_3 or CaO-content in the equilibrated slags.

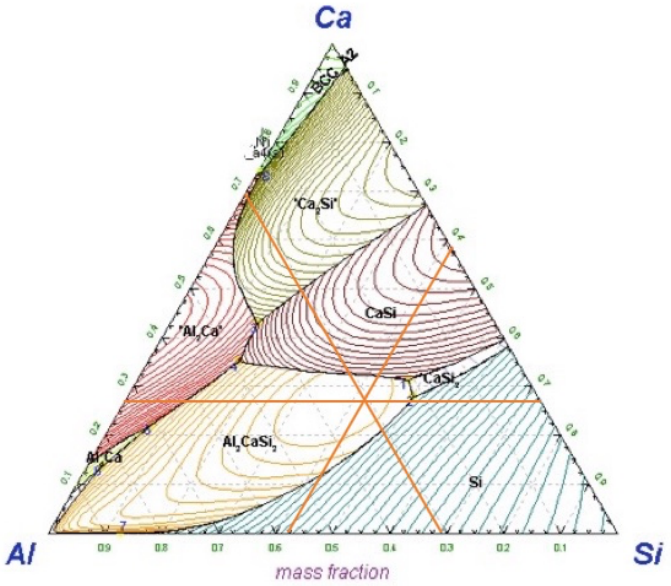

Figure 4.27: The Si-Al-Ca phase diagram with the marked composition of both the Si_2Al_2Ca phases in the metal from both slag experiments.

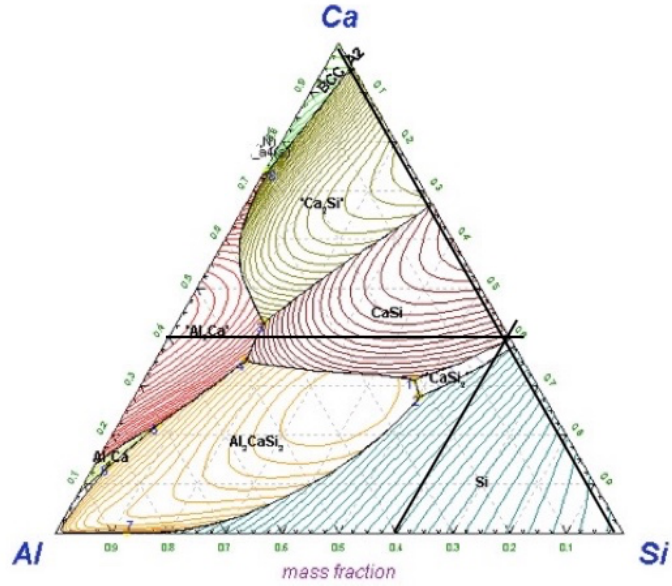

Figure 4.28: The Si-Al-Ca phase diagram with the marked composition of the Si_2Ca phase.

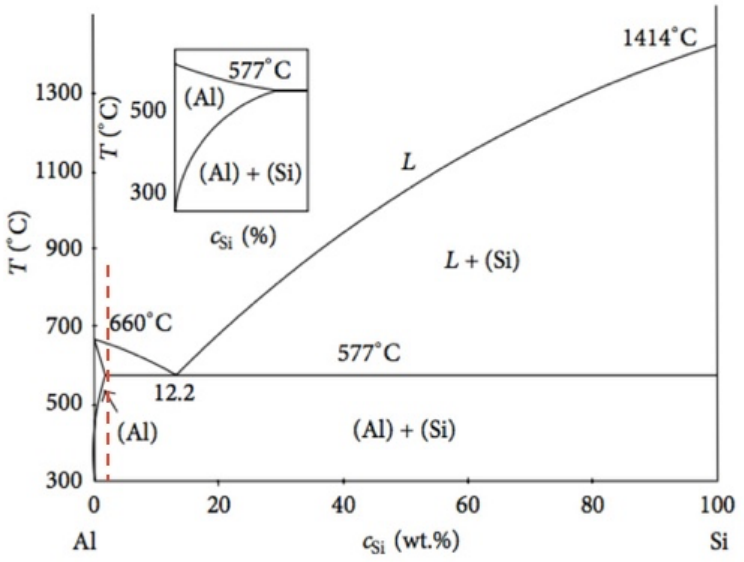

Figure 4.29: Marked composition of the Al-rich phase in the Si metal equilibrated with 35-65 wt% CaO-Al_2O_3 slag. [23]

Figure 4.27 shows the approximate marked composition of the mixed phase (Si_2Al_2Ca) phase present for both the metal from 35-65 wt% CaO-Al_2O_3 and 45-55 CaO-Al_2O_3 from the compositions listed in table 4.5 and 4.6. It is seen that the composition when assuming about 40 wt% Si, 35 wt% Al and 25 wt% Ca will be the Si_2Al_2Ca phase, which agrees well with the modeled results (see section 4.3.1). Figure 4.28 shows the approximate marked composition of the Si-Ca rich phase in the Si-Al-Ca phase diagram, when assuming about 60 wt% Si, and 40 wt% Ca. The theoretical composition is the just above the phase line between the SiCa and Si_2Ca, however, the modeled results shows that this is the Si_2Ca phase.

In figure 4.29, the composition of the Al-rich phase is marked, and at room temperature, it is seen that there will be an Al-Si phase which mainly composes of ∼97.5 wt% Al, with ∼ 2.5 wt% Si, and in the present case, traces of Ca.

In addtition to the phases presented here, one Si-rich phases (the matrix) were present in both metals equilibrated with 35-65 wt% CaO-Al_2O_3 slag (point 2 in figure 4.22) and with 45-55 wt% CaO-Al_2O_3 (point 3 in figure 4.23). The concentration of both these phases were ∼ 100 wt% Si.

4.2.3 Phases Present in $CaO-Al_2O_3$ Slags Equilibrated with Si

Phases in the slags were identified where the structure was bigger than 30 µm. After equilibration in the 35-65 wt% slag series, two phases were present in each slag sample, and figure 4.32 shows the compositions of the phases present. The grey and black points were observed in the 35-65 wt% slag series, while the red and blue points were observed in the 45-55 wt% slag series. As seen in figure 4.30 and 4.31, the phases are generally bigger in the 35-65 wt% slag series (imaged at 40x versus 200x images in the 45-55 wt% slag series). Therefore, most of the EPMA analysis in the 45-55 wt% slag series is done

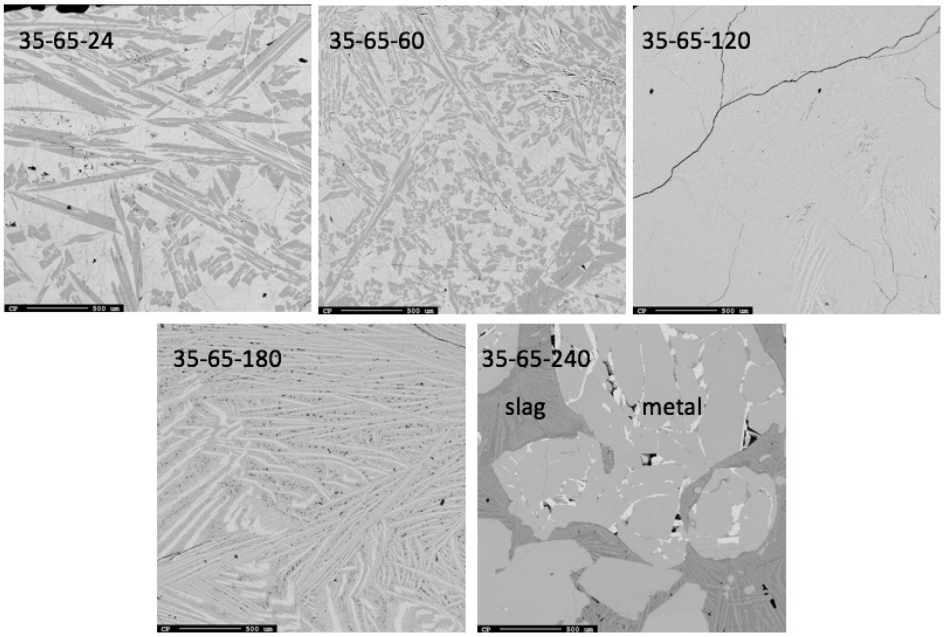

Figure 4.30: BSE images of the slags from all experiments in the 35-65 wt% $CaO-Al_2O_3$ slag series, taken at 40x magnification.

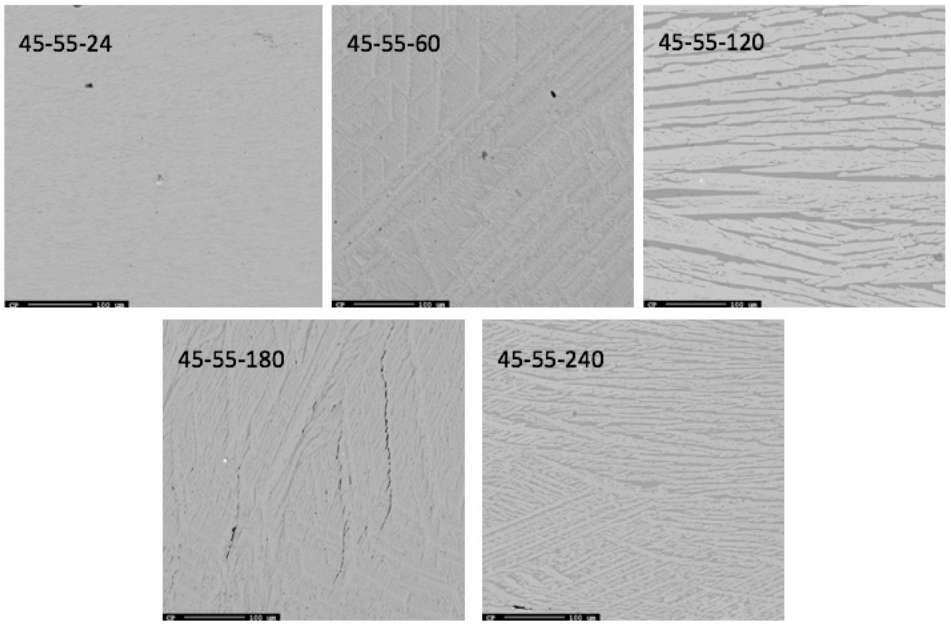

Figure 4.31: BSE images of the slags from all experiments in the 45-55 wt% CaO-Al_2O_3 slag series, taken at 200x magnification.

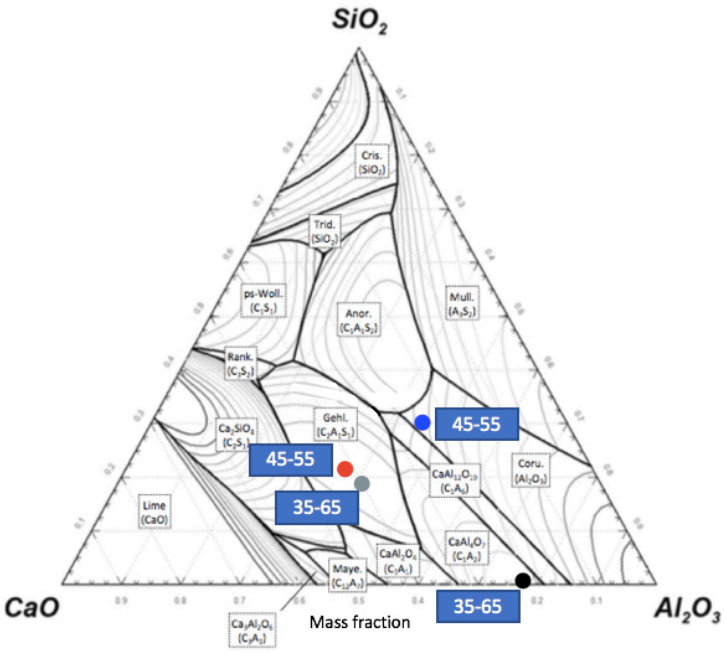

Figure 4.32: Marked phases in the slags after equilibration where the grey circle is the 40-40-20 wt% CaO-Al_2O_3-SiO_2, the black circle is approximately 22-75-1 wt%, CaO-Al_2O_3-SiO_2, the red circle is 41-36-22 wt%, CaO-Al_2O_3-SiO_2 and the blue circle is 24-44-30 wt% CaO-Al_2O_3-SiO_2.

Table 4.8: Averaged composition the slags after equilibration with Si metal calculated from EPMA analysis.

Slag	CaO	Al_2O_3	SiO_2	Phase in BSE image	Point (figure 4.32)	Estimated phase
35-65 wt%	22	75	1	Light	Black	$CaAl_4O_7$
	40	40	20	Dark	Grey	$Ca_2Al_2SiO_7$
45-55 wt%	41	36	22	Light	Red	$Ca_2Al_2SiO_7$
	24	44	30	Dark	Blue	Al_2O_3*

Both the red and grey point is in the gehlenite/melilite phase ($Ca_2Al_2SiO_7$). If looking at the modeled results in the next section, it seems more reasonable that the $CaAl_4O_7$ actually is the $CaAl_{12}O_{19}$ phase, as this is where the point would be if not taking the SiO_2 concentration into account, which is less than 1 wt%. The blue point is in the Al_2O_3 phase area, while the chemical composition of the actual phase is 24-44-30 wt%, CaO-Al_2O_3-

SiO_2, which makes it more reasonable that the phase is anorthite ($CaAl_2Si_2O_8$).

4.3 Thermodynamic Modelling

Solidification calculations in FactSage were performed by Kai Erik Ekstrøm, and the databases used were FSstel 7.3, FToxid 7.3, FactPS 7.3. The solidification calculations were done both assuming equilibrium cooling and Scheil-Gulliver cooling. The results obtained from both cooling mechanisms were almost identical for the metals, and the Scheil-Gulliver cooling mechanism was chosen.

4.3.1 Solidification Calculations for the Metals

The phases in the metals, calculated with FactSage will be shown in this section.

Table 4.9: Overview of the phases present in the metal equilibrated with the 35-65 wt% CaO-Al_2O_3 slag calculated with FactSage assuming Scheil-Gulliver cooling. All values are given in wt%.

Sample	**Si**	**Si_2Ca**	**Si_2Al_2Ca**	**Al (fcc)**
35-65-24	83.00	4.56	12.42	0
35-65-60	90.92	0.79	8.26	0
35-65-120	94.63	0	5.18	0.15
35-65-180	96.09	0	3.59	0.27
35-65-240	96.89	0	2.76	0.30

From table 4.9, it is seen that there will be four phases present in the metals equilibrated with the 35-65 CaO-Al_2O_3 slag. The amount of the Si-phase in the metal will increase with increasing metal/slag ratio, while the amount of the Si_2Al_2Ca phase decreases. When it comes to the Si_2Ca phase, it is only present at the samples 35-65-24 and 35-65-60 (a metal slag ratio of 1/1 and 2.5/1, respectively), and decreases when increasing the metal/slag ratio. At sample 35-65-120 (metal/slag ratio = 5/1), the phase disappears, and the Al phase gets introduced. From sample 35-65-120 to 35-65-240, the amount of the Al-phase increases.

Table 4.10: Overview of the phases present in the metal equilibrated with the 45-55 wt% CaO-Al_2O_3 slag calculated with FactSage assuming Scheil-Gulliver cooling. All values are given in wt%.

Sample	Si	Si_2Ca	Si_2Al_2Ca
45-55-24	74.00	14.00	12.00
45-55-60	86.76	5.57	7.64
45-55-120	92.46	2.49	5.02
45-55-180	94.62	1.51	3.83
45-55-240	95.77	1.05	3.13

From table 4.10 it is seen that there are three phases present in the Si-metal equilibrated with the 45-55 wt% CaO-Al_2O_3 slag. The amount of the Si phase decreases with increasing metal/slag ratio and is present at all metal/slag ratios. Also, the Si_2Ca phase is present at all metal/slag ratios and decreases with increasing metal/slag ratio. The same goes for the Si_2Al_2Ca phase, which is present at all metal/slag ratios and decreases with increasing metal/slag ratio.

4.3.2 Solidification Calculations for the Slags

The phases present in the slags after equilibrium with silicon will be presented here. The ”melilite” phase consists of 50 wt% $Ca_2Al_3O_7$ and 50 wt% Ca_2AlSiO_7.

Table 4.11: Overview of the present phases in the slag after equilibrium with Si metal, calculated with FactSage assuming equilibrium cooling. The final disappearance of all liquid is at 1391.94 °C for all samples. All values are given in wt%.

Sample	Melilite	$CaAl_4O_7$	$CaAl_{12}O_{19}$	$CaAl_2Si_2O_8$ (anorthite)
35-65-24	56.80	13.83	29.37	0
35-65-60	53.04	0	30.70	16.26
35-65-120	45.78	0	22.05	32.18
35-65-180	41.64	0	16.61	41.75
35-65-240	38.66	0	12.64	48.70

Table 4.12: Overview of the present phases in the slag after equilibrium with Si metal, calculated with FactSage assuming Scheil-Gulliver cooling. The final disappearance of all liquid is at 1442.81 °C for sample 36-65-24 and 1391.94 for the remaining samples. All values are given in wt%.

Sample	Melilite	$CaAl_4O_7$	$CaAl_{12}O_{19}$	$CaAl_2Si_2O_8$ (anorthite)
35-65-24	38.71	50.27*	1.83	9.18
35-65-60	53.04	0	30.70	16.26
35-65-120	45.78	0	22.05	32.18
35-65-180	41.64	0	16.61	41.75
35-65-240	38.66	0	12.64	48.70

Table 4.11 and 4.12 shows the phases present in the 35-65 wt% CaO-Al_2O_3 slag after equilibrated with Si-metal. Here, both the composition assuming equilibrium cooling and Scheil-Gulliver cooling because the obtained phases and values are different. When assuming equilibrium cooling, it is seen that the amount of the melilite phase, the $CaAl_{12}O_{19}$ phase decreases with increasing metal/slag ratio, while the amount of the Si-containing $CaAl_2Si_2O_8$ phase increases with increasing metal/slag ratio.

When considering Scheil-Gulliver cooling, there is no specific trend considering increases or decreases in the number of phases present in the slag.

The final disappearance of all liquid is at 1442.81 °C for sample 35-65-24 and 1391.94 °C for the remaining samples.

Table 4.13: Overview of the present phases in the 45-55 wt% slag after equilibrium with Si metal, calculated with FactSage assuming equilibrium cooling. All values are given in wt%.

Sample	Melilite	$CaAl_4O_7$	$CaAl_{12}O_{19}$	$CaAl_2Si_2O_8$ (anorthite)	$CaSiO_3$
45-55-24	72.98	20.96	6.06	0	0
45-55-60	69.75	0	13.97	16.28	0
45-55-120	61.27	0	6.92	31.81	0
45-55-180	56.56	0	2.57	40.86	0
45-55-240	52.36	0	0	46.79	0.86

Table 4.14: Overview of the present phases in the 45-55 wt% slag after equilibrium with Si metal, calculated with FactSage assuming Scheil-Gulliver cooling. The final disappearance of all liquid is at 1442.81 °C for sample 45-55-24 and 1391.94 °C for the remaining samples. All values are given in wt%.

Sample	**Melilite**	**$CaAl_4O_7$**	**$CaAl_{12}O_{19}$**	**$CaAl_2Si_2O_8$ (anorthite)**	**$CaSiO_3$**
45-55-24	69.25	28.48	0.38	1.89	0
45-55-60	63.15	13.30	3.92	19.63	0
45-55-120	60.92	0.70	6.39	31.99	0
45-55-180	56.56	0	2.57	40.86	0
45-55-240	52.36	0	0	46.79	0.86

Table 4.13 and 4.14 shows the phases present in the 45-55 wt% CaO-Al_2O_3 slag after equilibrated with Si metal. Here, both the composition assuming equilibrium cooling and Scheil-Gulliver cooling are included because the obtained phases and values are different. When assuming equilibrium cooling, it is seen that the amount of the melilite phase decreases with increasing metal/slag ratio, while the Al-rich $CaAl_4O_7$ phase is only present at a metal/slag ratio of 1. There is no specific trend when considering the $CaAl_{12}O_{19}$ phase. However, the amount of the Si-rich $CaAl_2Si_2O_8$ phase increases with increasing metal/slag ratio, and hence, increasing Si content in the melt. Traces of the Al free phase, $CaSiO_2$ is only present at a metal/slag ratio of 10.

The final disappearance of all liquid is at 1442.81 °C for sample 45-55-24 and 1391.94 °C for sample 45-55-60, 45-55-120, and 45-55-180, and 1257.43 °C for sample 45-55-240.

When considering Scheil-Gulliver cooling, the amount of the melilite phase decreases with increasing metal/slag ratio and the $CaAl_4O_7$ phase, until disappearance when reaching a metal/slag ratio of 7.5. The $CaAl_{12}O_{19}$ phase shows no specific trend. And also, here, the amount of the Si-rich $CaAl_2Si_2O_8$ phase increases with increasing metal/slag ratio. Traces of the Al-free $CaSiO_3$ phase is only present at the 10/1 metal/slag ratio.

4.4 Calculation of the Amount of phases (ImageJ)

The area fractions of the phases in the metal and slag samples were calculated using ImageJ by thresholding. Also, here, the error bars indicate a 95 % confidence interval calculated when two parallels were analyzed in ImageJ. However, all measurements do not have two parallels, and hence, no error bars. Some error bars are very small, and almost not visible in the graphical presentations.

4.4.1 Metals Equilibrated with 35-65 CaO-Al_2O_3 Slag

Three phases were clearly visible when imaging with backscatter electrons in the metal. However, the smallest phase with mainly aluminum was too small to differentiate with ImageJ. Therefore, only the area fraction (assumed equal to the volume fraction) of the Si_2Al_2Ca phase (white phase) was calculated. The area fraction of "the rest" was calculated by subtracting the amount of the Si_2Al_2Ca from 100 %. All binary images for the metal equilibrated with 35-65 wt% CaO-Al_2O_3 slag can be found in appendix C.1.

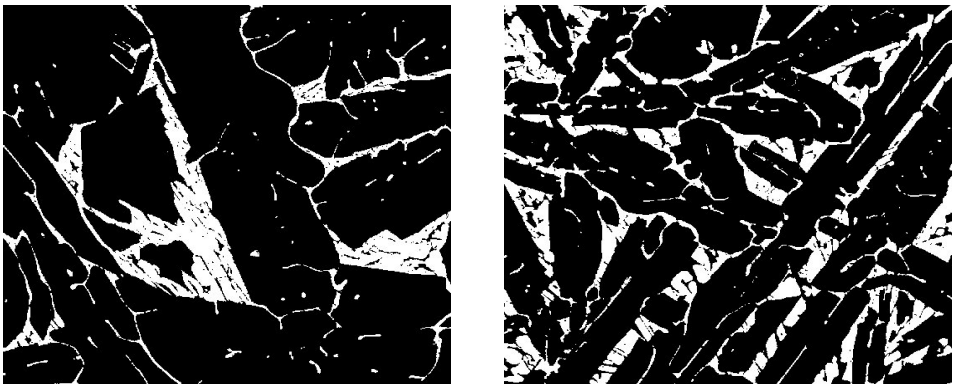

(a) Total area of the Si_2Al_2Ca phase in the metal from sample 35-65-24-1. The image is taken at 40x.

(b) Total area of only the Si_2Al_2Ca phase in the metal from sample 35-65-2. The image is taken at 40x.

Figure 4.33: Total area of Si_2Al_2Ca phase in sample 35-65-24-1 and 35-65-24-2.

Figure 4.33 is shown as an illustration of how all phases in all samples were calculated in ImageJ. The measured area is the white area in the pictures.

Table 4.15: Area fractions calculated by thresholding for all metal samples in the 35-65 wt% CaO-Al_2O_3 slag series.

Metal/slag ratio	Si_2Al_2Ca [%]	Si-matrix [%]
1	16.44 ± 4.72	83.56 ± 4.72
2.5	5.53 ± 2.16	94.47 ± 2.16
5	2.92 ± 1.04	97.08 ± 1.04
7.5	2.71 ± 0.99	97.29 ± 0.99
10	5.62 ± 4.13	97.35 ± 4.13

Table 4.15 shows averaged values of all measured area fractions for the metal samples. The light phase is the mixed, Si_2Al_2Ca phase, and the dark is the Si-matrix. It is worth mentioning that sample 45-55-240-2 (metal/slag ratio=10) is measured very close to the slag phase as opposed to the other samples, giving a higher value than expected of the amount of the light phase, hence, the significant deviation.

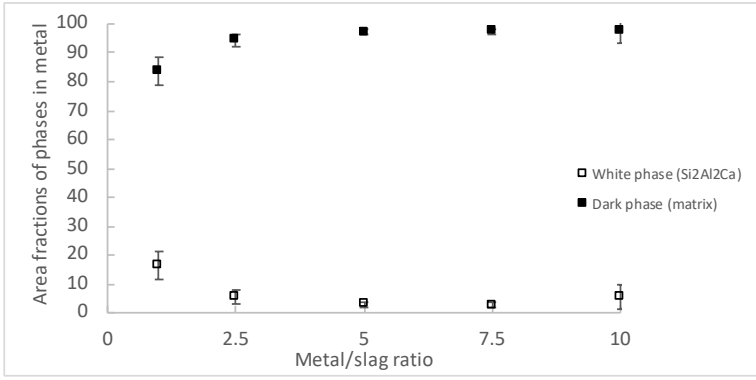

Figure 4.34: Calculated area fractions of the Si_2Al_2Ca (white) phase and the Si-matrix (dark phase) in the metal from 35-65 wt% CaO-Al_2O_3 experiments.

Figure 4.34 shows the amount of Si_2Al_2Ca phase (white phase) and the Si-matrix (dark phase) as a function of metal/slag ratio from the experiments with 35-65 wt% CaO-Al_2O_3 slag. There is a decrease in the amount of the Si_2Al_2Ca phase, and an increase in the Si-matrix when increasing the metal/slag ratio.

4.4.2 Metals Equilibrated with 45-55 CaO-Al_2O_3 Slag

In the metal from the experiments with 45-55 CaO-Al_2O_3 slag, it was possible to differentiate the three phases in ImageJ. First, the total area of the light-grey (Si_2Al_2Ca) phase and

the white phase (Si_2Ca) was calculated together, then only the white phase was calculated. To find the total area of the Si_2Al_2Ca phase, the area of the Si_2Ca phase was subtracted from the area of the Si_2Al_2Ca + Si_2Ca phase (light-grey phase + white in BSE images). All binary images for the metal equilibrated with 35-65 wt% CaO-Al_2O_3 slag can be found in appendix C.2.

(a) Total area of the Si_2Ca and Si_2Al_2Ca phase in the metal from sample 45-55-24-1. The image is taken at 40x.

(b) Total area of only the white phase in the metal from sample 45-55-24-1. The image is taken at 40x.

Figure 4.35: Total area of white + light-grey phase (a) and only the white phase (b).

Figure 4.35 shows the binary picture for the measured areas. The white areas in a) shows the total area for both the Si_2Al_2Ca phase and Si_2Ca phase in sample 45-55-24-1, and b) shows the total area of only the Si_2Ca phase.

Table 4.16: Area fractions calculated by thresholding for the metal from 45-55 CaO-Al_2O_3 experiments.

Metal/slag ratio	**Si_2Al_2Ca [%]**	**Si_2Ca [%]**	**Si-matrix [%]**
1	8.65 ± 1.92	13.60 ± 1.17	77.75 ± 3.09
2.5	2.49	6.17	91.34
5	1.87	6.01	92.13
7.5	0.995	5.73	93.28
10	0.60 ± 0.35	3.43 ± 0.82	95.97 ± 1.17

Table 4.16 shows averaged values of all measured area fractions for the metal samples.

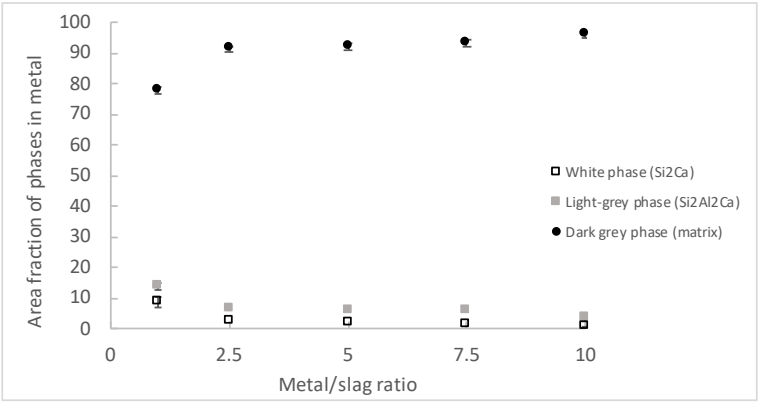

Figure 4.36: Calculated area fractions of the Si_2Ca (white) phase, Si_2Al_2Ca (light-grey) phase and the Si-matrix (dark phase) in the metal from 45-55 $CaO\text{-}Al_2O_3$ experiments.

Figure 4.36 shows the amount of Si_2Ca phase, the Si_2Al_2Ca phase and the Si-matrix as a function of metal/slag ratio from the experiments with 45-55 wt% $CaO\text{-}Al_2O_3$ slag. There is a decrease of the amount of the Si_2Ca phase and the Si_2Al_2Ca phase, and an increase of the amount of the Si-matrix when increasing the metal/slag ratio.

Chapter 5

Discussion

This chapter will discuss results from the previous chapter and be compared with other relevant works and thermodynamic modeled data. First, important points regarding the preparation of the slags will be discussed, then the distribution of Al and Ca between Si in equilibrium with the slags will be discussed, and the activity coefficients of Al and Ca in Si will be calculated. Then, the effect of equilibrium time will be discussed. The phases present in the metal and the slag will also be discussed, with the main focus being the phases in the metals. Lastly, an evaluation of the experimental set-up will be done, together with a consideration of the reproducibility of the results obtained in the present work.

5.1 Important Points Regarding the Preparation of Slags

The target compositions and the measured analyzed slag samples were significantly different. The target compositions were:

- 45-55 wt% CaO-Al_2O_3
- 55-45 wt% CaO-Al_2O_3

For preparing the 45-55 wt% CaO-Al_2O_3 slag, 900 grams of CaO and 1100 grams of Al_2O_3 were mixed, and for preparing the 55-45 wt% CaO-Al_2O_3 slag, 1100 grams of CaO and 900 grams of Al_2O_3 were mixed. During the preparation of the slags, it was seen that a lot of gas was exhausted from the mixture, as the gas was accumulated in the middle of

the powder mixture, and stirring had to be done to avoid gas explosions. There are two possibilities of what happened with the CaO; either, the CaO had reacted with moisture or CO_2 in the air prior to melting, which could either have caused dehydration or calcination when the temperature was increased:

$$\mathrm{Ca(OH)_2} \longrightarrow \mathrm{CaO} + \mathrm{H_2O} \tag{5.1}$$

Eq. (5.1) is an exothermic reaction above $\sim$ 825 °C, and as the CaO dehydrates, the powder will "puff up," and leave the crucible.

The calcination will go by the following reaction, which also will lead to CaO leaving the crucible:

$$\mathrm{CaCO_3} \longrightarrow \mathrm{CaO} + \mathrm{CO_2} \tag{5.2}$$

The slags were analyzed with XRF and EPMA, and analysis gave similar results, as showed in table 5.1. As seen from the table, the obtained CaO concentrations are much lower than the targeted ones, and the highest loss of CaO are observed from "slag 1", where the targeted composition was 45-55 wt% CaO-Al_2O_3. For simplicity, it was therefore decided to change the referring and naming of the slags, whereas, the 45-55 wt% CaO-Al_2O_3 slag was renamed to 35-65 wt% CaO-Al_2O_3 and the 55-45 wt% CaO-Al_2O_3 was renamed to 45-55 wt% CaO-Al_2O_3

Table 5.1: Measured initial slag compositions, by XRF and EPMA. "Slag 1" is the targeted 45-55 wt% CaO-Al_2O_3 slag, and "slag 2" is the targeted 55-45 wt% CaO-Al_2O_3.

	Slag 1			**Slag 2**		
	SiO_2	**CaO**	**Al_2O_3**	**SiO_2**	**CaO**	**Al_2O_3**
XRF	0.31	34.16	64.55	0.37	41.61	52.68
EPMA	0	35.9	65.5	0	49.1	52.7

5.2 Distribution of Al and Ca Between Si and CaO-Al_2O_3 Slags

5.2.1 Effect of Metal/Slag Ratio

As expected, the concentration of Al and Ca decreases with increasing metal/slag ratio for both slag compositions in general. The Al and Ca concentrations are generally high in Si when equilibrating with CaO-Al_2O_3 slags, with the highest Al and Ca concentrations in the silicon equilibrated with 35-65 wt% CaO-Al_2O_3 slag being 9.74 wt% and 6.13 wt% Ca, respectively. For the Si metal equilibrated with 45-55 wt% CaO-Al_2O_3 slag, the highest Al and Ca concentrations were 4.57 wt% and 11.39 wt%, respectively. Both of these highest concentrations were obtained in the experiments where the metal/slag ratio was 1/1. All values presented in the following discussion are based on EPMA analysis and image analysis. ICP-MS was also conducted on the metal samples, and these results will be compared with the results from EPMA.

Table 5.2: Compared concentrations of Si, Al, and Ca obtained concentrations from ICP-MS and calculated values from EPMA. All values are given in wt%.

	EPMA			ICP-MS		
Metal/slag ratio	**Si**	**Al**	**Ca**	**Si**	**Al**	**Ca**
35-65 wt%						
1/1	84.12	9.74	6.13	94.2	4.58	2.86
2.5/1	93.49	4.33	2.17	96.5	2.37	1.09
5/1	95.81	3.01	1.18	94.8	4.40	1.95
7.5/1	96.73	2.19	1.08	98.5	1.11	0.476
10/1	94.27	3.58	2.15	99.0	1.23	0.478
45-55 wt%						
1/1	84.04	4.57	11.39	91.0	4.44	6.05
2.5/1	93.79	1.42	4.79	89.1	4.35	5.84
5/1	94.48	1.07	4.45	96.0	1.71	1.52
7.5/1	95.48	0.61	3.91	97.0	0.893	0.967
10/1	97.27	0.38	2.35	98.1	1.33	1.22

However, as seen in table 5.2, the Al and Ca concentrations on Si in equilibrium with 35-65 wt% CaO-Al_2O_3 slag calculated from EPMA analysis are somewhat higher than the ones obtained from ICP-MS. With the most considerable differences being in the 1/1 metal slag ratios. For the Al concentrations in the metals from the 45-55 wt% slag series, the results are in relatively good agreement, except where a slightly higher Al concentration is observed in 7.5/1 from EPMA compared to the measures concentration in 10/1 from ICP-

MS analysis. The Ca concentrations calculated from EPMA are higher in general besides, the sample where the metal/slag ratio is 2.5/1; however, the values are close.

The metal/slag ratio was varied from 1/1 to 10/1 for getting an (ideally) straight line across compositions in the lower part of the CaO-Al_2O_3-SiO_2 phase diagram. The most representative work to compare the results in this study, is the work by Morita et al. [61] who investigated the equilibrium between Si and CaO-Al_2O_3-SiO_2 slag system in the whole liquid region at 1550 °C.

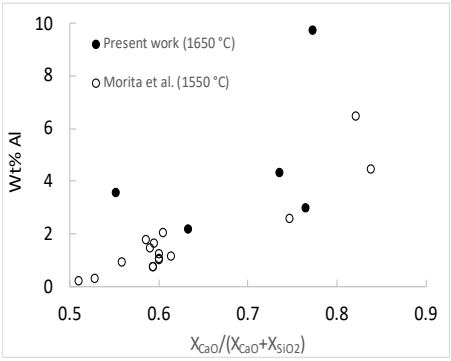

(a) The relation between wt% Al in Si in equilibrium with 45-55 wt% CaO-Al_2O_3 slag and $X_{CaO}/(X_{CaO} + X_{SiO_2})$, compared with data from Morita et al. (2000)

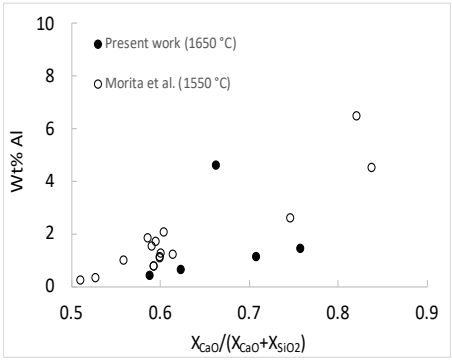

(b) The relation between wt% Al in Si in equilibrium with 45-55 wt% CaO-Al_2O_3 slag and $X_{CaO}/(X_{CaO} + X_{SiO_2})$, compared with data from Morita et al. (2000)

Figure 5.1: Comparison of Al concentrations with data from Morita et al. [61]

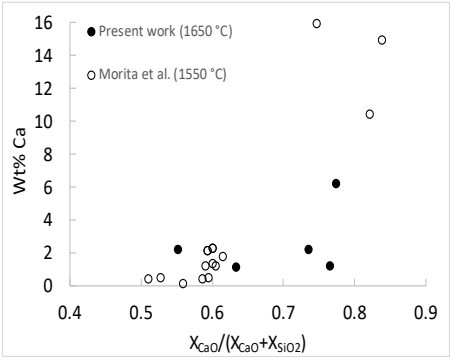

(a) The relation between wt% Ca in Si in equilibrium with 35-65 wt% CaO-Al_2O_3 slag and $X_{CaO}/(X_{CaO} + X_{SiO_2})$.

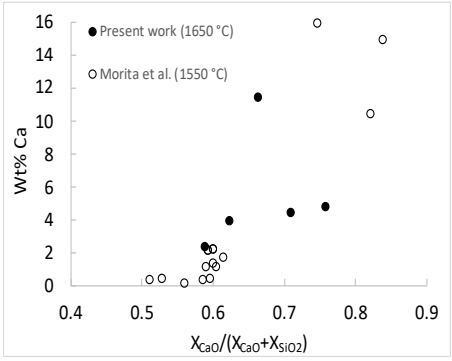

(b) The relation between wt% Ca in Si in equilibrium with 45-55 wt% CaO-Al_2O_3 slag and $X_{CaO}/(X_{CaO} + X_{SiO_2})$.

Figure 5.2: Comparison of Ca concentrations with data from Morita et al. [61]

The Al concentration in equilibrium with Si 35-65 and 45-55 wt% CaO-Al_2O_3 as a function of $X_{CaO}/(X_{CaO}+X_{SiO_2})$ is shown in figure 5.1. As seen in the figure, the concentrations in the present work are generally in good agreement, but somewhat higher than those obtained from Morita et al. [61] for the Si metal equilibrated with 35-65 wt% CaO-Al_2O_3 slag. Explanations for this could be the 100 °C higher temperature or the higher Al_2O_3 concentrations in the present work. Morita et al. [61] states that their study was in good agreement with the study obtained from Weiss and Schwerdtfeger [62] in SiO_2-rich slags in regards to the Al content, despite the temperature difference of 50 °C. They also compared the obtained distribution of Al and Ca with the work by Fujiwara et al. [63] at 1600 °C, and their results are in reasonable agreement, despite the temperature difference of 50 °C. This indicates that the temperature difference between the present work and Morita et al. [61] cannot be the reasoning behind the higher obtained Al-concentrations. However, the trend seems to be similar, and it is clear that the weight percent of Al increases with increasing $X_{CaO}/(X_{CaO} + X_{SiO_2})$ ratio in the slag.

For the Ca content in the Si metal equilibrated with 35-65 and 45-55 wt% CaO-Al_2O_3 slags, the concentration is around the same level at $X_{CaO}/(X_{CaO} + X_{SiO_2})$ = 0.6. However, as this present work only has one-two points of data for the 35-65 wt% CaO-Al_2O_3 slag in this area, it is not possible to conclude with anything, but it is seen that the Ca concentrations in the present work are higher. At $X_{CaO}/(X_{CaO}+X_{SiO_2})$ values around 0.70 and higher, the present work shows lower concentrations. However, the trend is similar; the Ca concentration increases with increasing $X_{CaO}/(X_{CaO} + X_{SiO_2})$.

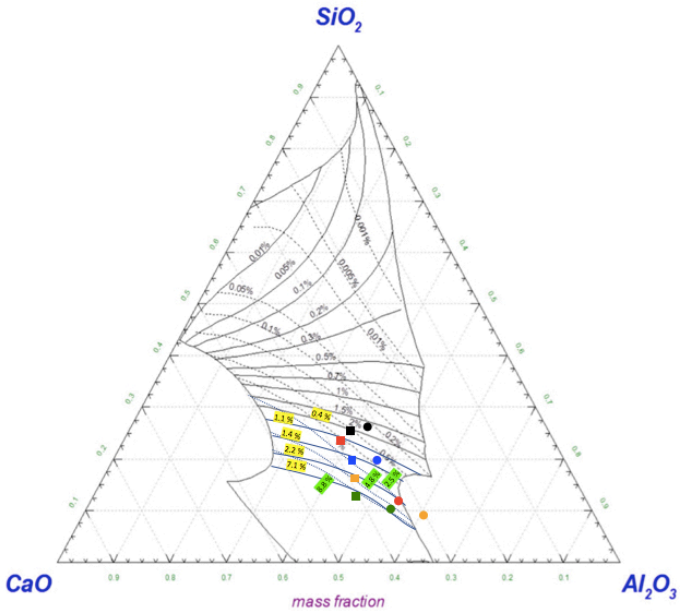

Figure 5.3: CaO-Al_2O_3-SiO_2 phase diagram at 1600 °C with suggestions to isoconcentration lines for Al (full lines) and Ca (dashed lines), obtained from the experimental data in the present work. Where the circles and squares represents concentrations obtained from equilibrium experiments with 35-65 and 45-55 wt% CaO-Al_2O_3 slags, respectively. Green depicts a metal/slag ratio of 1/1, yellow = 2.5/1, red = 5/1, blue = 7.5/1 and black = 10/1. The phase diagram is obtained from FactSage. [4]

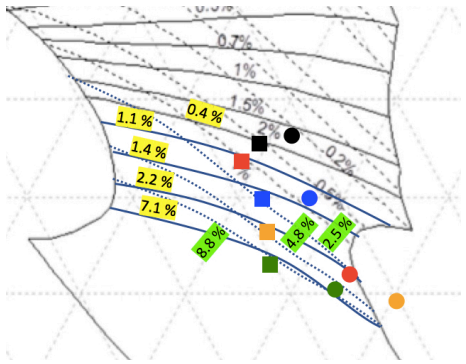

Figure 5.4: CaO-Al_2O_3-SiO_2 phase diagram with suggestions to isoconcentration lines zoomed in.

Figure 5.3 and 5.4 shows the CaO-Al_2O_3-SiO_2 phase diagram at 1600 °C obtained from FactSage [4] and the plotted slag concentrations for the 35-65 (circles) and 45-55 wt% (squares) CaO-Al_2O_3 in equilibrium with silicon with various metal/slag ratios, where the

green represents a metal/slag ratio of 1/1, yellow is 2.5/1, red is 5/1, blue is 7.5/1 and the black point are 10/1. The suggested isoconcentration lines (blue lines) are drawn based on the results obtained in the present work and based on average values where there is more than one point on the line. The full lines represent the Al isoconcentration curves with yellow writing, and the stippled lines represent the Ca concentration lines with green writing.

The phase diagram is for 1600 °C, and the experiments run in this thesis are run at 1650 °C. Therefore there will be some small errors due to the temperature difference of 50 °C, and it is seen that the yellow point is outside the liquidus region at 1600 °C, but not for 1650 °C. However, the results are still worth comparing. When increasing the temperature with 50 °C, the isothermal section will be slightly bigger, as seen in figure 2.12. As mentioned earlier, Morita et al. [61] compared their obtained values for Al and Ca concentrations after equilibrating Si with CaO-Al_2O_3-SiO_2 slags at 1550 °C with Fujiwara et al. [63] who did similar experiments at 1600 °C, and their obtained concentrations for Al and Ca were in good agreement.

In general, it is seen that with decreasing SiO_2 concentration in the slag, the Al and Ca concentration increases. Since there is no data available in this diagram for Al concentrations above 2 %, and it is not known by which magnitude the concentration will increase, it will be challenging to state if the concentrations obtained in this study are too high or too low compared to this diagram for all the points. For the black point (circle), with a metal/slag ratio of 10/1, it is seen that the theoretical Al concentration at the plotted slag composition would be 2 wt %, while the measured value is 3.58 wt %. The higher concentration can be explained by the analyzed metal in the 10/1 experiments were measured very close to the slag, as opposed to all the other metal samples, which was measured approximately in the middle of the metal phase. Despite this, the concentrations measured from the 10/1 experiments were included to emphasize how much the concentration gradient between the slag- and metal phase influences the Al and Ca concentrations in the metal, although there is more metal in equilibrium.

For the 35-65 wt% slag series, in the experiment with a metal/slag ratio of 5 (red circle), the Al concentration is 3.01 wt%, which seems to be a relatively good fit, if comparing with the diagram, and if the solid Al-lines would be extrapolated. When it comes to the blue circle, and a metal/slag ratio of 7.5/1, the Al concentration is lower than the Al concentration at 10/1, and it is explained above why this is the case. If only considering the Al concentration, it is reasonable that it is lower for a metal/slag ratio of 7.5/1 as opposed

to a metal/slag ratio of 5/1. However, the SiO_2 concentration is lower than expected for the experiment with a metal/slag ratio of 7.5/1, where the blue circle is expected to be above the red circle in the diagram. The yellow circle, where there is a metal/slag ratio of 2.5/1, the Al concentration is 4.33 wt%, which fits well with the overall trend. The green circle, with a metal/slag ratio of 1/1, shows the highest Al concentration as expected, with 9.74 wt %. Taken this into consideration, there is a strong indication that the Al concentration in Si in equilibrium with CaO-Al_2O_3-SiO_2 slags increases exponentially with increasing CaO and Al_2O_3 concentrations in the slag. For the Ca concentrations, in the black point, where the metal/slag ratio is 10/1, the concentration is 2.15 wt% in the present work. Theoretically, the concentration should be 0.2 wt% at this particular slag composition in equilibrium with Si. At the red circle, the Ca concentration where the metal/slag ratio is 5/1, is higher than in the metal with a 7.5/1 metal/slag ratio, which is expected. Overall, the Ca concentrations seem to be in relatively good agreement when plotting in the diagram and extrapolating the isoconcentration lines.

For the isoconcentration lines obtained from equilibria experiments with 45-55 wt% CaO-Al_2O_3 slag, the Al concentrations are in general too low compared with the diagram. Looking at the yellow (2.5/1) and green squares (1/1), it is seen that the SiO_2 concentration is higher for the metal/slag ratio of 1/1 compared to 2.5/1, which should not be the case, because more Si metal should generate more SiO_2 in the slag. However, the Al concentration at a metal/slag ratio of 1/1 is measured to be 4.57 wt%, while when extrapolating the modeled isoconcentration lines, the Al concentration should be around 5 wt%, giving the smallest point of error for this series. The yellow square, with the lowest SiO_2 concentration, has a measured concentration of 1.42 wt% Al, which seems to be too low if extrapolating the existing isoconcentration lines. Considering the Ca concentrations, in the black square where the metal/slag ratio is 10/1, the measured concentration is 2.35 wt%, while the point is at the 0.5 wt% line, while the red square with a metal/slag ratio of 5/1 is at the 1 wt% line, while the measured concentration is 4.45 wt%. The obtained Ca concentrations in the 45-55 wt% slag series seems, therefore, to be too high if compared with the diagram. However, looking at the trend for the Ca concentrations in general, it seems to be as expected, where the Ca concentration increases with increasing CaO concentrations as seen in figure 5.4, where the Ca concentrations are higher in the square points compared to the circles. Moreover, a similar trend is seen for the Al concentrations, which increases with increasing Al_2O_3 content.

All experiments with the exact parameters in this study were modeled in FactSage. Figure

5.5 and 5.6 shows the experimental measured concentrations of Al and Ca for the Si-metal equilibrated with 35-65 wt% CaO-Al_2O_3 slag, and with 45-55 wt% CaO-Al_2O_3 slag compared with results from FactSage. The Al concentrations in the 35-65 wt% CaO-Al_2O_3 experiments are all higher than the theoretical ones from FactSage. However, the experimental Ca concentrations seem to have a relatively good fit with the theoretical concentrations, besides from the concentration obtained from the experiment with 10/1 metal slag ratio due to reasons mentioned before; the measurements were done very close to the slag, giving unrealistic high values compared to the other measured concentrations. This indicates that the system has not reached equilibrium.

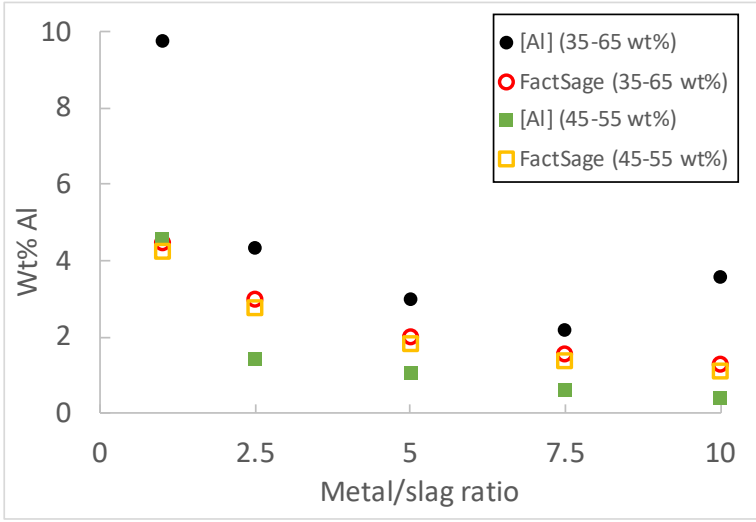

Figure 5.5: Comparison of the experimentally obtained Al concentrations and modeled concentrations from FactSage.

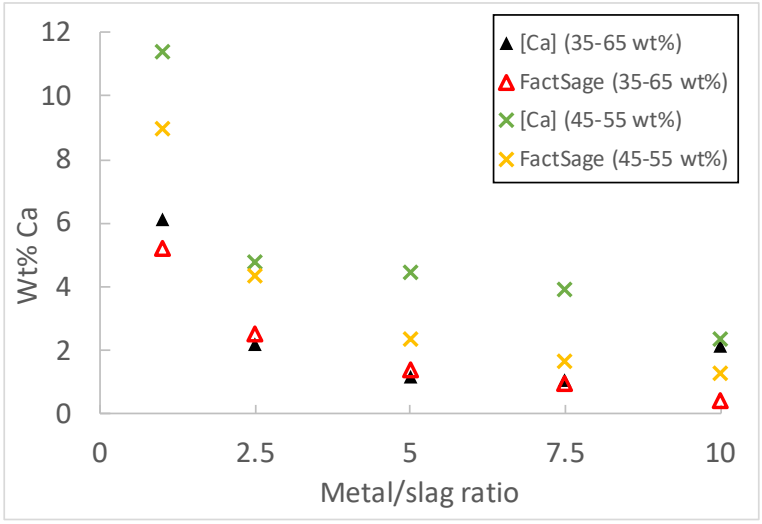

Figure 5.6: Comparison of the experimentally obtained Al concentrations and modeled concentrations from FactSage.

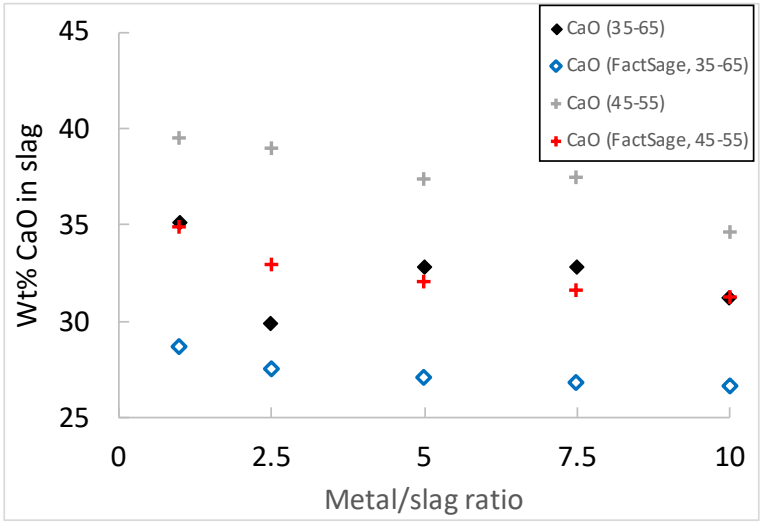

Figure 5.7: Concentration of CaO as a function of metal/slag ratio, compared with the theoretical concentrations calculated from FactSage.

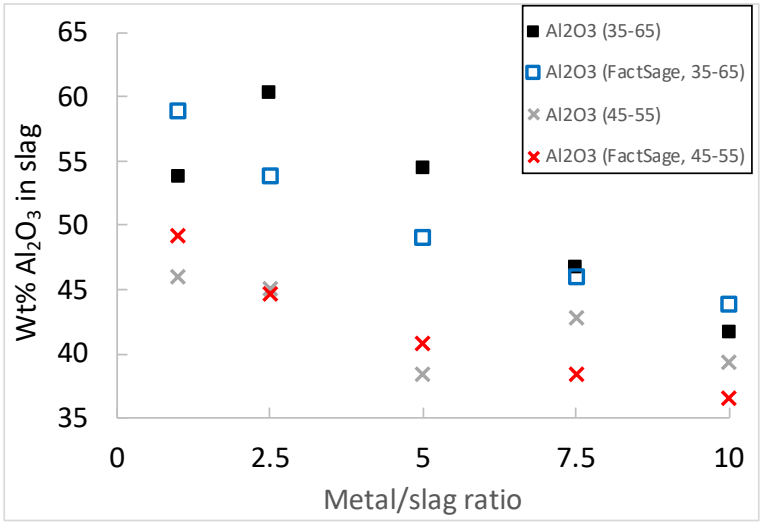

Figure 5.8: Concentration of Al_2O_3 as a function of metal/slag ratio, compared with the theoretical concentrations calculated from FactSage.

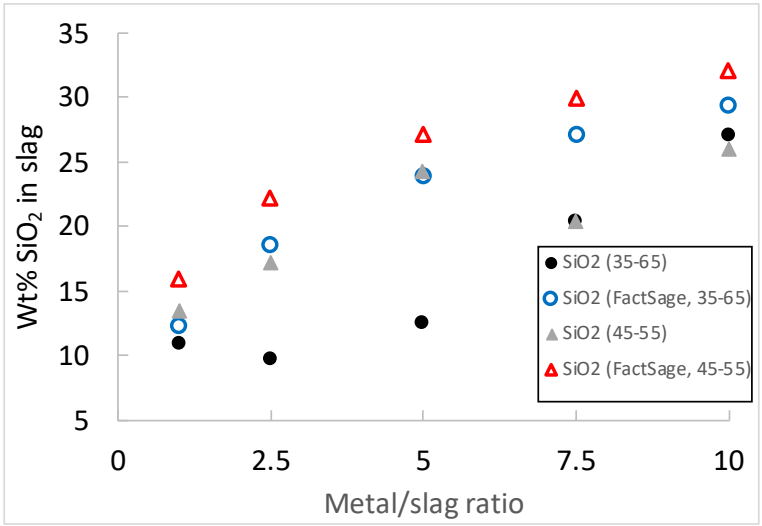

Figure 5.9: Concentration of SiO_2 as a function of metal/slag ratio, compared with the theoretical concentrations calculated from FactSage.

As illustrated in figure 5.7, 5.8 and 5.9, the slag concentrations obtained in the present work are not completely in agreement with the modeled results from FactSage. The CaO concentrations in the present work are slightly higher than the modeled results, but the trend

is in good agreement, as the concentrations should decrease step-wise when increasing the Si concentration in the system. The Al_2O_3 concentrations should also decrease step-wise with increasing metal/slag ratio and increasing Si concentration, and the obtained values in the present work are slightly higher for 2.5/1 and 5/1 than the theoretical concentrations, and slightly lower for the experiment with the largest amount of Si. When it comes to the SiO_2 concentrations in the slag, it should increase when increasing the mass of Si. One experiment worth highlighting is the one with a metal/slag ratio of 2.5/1 in 35-65 wt% slag series. Where all oxide concentrations are out of trend, and as seen in figure 5.4, the yellow circle which represents this point are out of the line. This could most likely be due to inhomogeneities in the slag pieces used in this particular experiment.

Figures 5.5 and 5.6 illustrates the concentration of Al and Ca obtained experimentally and from FactSage. It seems like the obtained concentrations modeled in FactSage with respect to the experiments in the present work is in better agreement with the ones obtained from the CaO-Al_2O_3-SiO_2 phase diagram at 1600 °C. Although the modeled Al-concentrations are also higher (except for the metal/slag ratio of 1/1), than the measured concentrations in this study, they seem to fit relatively well. When comparing the specific modeled concentrations with the ones obtained from the phase diagram, the specific modeled results are also lower. The temperature difference could explain why all the Ca concentration is higher than the modeled in the diagram, but that does not explain the lower Al-concentrations in the present work.

As mentioned earlier, Morita et al. [61] compared their results at 1550 °C with the work by Fujiwara et al. [63] at 1600 °C, and their results were in good agreement, despite the temperature difference. Morita et al. [61] also states that their results are in good agreement with Weiss and Schwerdtfeger [62] at 1500 °C with respect to Al, but they obtained higher Ca concentrations. Morita et al. [61] suggest that the temperature difference between their study and the one by Weiss and Schwerdtfeger [62] may be the cause of the concentration differences. The temperature difference can be directly related to the present study; comparing the Ca concentrations to the isoconcentration lines for Ca in the phase diagram, the obtained values are higher than those at 1600 °C. This may indicate that the data in general in the CaO-Al_2O_3 rich region are very uncertain. Also, there has not been carried out equilibrium studies in this particular system at 1650 °C, and the temperature dependence could have an impact.

5.2.2 Activity Coefficients in the CaO-Al_2O_3-SiO_2 System

The activity coefficients of Al and Ca in Si were calculated based on their respective concentrations. Some assumptions were made, and the activity of Si was assumed to be the same as the mole fraction. The activities of Al_2O_3, CaO, and SiO_2 were found by plotting in the isoactivity diagrams by Rein and Chipman [64] at 1600 °C, even though the experiments were run at 1650 °C. The equilibrium constants of eq. (5.3) and (5.7) are from FactSage. The interaction coefficients of Ca and Al was not considered in the calculations, as it is not recommended for more highly alloyed materials, as stated by Sigworth. [72] Pelton and Bale [58] recommend using modified approach interaction coefficients, similar to Darken's Quadratic formalism, as showed in section 2.4.6. However, this was not considered in these calculations.

All data used for the calculations and an example calculation can be found in appendix F. To convert the activity of Al_2O_3 to $AlO_{1.5}$, the relation $a^2_{Al_2O_3} = a^4_{AlO_{1.5}}$ was used, as the isoactivity diagram from Rein and Chipman [64] is valid for $AlO_{1.5}$.

The activity coefficient of Al was calculated by the equilibrium:

$$3\,\mathrm{Si} + 2\,\mathrm{Al_2O_3} \rightleftharpoons 3\,\mathrm{SiO_2} + 4\,\mathrm{Al} \tag{5.3}$$

With the equilibrium constant:

$$K = \frac{a^4_{Al} \cdot a^3_{SiO_2}}{a^3_{Si} \cdot a^4_{AlO_{1.5}}} \tag{5.4}$$

With the equilibrium constant: K = 4.12×10^{-12} at 1923 K. [4]

We have that:

$$a_{Al} = X_{Al} \cdot \gamma^0_{Al} \tag{5.5}$$

Which gives:

$$\gamma^4_{Al} = \frac{K \cdot a^3_{Si} \cdot a^4_{AlO_{1.5}}}{X^4_{Al} \cdot a^3_{SiO_2}} \tag{5.6}$$

The activity coefficient of Ca was calculated from the equilibrium:

$$\mathrm{Si} + 2\,\mathrm{CaO} \rightleftharpoons \mathrm{SiO_2} + 2\,\mathrm{Ca} \tag{5.7}$$

With the equilibrium constant:

$$K = \frac{a_{SiO_2} \cdot a_{Ca}^2}{a_{Si} \cdot a_{CaO}^2} \tag{5.8}$$

With the equilibrium constant: K = 6.33 $\times$ 10^{-8} at 1923 K. [4]

We have that:

$$a_{Ca} = X_{Ca} \cdot \gamma_{Ca}^0 \tag{5.9}$$

Which gives:

$$\gamma_{Ca}^2 = \frac{K \cdot a_{CaO}^2 \cdot a_{Si}}{X_{Ca}^2 \cdot a_{SiO_2}} \tag{5.10}$$

Table 5.3: Calculated activity coefficients of Al and Ca in Si in equilibrium with 35-65 wt% and 45-55 wt% CaO-Al_2O_3 slags, compared with relevant other works.

	35-65 wt% CaO-Al_2O_3		**45-55 wt% CaO-Al_2O_3**				
Metal/slag ratio	γ_{Al}^0	γ_{Ca}^0	γ_{Al}^0	γ_{Ca}^0	**Reference**	γ_{Al}^0	γ_{Ca}^0
1/1	0.407	0.008	1.43	0.004	Morita et al. [61]	0.23	0.0028
2.5/1	0.712	0.012	49.37	0.093	Dumay et al. [42]	0.65 $\pm$ 0.2	0.003 $\pm$ 0.001
5/1	0.368	0.056	3.14	0.004	Weiss et al. [62]	0.56	NA
7.5/1	1.164	0.018	2.99	0.019			
10/1	0.315	0.002	2.08	0.001			

Table 5.3 shows the calculated activity coefficients of Al and Ca based on their respective concentrations and mole fractions, compared with other relevant works. The activity coefficient of Al at a metal/slag ratio of 2.5/1 in the 45-55 wt% slag is considered to be an outlier, as the SiO_2 activity for this point was lower by a factor of 10 in this particular point, giving an unrealistic high activity coefficient (γ_{Al}^0 = 49.37), compared to the other calculated activity coefficients.

Dumay et al. [42] calculated the activity coefficient at high-alumina activities in FeSi65, and found γ_{Al}^0 to be 0.65$\pm$ 0.2, which fits well with their earlier study, where they obtained γ_{Al}^0 = 0.55 $\pm$ 0.1, and with Weiss and Schwerdtfeger [62], which found γ_{Al}^0 to be 0.56 for

pure silicon equilibrated with SiO_2-saturated CaO-Al_2O_3-SiO_2 slags. In the 35-65 wt% slag series, γ^0_{Al} are in the range 0.315-1.164, which are in the same range as the obtained results from Dumay et al. [42]. For the 45-55 wt% slag series, the values are less in agreement, where γ^0_{Al} are in the range 1.43-49.37. If discarding γ^0_{Al} = 49.37, which was obtained due to unreasonably low SiO_2 activities, the range would be 1.43-3.14, which also are higher than the reported values. Comparing with the work by Morita et al. [61] and inserting the temperature 1923 K in their relations shown in table 2.1, it is found that γ^0_{Al} = 0.23, where the present work from the 35-65 wt% slag series shows somewhat higher values, but are in better agreement as opposed to the 45-55 wt% slag series, where the activity coefficients are significantly higher.

Dumay et al. [42] also calculated the activity coefficient of Ca with the same conditions, and found γ^0_{Ca} to be 0.003 $\pm$ 0.001, however, they report significant scattering in their values. In the 35-65 wt% slag series, the γ^0_{Ca} is found to be in the range 0.002-0.056, and 0.001-0.093 in the 45-55 wt% slag series. Comparing with the calculated activity coefficient by Morita et al. [61], and inserting the temperature 1923 K in the formula given in table 2.1, γ^0_{Ca} = 0.0028 which are in relatively good agreement for the lower obtained range of activity coefficients in the present work.

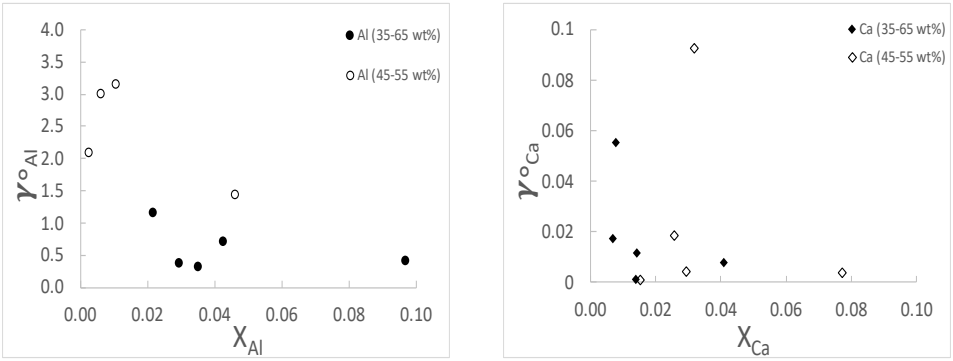

(a) The relation between γ^0_{Al} and X_{Al}.

(b) The relation between γ^0_{Ca} and X_{Ca}.

Figure 5.10: Calculated activity coefficients as a function of mole fractions of Al and Ca.

One crucial point here is that the system in the present work is not considered to be very pure or infinite dilute. Sigworth [72] states that a system can be considered infinite dilute when the Si concentration is above $\sim$99 %, which makes the results in the present work not directly comparable. As seen in figure 5.10, the calculated activity coefficients do decrease with increasing X_{Al} or X_{Ca}; however, the values are scattered.

To summarise, the calculated activity coefficients from the 35-65 wt% slag series are in best agreement with respect to γ^0_{Al} with the other present work, where the activity coefficients in the 45-55 wt% slag series are significantly higher. The activity coefficient of Ca is in good agreement with both Morita et al. [61] and Dumay et al. [42] where the γ^0_{Ca} is in a magnitude of 10^{-3}. However, some values in the present work are higher by a factor of 10.

5.2.3 Effect of Equilibrium Time

The Al concentration in Si in equilibrium with CaO-Al_2O_3 slags is shown in figure 5.11 and the Al concentration decreases significantly when the CaO/Al_2O_3 increases, while the Ca concentration increases, as shown in figure 5.12. If equilibrium is assumed, the change in equilibrium concentrations should be mainly due to the change in the activity coefficients of Al and Ca in Si. This can also be seen from table 5.4, where the concentration of Al_2O_3 has decreased, for the 35-65 wt% CaO-Al_2O_3 experiments. A decrease is also observed in the Al_2O_3 concentration in the 45-55 wt% CaO-Al_2O_3 after all experiments. Also, a large increase in SiO_2 concentration is observed, which is due to an increase in the SiO_2 activity in the slag caused by more Si metal in the experiments, and thus, the CaO and Al_2O_3 activity decrease due to the increase of the SiO_2 content in the slag. The reduction of CaO was also observed for all experiments, except for the metal/slag ratio of 1/1 in the 35-65 wt% series, which is a strong indication of error in the measured CaO concentration. As seen in figure 5.13, the CaO/Al_2O_3 ratio remains relatively constant for the 45-55 wt% series, while increasing slightly in the 35-65 wt% series. Looking at the obtained Al and Ca concentrations together with this, it can be stated that more Al_2O_3 reduces to Al in the 35-65 wt% series, compared to the 45-55 wt% series. Simultaneously, less CaO is reduced, leading to lower Ca concentrations.

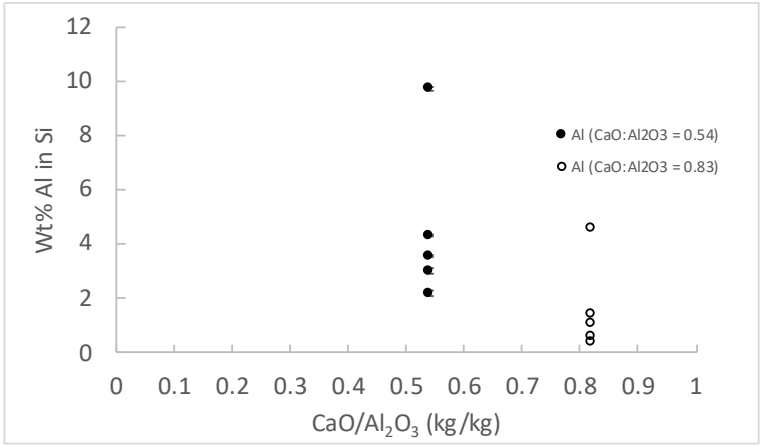

Figure 5.11: The concentration of Al in Si in equilibrium as a function of the CaO/Al_2O_3 ratio.

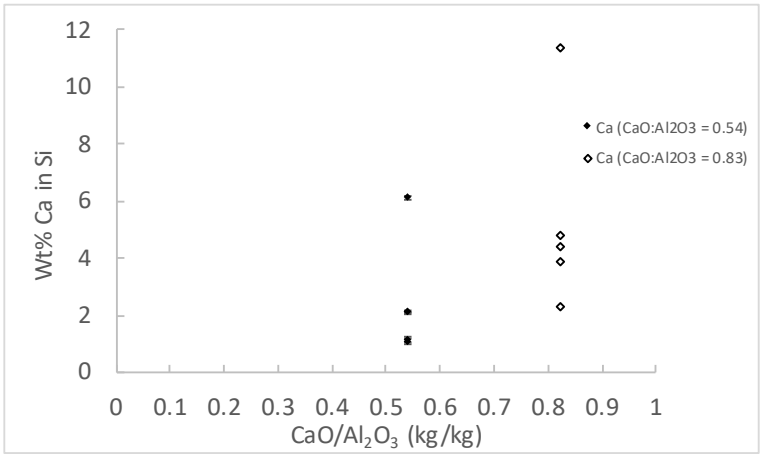

Figure 5.12: The concentration of Ca in Si in equilibrium as a function of the CaO/Al_2O_3 ratio.

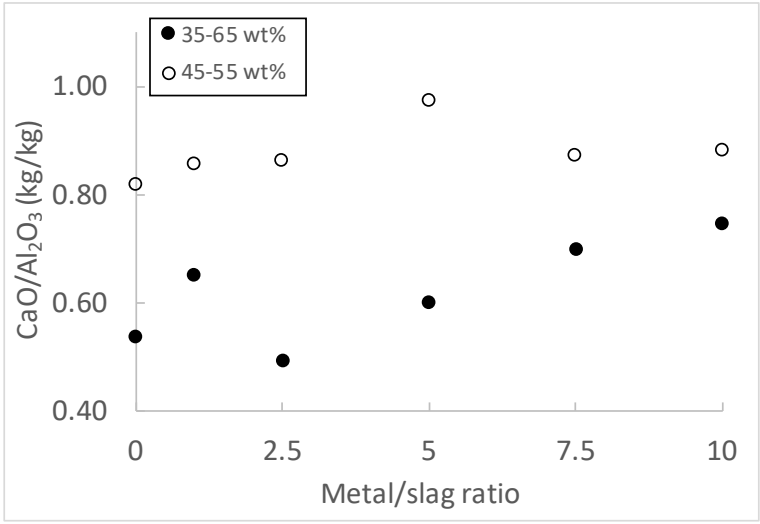

Figure 5.13: The CaO/Al_2O_3 ratio as a function of the metal/slag ratio.

Table 5.4: Overview of the slag compositions before and after experiments, with the Al and Ca concentrations in the Si after equilibria experiments.

	Initial			Final				
Metal/slag ratio	**SiO_2**	**CaO**	**Al_2O_3**	**SiO_2**	**CaO**	**Al_2O_3**	**[Al]**	**[Ca]**
35-65 wt%								
1/1	0.31	34.16	64.55	11.03	35.14	53.83	9.74	6.13
2.5/1	0.31	34.16	64.55	9.82	29.89	60.28	4.33	2.17
5/1	0.31	34.16	64.55	12.66	32.86	54.58	3.01	1.18
7.5/1	0.31	34.16	64.55	20.40	32.82	46.78	2.19	1.08
10/1	0.31	34.16	64.55	27.08	31.18	41.74	3.58	2.15
45-55 wt%								
1/1	0.37	41.61	52.68	13.52	39.52	46.06	4.57	11.39
2.5/1	0.37	41.61	52.68	17.22	38.95	45.13	1.42	4.79
5/1	0.37	41.61	52.68	24.26	37.37	38.37	1.07	4.45
7.5/1	0.37	41.61	52.68	20.48	37.44	42.86	0.61	3.91
10/1	0.37	41.61	52.68	26.05	34.64	39.31	0.38	2.35

The holding time for all experiments was one hour, which was assumed to be long enough time to approach equilibrium. Dumay et al. [42] equilibrated FeSi65 with CaO-Al_2O_3-

SiO_2 slags 1350 °C, 1450 °C and 1500 °C, at holding times between 12-48 h. They state that the Al concentration increases with temperature for all the slag compositions they investigated and that the effect is more pronounced when the Al_2O_3 concentration is high. Their highest concentration of Al_2O_3 in the slag was 40.7 wt%, and the concentration of CaO and SiO_2 28.4 wt% and 30.8 wt%, respectively. They also state that the Ca concentration in the FeSi65 increases with increasing CaO content in the start-slag. If compared with their study, both slags in the present study will be considered "high Al_2O_3 concentrations". The slag composition after equilibrium were 41.0 wt% Al_2O_3, 28.8 wt% CaO and 31.0 wt% SiO_2, and the present work agrees well with the findings of Dumay et al. [42] Jakobsson [33] states that, in his most Al_2O_3-rich slags, with a composition of 50.1 wt% CaO, 38.9 wt% Al_2O_3 and 10.7 wt% SiO_2, a significant reduction in general of Al_2O_3 was observed in the first three hours of holding time, as well as reduction of CaO. This is an indication that the predominating reaction at first was the dissolution of Ca and Al into the silicon phase. This was also the case for all experiments carried out in the present work. Also, after three hours and further, the SiO_2 concentration decreased while the CaO and Al_2O_3 concentration increased. He also states that the Ca and Al concentration were approximately the same after six hours and somewhat higher after nine hours, and he concludes that the equilibrium time concerning Ca and Al was three hours. The reasoning behind the increased concentration between six and nine hours was the decrease in the activity of SiO_2, and increased activity of CaO and Al_2O_3 caused by the decrease of SiO_2 content in the slag. However, Weiss and Swcherdtfeger [62] states that the Al concentration in the Si metal increases, while the Ca content decreases with increasing Al_2O_3 concentration in the slag. It is important to bear in mind that these exact parameters in the present work have not been investigated before. Thus, it is not possible to conclude with the decreasing trend of Ca with increasing Al_2O_3 content. In the present work, the CaO concentration is not constant for the two slag systems when increasing the Al_2O_3 concentration. Therefore it is not possible to directly conclude if the statement from Weiss and Swcherdtfeger [62] would fit the present system as the CaO-concentration simultaneously increased with increased Al_2O_3 concentration.

This could mean that the one-hour holding time in the present work is not long enough to reach equilibrium, as only a decrease of CaO and Al_2O_3 concentrations and an increase in SiO_2 concentration is observed. Also, higher concentrations of Al and Ca than expected were observed when measuring near the slag for the 35-65 wt% slag series, which also is an indication of not reaching equilibrium. However, Ding et al. [73] equilibrated Mn-Si-C_{sat} metal with a MnO-SiO_2-CaO-Al_2O_3 slag and CO-atmosphere (1 atm) to in-

vestigate the equilibrium between the equilibrium distribution of manganese and silicon between the slag and the metal. They found that the equilibrium content of Si in the metal is mainly controlled by temperature, the SiO_2-content of the slag, and the mass ratio R=(CaO+MgO)/Al_2O_3. They determined that the Si-content in the metal increases with increasing temperature, and increases with increasing SiO_2 content in the slag, and decreases with increasing R-ratio. This reasoning is based on slag/metal/gas equilibrium.

$$2\,(\mathrm{MnO}) + \mathrm{Si} \rightleftharpoons 2\,\mathrm{Mn} + (\mathrm{SiO_2}) \tag{5.11}$$

However, they are stating that when only slag/metal equilibrium is considered and established (as in reaction (5.11)), the system is said to be at "partial slag/metal equilibrium," whereas the reaction is little dependent on the temperature, pressure and the composition of the slag phase. In the system of Ding et al. [73], complete equilibrium is reached when the slag, metal, and the gas phase are in equilibrium. When considering the system relevant for this thesis, the system is completely in equilibrium when the metal and the slag phase are in equilibrium, because these are the two variables in the system if neglecting formation of SiO(g) through reactions with the crucible. Hence, since the experiments are run in an argon atmosphere, the gas-phase equilibrium can be neglected for this system. Ding et al. [73] also states that when the metal/slag ratio is large, less time is required to reach equilibrium than with smaller metal/slag ratios. Their metal/slag ratio was 8.5/1, and their holding time was three hours at 1700 °C and five hours at 1600 °C. All the before-mentioned studies have more slag than metal except for this one. However, the metal-slag system is different and may not be directly comparable with respect to equilibrium time and the change in slag compositions, as the SiO_2 concentration will increase with an increasing amount of Si metal, which has been observed for almost all experiments conducted in the present work.

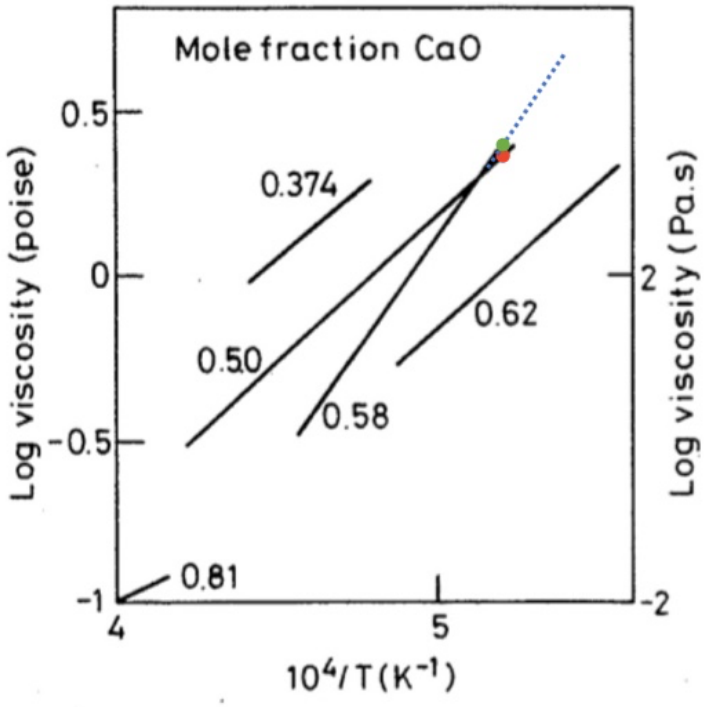

Figure 5.14: Viscosities in the CaO-Al_2O_3 melt system, as a function of reciprocal temperature (log(1/1650)). Green point: 35-65 wt% CaO-Al_2O_3, red point: 45-55 wt% CaO-Al_2O_3 slag. [34]

One important factor to consider with respect to equilibrium time is the viscosity of the system. Figure 5.14 shows the viscosity of CaO-Al_2O_3 melts as a function of reciprocal temperature, and the compositions of the slags in this system are plotted. The line with X_{CaO} = 0.58 was extrapolated to fit the temperature in the present system. As seen from the diagram, the 35-65 wt% slag will have a slightly higher viscosity than the 45-55 wt% slag. The mole fraction of CaO in the least viscous system is 0.6, and the 0.58 line was chosen as the most conservative estimate. The most viscous slag is expected to have the longest equilibrium time, as diffusivity is inversely proportional to viscosity, according to the Stoke-Einstein equations, as shown in eq. (2.21). However, from the figure, it is seen that the difference in viscosity for the two slags in the present work is relatively small. In table 2.1, the equilibrium time for various studies is given, where the equilibrium time is varied between 3-48 h. All studies listed in the table have SiO_2 in the system, which makes the studies not directly comparable, and the temperature in the present work is higher than in the other studies.

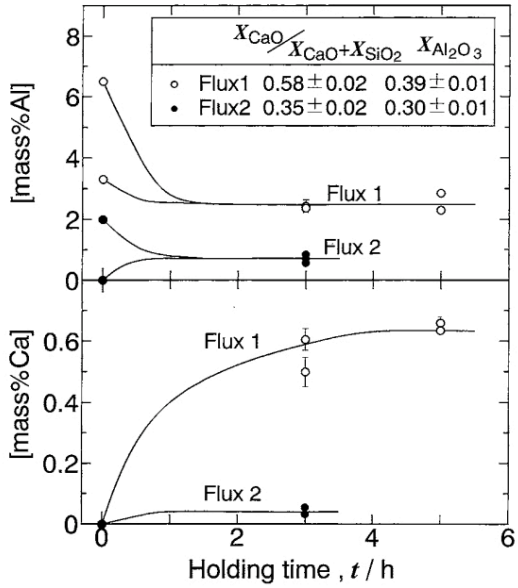

Figure 5.15: Wt% Ca and Al in equilibrium with Si as a function of holding time. [63]

However, Fujiwara et al. [63] equilibrated Si with CaO and Al_2O_3 saturated CaO-Al_2O_3-SiO_2 slags and investigated the required holding time for the system as showed in figure 5.15. Even though their holding times were between three-five hours, it is seen that equilibrium was reached after one hour when $X_{CaO}/(X_{CaO}+X_{SiO_2})$ = 0.35 and $X_{Al_2O_3}$ = 0.30 (flux 1), and the Ca concentration in the Si metal was at the lowest, 0.02 wt%. This leads to the belief that the mass transfer in the most viscous slag ceases after a short amount of time due to the system's diffusion limit. When $X_{CaO}/(X_{CaO}+X_{SiO_2})$ = 0.58 and $X_{Al_2O_3}$ = 0.39 (flux 2), the Ca concentration increased greatly to 0.6 wt%, but the equilibrium time was longer, and was reached after about four hours, where the concentration difference was constant at 0.6 wt%. Considering the equilibrium time with respect to Al, it was reached after about 1.5 hours for both before-mentioned slags. When equilibrated with flux 1, the concentration flattened out at about 2.7 wt%, and at about 0.9 wt% when Si was equilibrated with flux 2.

5.3 Phase Composition of Silicon in Equilibrium with $CaO\text{-}Al_2O_3$ Slags

As mentioned in section 2.7, studies on Si-Al-Ca alloys are limited. The phases obtained in Si after equilibration with 35-65 wt% and 45-55 wt% $CaO\text{-}Al_2O_3$ have been investigated, and in general, the results agree well with the literature. Also, solidification calculations assuming Scheil-Gulliver cooling and equilibrium cooling was conducted in FactSage, both calculations showed almost identical results.

5.3.1 Silicon in Equilibrium with 35-65 wt% $CaO\text{-}Al_2O_3$ Slag

Three phases were present in the Si metal in equilibrium with 35-65 wt% $CaO\text{-}Al_2O_3$ slag; one Al-rich phase, one Si_2Al_2Ca phase, and one Si-rich phase (the matrix). From image analysis, it was seen that the overall amount of phases decreased with increasing metal/slag ratio, which is as expected.

Table 5.5: Mole fractions of the Si-Al-Ca phase in the Si metal in equilibrium with 35-65 wt% $CaO\text{-}Al_2O_3$ slags.

Metal/slag ratio	Si	Al	Ca
1/1	0.401	0.401	0.198
2.5/1	0.405	0.397	0.198
5/1	0.403	0.399	0.199
7.5/1	0.405	0.398	0.196
10/1	0.406	0.396	0.198

As seen from table 5.5, there is about 40 mol% Si, 40 mol% Al and 20 mol% Ca in the mixed Si-Al-Ca phase in the Si metal equilibrated with 35-65 wt% $CaO\text{-}Al_2O_3$ slag. The estimated phase is then Si_2Al_2Ca, which agrees well with the plotted composition in the Si-Al-Ca phase diagram, as seen in figure 4.27 in the results-section.

Anglezio et al. [68] investigated Si-Al-Ca alloys, and they found presence of two phases in Si, in addition to the matrix; one Si_2Al_2Ca phase and one Si_2Ca phase. The two phases mentioned were also observed by Margaria et al. [69]. However, the Si_2Ca phase was not observed in this metal equilibrated with the most Al-rich slag, whereas a Al-rich phase were observed instead. If only considering Si and Al in the system, the Al rich phase is found in the phase diagram as showed in figure 4.29.

Qualitatively, the modeled results are in good agreement with the experimental observations, besides, presence of the Si_2Ca phase were found for the metal/slag ratios 1/1 and 2.5/1, as showed in 5.6, where the experimental amounts of phases are compared with the modeled in FactSage (Fact.). Looking at the Si_2Al_2Ca phase, higher amounts were found in the present study at a metal/slag ratio of 1/1, compared to the modeled results, for the other metal/slag ratios, smaller amounts of the phase was detected. The Al-rich phase was not possible to quantify in ImageJ, since it is so small, therefore after studying the BSE images, an estimation of 1 % was decided for the metal/slag ratios of 1/1, 2.5/1 and 5/1, and 0.5 % for the 7.5/1, and 10/1. The modeled results, on the other hand, shows no presence of the Al-rich phase in the metal/slag ratios 1/1 and 2.5/1, and that the amount of Al-rich phase increases with increasing metal/slag ratio from 5/1 to 10/1. As the estimation is highly uncertain, the errors may be large. However, detection of the Al-rich phase was done for all metal samples, and from inspecting the images, the amount decreased with increasing metal/slag ratio. The amount of the Si-matrix obtained in the experiments agrees relatively well with the modeled results from FactSage. As mentioned earlier, the fraction of Si for the 10/1 metal slag ratio is unreasonably low, due to measurements very near the slag. The fractions of the phases were quantified in ImageJ by thresholding, and the method in itself may cause errors because each image was analyzed individually and manually. As seen in table 5.7, the equilibrium solidification calculations are almost identical to the results from Scheil-Gulliver cooling. This could be an indication of that the present system is not far from equilibrium, as the results obtained from the experiments and the modeled equilibrium calculations are within the same order of magnitude, and some values are close.

Table 5.6: Comparison of the fraction of the phases calculated with ImageJ and FactSage, assuming Scheil cooling in the Si metal equilibrated with 35-65 wt% CaO-Al_2O_3 slag.

Metal/slag	Exp. Si_2Al_2Ca	Fact. Si_2Al_2Ca	Exp. Si_2Ca	Fact. Si_2Ca	Exp. Al (fcc)	Fact. Al (fcc)	Exp. Si	Fact. Si
1/1	16.44	12.42	0	4.56	1	0	84.12	83.00
2.5/1	5.53	8.26	0	0.79	1	0	93.49	90.92
5/1	2.92	5.18	0	0	1	0.15	95.81	94.63
7.5/1	2.71	3.59	0	0	0.5	0.27	96.73	96.09
10/1	5.62	2.76	0	0	0.5	0.30	94.27	96.89

Table 5.7: Comparison of solidification calculations assuming Scheil-Gulliver- and equilibrium cooling, from FactSage.

Metal/slag ratio	Scheil-Gulliver Si_2Al_2Ca	Equilibrium Si_2Al_2Ca	Scheil-Gulliver Si_2Ca	Equilibrium Si_2Ca	Scheil-Gulliver Al (fcc)	Equilibrium Al (fcc)	Scheil-Gulliver Si	Equilibrium Si
1	12.42	12.42	4.56	4.56	0	0	83.00	83.00
2.5	8.26	8.26	0.79	0.78	0	0	90.92	90.92
5	5.18	5.19	0	0	0.15	0.15	94.63	94.63
7.5	3.59	3.60	0	0	0.27	0.26	96.09	96.09
10	2.76	2.78	0	0	0.30	0.28	96.89	96.89

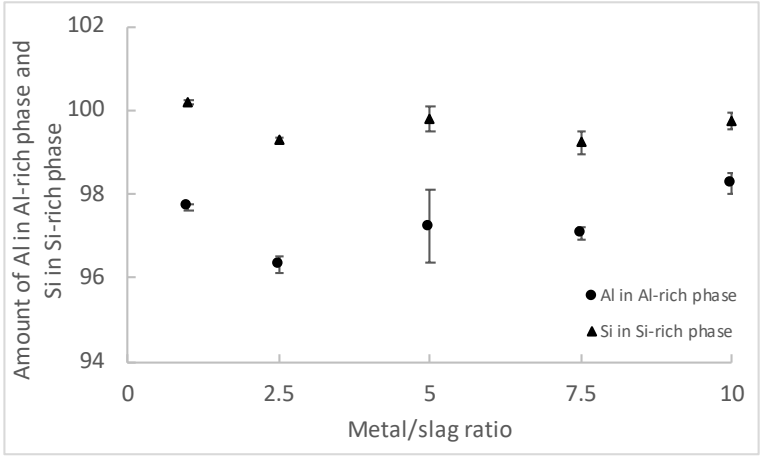

Figure 5.16: The concentration of Si and Al in the Si-rich phase and Al-rich phase, respectively in the metal equilibrated with 35-65 wt% $CaO\text{-}Al_2O_3$ slag. All values are given in wt%.

Figure 5.16 shows the amount of Al in the Al-rich phase and the amount of Si in the Si-rich phase in the metal equilibrated with 35-65 wt% $CaO\text{-}Al_2O_3$ slag as a function of metal/slag ratio. Here, the Al-content in the Al-rich phase is $\sim$ 97 wt%, and the Si-content in the Si-rich phase is $\sim$ 100 wt%. Similar phenomenon are observed in all phases present in the metals, as seen in the tables 4.4, 4.5, 4.6, and 4.7 in the results section. The values are relatively constant, which means that averaging all values between all phases to get an overall composition, will not result in a significant error of the values.

5.3.2 Silicon in Equilibrium with 45-55 wt% CaO-Al_2O_3 Slag

Presence of three phases were observed in the Si metal in equilibrium with 45-55 wt% CaO-Al_2O_3 slag; one Si_2Al_2Ca phase, one Si_2Ca phase, and one Si-rich phase (the matrix). As expected, it was seen that the general amount of phases decreased with increasing metal/slag ratio.

Table 5.8: Mole fractions of the Si_2Al_2Ca phase in the Si metal in equilibrium with 45-55 wt% CaO-Al_2O_3 slags.

Metal/slag ratio	Si	Al	Ca
1/1	0.397	0.400	0.203
2.5/1	0.401	0.399	0.199
5/1	0.406	0.393	0.200
7.5/1	0.412	0.389	0.200
10/1	0.407	0.395	0.199

Table 5.9: Mole fractions of the Si_2Ca phase, in the Si metal in equilibrium with 45-55 wt% CaO-Al_2O_3 slags.

Metal/slag ratio	Si	Al	Ca
1/1	0.657	0.010	0.333
2.5/1	0.653	0.012	0.335
5/1	0.655	0.012	0.332
7.5/1	0.658	0.012	0.330
10/1	0.657	0.013	0.330

Also here, as seen from table 5.8, about 40 mol% Si, 40 mol% Al and 20 mol% is present in the Si_2Al_2Ca phase in the Si metal equilibrated with 45-55 wt% CaO-Al_2O_3 slag. Estimating the phase based on the mole fractions leads to the Si_2Al_2Ca phase, which agrees well with the plotted composition in the Si-Al-Ca phase diagram, as seen in figure 4.27 in the results-section, which is an observed phase by Anglezio et al. [68] and Margaria et al. [69] together with the Si_2Ca phase, as previously discussed. As seen in table 5.9, the Si-Ca-rich phase has about 66 mol% Si and 33 mol%, leading to a Si_2Ca phase. Margaria et al. [69] writes that the Si_2Ca phase can contain up to 2 % Al, and this agrees well with the findings in the present work, where approximately 1 wt% Al was found in the phase. However, when plotting the amount of Si, Al, and Ca in the Si-Al-Ca phase diagram, which is

weight-based, the phase diagram shows that it should be the SiCa. However, the point is just above the phase line separating the SiCa and the Si_2Ca phase. Thus, it is reasonable to assume that the Si-Ca-rich phase is the Si_2Ca phase, when taking the mole fractions into account, and the modeled results. In the Si_2Al_2Ca phase, comparing the fractions of the phases with the results from the modeling, it is seen that the experimental values are lower for all metal/slag ratios. The amount of the Si_2Ca phase is in fairly good agreement when the metal/slag ratio is 1/1 and 2.5/2, but for the 5/1, 7.5/1, and 10/1, the values presented in the present work are higher. In the Si phase (the matrix), the modeled results are in good agreement for all metal/slag ratios. As seen in table 5.11, the equilibrium solidification calculations are also here almost identical to the results from Scheil-Gulliver cooling. As the results obtained from the experiments and the modeled equilibrium calculations are within the same order of magnitude, and some values are close, this could indicate approaching equilibrium.

Table 5.10: Comparison of the fractions of the phases calculated with ImageJ and FactSage, assuming Scheil cooling in the Si metal equilibrated with 45-55 wt% $CaO\text{-}Al_2O_3$ slag.

Metal/slag	**Exp. Si_2Al_2Ca**	**Fact. Si_2Al_2Ca**	**Exp. Si_2Ca**	**Fact. Si_2Ca**	**Exp. Si**	**Fact. Si**
1/1	8.64	12.00	13.60	14.00	77.75	74.00
2.5/1	2.49	7.64	6.17	5.57	91.34	86.76
5/1	1.87	5.02	6.00	2.49	92.13	92.46
7.5/1	1.00	3.83	5.73	1.51	93.28	94.62
10/1	0.60	3.13	3.43	1.05	95.97	95.77

Table 5.11: Comparison of solidification calculations assuming Scheil-Gulliver- and equilibrium cooling, from FactSage in the 45-55 wt% $CaO\text{-}Al_2O_3$ slag series.

Metal/slag ratio	**Scheil-Gulliver Si_2Al_2Ca**	**Equilibrium Si_2Al_2Ca**	**Scheil-Gulliver Si_2Ca**	**Equilibrium Si_2Ca**	**Scheil-Gulliver Si**	**Equilibrium Si**
1	12.00	11.81	14.00	14.00	74.00	74.16
2.5	7.64	7.64	5.57	5.56	86.76	86.77
5	5.02	5.02	2.49	2.49	92.46	92.46
7.5	3.83	3.81	1.51	1.51	94.62	94.63
10	3.13	3.11	1.05	1.05	95.77	95.79

5.3.3 Phases Present in the Slags Equilibrated with Silicon

The phases present in the slags were identified where the structure was bigger than 30 µm. The area fraction (assuming equal to volume fraction) of each phase was calculated using ImageJ for all experiments where the phases were detectable, and these values, together with plotted compositions in the CaO-Al_2O_3-SiO_2 phase diagram are compared with the thermodynamic calculations. The phases in the 35-65 wt% slag were generally bigger than the phases in the 45-55 wt%. Since the structure was very fine in most of the samples from the 45-55 wt% slag series, they are analyzed with a defocused beam, besides for sample 45-55-120 and 45-55-240. Analyzing with a defocused beam gives an averaged composition of the slag, not making it possible to identify the phase compositions.

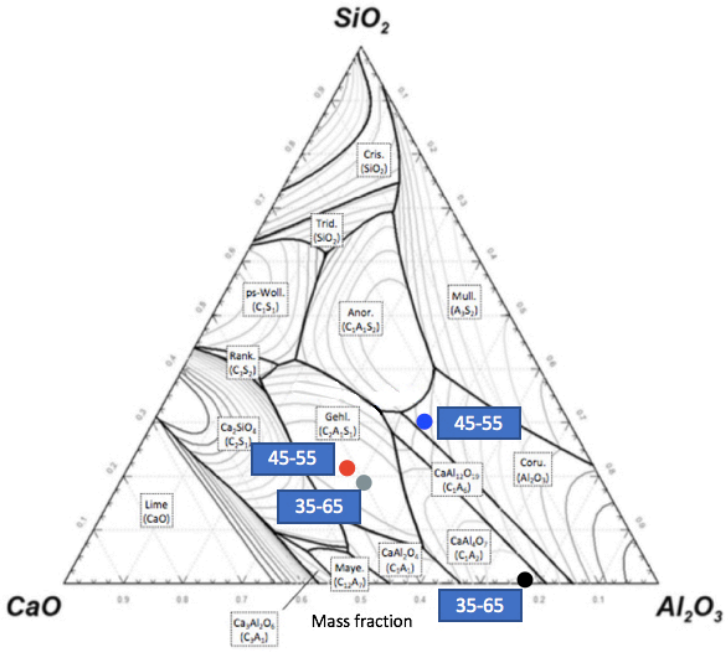

Figure 5.17: Marked phases in the slags after equilibration where the grey circle is the 40-40-20 wt% CaO-Al_2O_3-SiO_2, the black circle is approximately 22-75-1 wt%, CaO-Al_2O_3-SiO_2, the red circle is 41-36-22 wt%, CaO-Al_2O_3-SiO_2, the blue circle is 24-44-30 wt% and CaO-Al_2O_3-SiO_2.

Table 5.12-5.14 shows the composition of the phases present in the 35-65 wt% slag equilibrated with Si. Here, only two phases were present in the slag, whereas FactSage suggests 3-4 phases present. The equilibrium calculations and Scheil-Gulliver calculations are in good agreement besides the experiments with a metal/slag ratio of 1/1. However, the

experimental work in the 1/1 sample is in best agreement with the equilibrium cooling calculations, where FactSage calculated 56.80 wt% melilite, and the experimental results show 68.01 wt% melilite. Considering the $CaAlO_7$ phase, (black point in figure 5.17), the composition is 22-75-1 wt% CaO-Al_2O_3-SiO_2. If not taking the 1% SiO_2 into account, the point would end up in $CaAl_{12}O_{19}$ phase, which seems more reasonable when compared with the modeled results. In the melilite phase, the experimental results are in relatively good agreement with the modeled results. Sample 7.5/1 stood out and was measured with a defocused beam. If the experimentally measured $CaAlO_7$ phase is $CaAl_{12}O_{19}$, the sample with a metal/slag ratio of 1/1 fits best with the equilibrium calculations. However, the rest of the samples shows higher concentrations of the $CaAl_{12}O_{19}$ phase, probably because FactSage measured a third phase, $CaAl_2Si_2O_8$.

Table 5.12: Equilibrium solidification calculations from the 35-65 wt% slag.

Metal/slag ratio	**Melilite**	**$CaAl_4O_7$**	**$CaAl_{12}O_{19}$**	**$CaAl_2Si_2O_8$**
1/1	56.80	13.83	29.37	0
2.5/1	53.04	0	30.70	16.26
5/1	45.78	0	22.05	32.18
7.5/1	41.86	0	16.61	41.75
10/1	38.66	0	12.64	48.70

Table 5.13: Scheil-Gulliver solidification calculations from the 35-65 wt% slag.

Metal/slag ratio	**Melilite**	**$CaAl_4O_7$**	**$CaAl_{12}O_{19}$**	**$CaAl_2Si_2O_8$**
1/1	38.71	50.27	1.83	9.18
2.5/1	53.04	0	30.70	16.26
5/1	45.78	0	22.05	32.18
7.5/1	41.64	0	16.61	41.75
10/1	38.66	0	12.64	48.70

Table 5.14: Experimental results from the 35-65 wt% slag.

Metal/slag ratio	**Gehlenite/ melilite**	**$CaAlO_7$**
1/1	68.01	31.95
2.5/1	46.92	53.08
5/1	56.00	44.00
7.5/1	defocused beam	defocused beam
10/1	36.85	63.15

Table 5.15-5.17 shows the composition of the phases present in the 45-55 wt% slag equilibrated with Si. Only two phases were identified in the slag, whereas the FactSage calculations show the presence of 3-4 phases. In the 5/1 slag, FactSage agrees in both the equilibrium and Scheil-Gulliver solidification calculations. Comparing these to the experimental results, they are in relatively good agreement. The experimental results show 74.69 wt% melilite, while FactSage calculated 60.92 % of this phase. When it comes to the $CaAl_2Si_2O_8$ phase, when plotting it in the $CaO\text{-}Al_2O_3\text{-}SiO_2$ phase diagram, the point ends up at the corundum (Al_2O_3) area. However, the composition of this phase is 24-44-30 wt% $CaO\text{-}Al_2O_3\text{-}SiO_2$, which makes it more reasonable to assume that the phase is $CaAl_2Si_2O_8$, as the phases are close in the phase diagram. If assuming this, the results are in good agreement as well. The present results show 25.31 wt% of the $CaAl_2Si_2O_8$ phase, while FactSage calculated 31.99 wt% of this phase. The 10/1 experiments are also in relatively good agreement with FactSage, where the present work shows 64.84 wt% melilite, and FactSage calculated 52.36 wt%. When it comes to the $CaAl_2Si_2O_8$ phase, EPMA and image analysis determined 35.16 wt% of the phase, while FactSage calculations show an amount of 46.79 wt%.

Table 5.15: Equilibrium solidification calculations from the 45-55 wt% slag.

Metal/slag ratio	**Melilite**	**$CaAl_4O_7$**	**$CaAl_{12}O_{19}$**	**$CaAl_2Si_2O_8$**	**$CaSiO_3$**
1/1	72.78	20.96	6.06	0	0
2.5/1	69.75	0	13.97	16.28	0
5/1	61.27	0	6.92	31.81	0
7.5/1	56.56	0	2.57	40.86	0
10/1	52.36	0	0	46.79	0.86

Table 5.16: Scheil-Gulliver solidification calculations from the 45-55 wt% slag.

Metal/slag ratio	**Melilite**	**$CaAl_4O_7$**	**$CaAl_{12}O_{19}$**	**$CaAl_2Si_2O_8$**	**$CaSiO_3$**
1/1	69.25	28.48	0.38	1.89	0
2.5/1	63.15	13.30	3.92	19.63	0
5/1	60.92	0.70	6.36	31.99	0
7.5/1	56.56	0	2.57	40.86	0
10/1	52.36	0	0	46.79	0.86

Table 5.17: Experimental results from 45-55 wt% slag.

Metal/slag ratio	**Gehlenite/ melilite**	**$CaAl_2Si_2O_8$**
1/1	defocused beam	defocused beam
2.5/1	defocused beam	defocused beam
5/1	74.69	25.31
7.5/1	defocused beam	defocused beam
10/1	64.84	35.16

5.4 Evaluation of Experimental Set Up

The main goal of this thesis was to investigate the equilibrium between Si and CaO-Al_2O_3 slags. All experiments were performed in a closed induction furnace. The heat is applied electrically to the crucible, which makes it easy to control the heat. As the crucible has to be placed in the furnace before heating, the effective holding time was longer than the one hour holding time, as the time was set to start when reaching 1650 °C. The design of the furnace makes it not possible to take out the crucible for controlled cooling, and therefore, after one hour, the power was shut off and cooled to room temperature before opening the furnace and taking it out. The furnace was always evacuated to at least 3.0×10^{-3} mbar, flushed with argon three times before each experiment, and then filled with argon with a purity of 5N or 6N, leading to very low oxygen partial pressures in the system.

The operating temperature is just above the melting temperature of the most Al_2O_3 rich slag; 35-65 wt% CaO-Al_2O_3, and completely melting of all materials were observed after all experiments.

The separation of the metal and the slag was challenging, as relatively large crucibles were used (D_i = 70 mm, h_i = 150 mm), and 24 g of slag were used for each experiment, resulting in a very thin slag layer. Therefore, it was decided to use EPMA as an analyzing method for the slags, because, then, it is possible to mount samples with other parts of the crucible, and still get relatively reliable results even though only the surface is analyzed. If the slag samples were to be analyzed with ICP-MS, there would have been big chances of getting metal contaminations in the slag. One drawback of EPMA as an analysis method for both the slag and the metal is that if the samples are not entirely homogeneous, the results may deviate from the real concentration. However, three points at different areas for each phase present of the sample were measured, and all values were in good agreement. The slag before equilibration was also analyzed with both XRF and EPMA, and those results were also in good agreement.

Calculations based on EPMA analysis and calculated fractions of the phases present with ImageJ by thresholding were done to determine the overall concentrations in the metal and the slag. The threshold method in itself could cause significant errors, as every image is analyzed manually, and based on contrasts in the BSE images. All images should be representative for the whole sample, which may not always be the case.

As mentioned earlier, when preparing the slags, the CaO concentration in the slags was significantly lower than the target composition, due to either hydration or carbonation of

the CaO powder.

5.5 Reproducibility of Results

Two parallels with equal metal/slag ratios with the same slag were conducted for each series, except for the metal/slag ratios 2.5/1, 5/1, and 7.5/1 in equilibrium with 45-55 wt% CaO-Al_2O_3 slag due to time constraints caused by the COVID-19 situation. A 95 % confidence interval was calculated based on the average values between the two replicate splits were calculated for all concentrations presented in the Si metal, and the errors were in general small.

The time needed to reach equilibrium in the system has not been investigated and was assumed to be one hour. As discussed earlier, higher concentrations of Al and Ca were found in the 10/1 metal/slag ratio in the 35-65 wt% slag series, due to measurements very near the slag. This could be an indication of not reaching equilibrium. In the sample with a metal/slag ratio of 2.5/1 in the 35-65 wt% slag series, all oxide concentrations were out of trend, which most likely is due to inhomogeneities in the slag used for this particular experiment.

Chapter 6

Conclusion

SoG silicon was equilibrated with 35-65 wt% CaO-Al_2O_3 and 45-55 wt% CaO-Al_2O_3 slags at 1650 °C. The equilibrium time used was one hour. Different metal/slag ratios were tested; a metal slag ratio of 1/1, 2.5/1, 5/1, 7.5/1, and 10/1, where the mass of the slag was kept constant at 24 g. All experiments were also thermodynamically modeled in FactSage 7.1, and the modeled and experimental results were in relatively good agreement. The concentration trends of Al and Ca are in good agreement with previously published work.

6.1 Distribution of Al and Ca Between Si and CaO-Al_2O_3 Slags

- The concentration of Al and Ca decreases with increasing metal/slag ratios for 35-65 wt% and 45-55 wt% CaO-Al_2O_3 slags. An increase for the metal/slag ratio 10/1 in the 35-65 wt% slag was observed, but this was due to measurements very near the slag and is considered as an exception. For the 35-65 wt% CaO-Al_2O_3 slag series, the Al concentrations were 2.19 $\pm$ 0.23-9.74 $\pm$ 0.14wt% and the Ca concentrations were between 1.08 $\pm$ 0.10-6.13 $\pm$ 0.05 wt%. For the 45-55 wt% CaO-Al_2O_3 slag series, the Al concentrations were 0.38 $\pm$ 0.20- 4.57 $\pm$ 0.02, and the Ca concentrations were between 2.35 $\pm$ 0.02-11.39 $\pm$ 0.10 wt%.

- The activity coefficients of Al and Ca in Si was determined to be in the range γ^0_{Al} = 0.32-1.16 and γ^0_{Ca} = 0.002-0.056 for the 35-65 wt% slag series. In the 45-55 wt% CaO-Al_2O_3 slag series, the activity coefficients were determined to be in the range γ^0_{Al} = 1.43-3.14 and γ^0_{Ca} = 0.001-0.093.

- The obtained SiO_2 concentrations after the equilibria experiments increases with an increased amount of Si in the system. For the 35-65 and 45-55 wt% CaO-Al_2O_3 slags, the concentrations were between 9.83-27.08 wt% and 13.52-26.05 wt%, respectively.

6.2 Identification of Phases Present in Metals and Slags

- In the silicon metal equilibrated with the 35-65 wt% CaO-Al_2O_3 slag, three prominent phases were present; a Si_2Al_2Ca phase, one Al-rich phase, which were determined to be fcc Al, and the Si-matrix with $\sim$ 100 % Si.
- In the silicon metal equilibrated with the 45-55 wt% CaO-Al_2O_3 slag , three prominent phases were present; one Si_2Ca phase, one Si_2Al_2Ca phase and the Si-matrix.
- The area fractions (assumed to be equal to volume fractions) of the phases were calculated, and in general, the amount of phases decreases with increasing metal/slag ratio.
- The identification of the phases were in good agreement with the modeled results from FactSage.
- In the 35-65 wt% slag series, the Si_2Al_2Ca, the fraction of the phase was in the range 2.71 $\pm$ 0.99 - 16.44 $\pm$ 4.72 %, whereas the results from FactSage were in the range 2.76-12.42 %. The experimental results showed no presence of the Si_2Ca phase, while FactSage showed the presence of the Si_2Ca phase for the 1/1 and 2.5/1 experiments with 4.56 wt% and 0.79 wt%, respectively. The Al-rich phase was assumed to be in the range 0.5-1 wt% from highest to lowest metal/slag ratio, while FactSage showed no presence of the Al-rich phase in the 1/1 and 2.5/1 metal/slag ratio experiments, and from experiment 5/1-10/1, the fraction of the Al-rich phase was in the range 0.15-0.30 wt%. The fraction of the Si-matrix was experimentally determined to be between 83.56 $\pm$ 4.72 - 97.35 $\pm$ 4.13 wt%, while the fractions from FactSage were in the range 83.00-96.89 wt%.
- In the 45-55 wt% slag series, the fraction of the Si_2Al_2Ca phase was in the range 0.60$\pm$ 0.35 - 8.64 $\pm$ 1.92 wt%. Modeled results from FactSage showed that the Si_2Al_2Ca phase was in the range 3.13-12.00 wt%. The fraction of the Si_2Ca phase was in the range 3.43 $\pm$ 0.82 - 13.60 $\pm$ 1.17. Modeled results from FactSage showed that the Si_2Ca phase was in the range 3.43-13.60 wt%. The fraction of the Si-matrix was determined to be between 77.75 $\pm$ 3.09 - 95.95 $\pm$ 1.17. From the modeled

results from FactSage, the Si-matrix fraction was determined to be 74.00-95.77 wt%.

- Two phases were observed in the slags, which was determined to be melilite and a $CaAl_{12}O_{19}$ phase with fractions of 36.85-68.01 wt% and 31.94-63.15 wt%, respectively. In the 45-55 wt% slag, the phases were determined to be melilite and $CaAl_2Si_2O_8$, with fractions of 64.84-74.69 wt% and 25.31-35.16 wt%, respectively.
- Solidification calculations from FACTSAGE showed the presence of three to four phases in the slags. However, with respect to the observed phases experimentally, the results were in reasonable agreement.

Chapter 7

Future Work

The equilibrium time needed for this system should be investigated to determine if one hour is enough time to reach equilibrium. This can be done by measuring the concentration gradients of Al and Ca in the Si metal as a function of time. It would be interesting to investigate the effect of temperature in this system and to see how the Al and Ca concentrations possibly may be affected by temperature when Si is in equilibrium with CaO-Al_2O_3 slags.

Different metal/slag ratios could also be investigated and compared with the same ratios used in this work. For example, using the same ratios as this work, only more slag than metal, to see how it affects the Al and Ca concentrations in the metal.

Different slag compositions could also be investigated, and since the concentration of CaO in the more CaO-rich slag was lower than anticipated, it would be an interesting extension of this work to see how the system changes when the concentration of CaO is higher than Al_2O_3.

Bibliography

[1] Michael Schmela, Raffaele Rossi, Naomi Chevillard, Mariano Guillén Paredes, and Máté Heisz. Global Market Outlook 2019-2023. In *SolarPower Europe*, 2019.

[2] Dr Simon Philipps, Fraunhofer Ise, Werner Warmuth, and PSE Projects GmbH. Photovoltaics Report. page 48, 2020.

[3] G. Tranell. SiSal Pilot: Innovative pilot for Silicon production with low environmental impact using secondary Aluminium and silicon raw materials, 2019.

[4] C. W. Bale, P. Chartrand, S. A. Degterov, G. Eriksson, K. Hack, R. Ben Mahfoud, J. Melançon, A. D. Pelton, and S. Petersen. FactSage thermochemical software and databases. *Calphad*, 26(2):189–228, June 2002.

[5] Johan Tuset, Anders Schei, and Halvard Tveit. *Production of high silicon alloys*. Tapir, 1998.

[6] European Commision. Communication from the commission to the European parliament, the council, the European economic and social committee and the committee of the regions, 2014.

[7] CRM Alliance. Silicon Metal, 2017.

[8] EU ETC. The EU Emissions Trading System, 2020.

[9] MarketsandMarkets™. Silicone Market worth $28.6 billion by 2024. 2019.

[10] Arnulf Jaeger-Waldau. PV Status Report 2017. In *EU Science Hub - European Commission*, November 2017.

[11] Roskill Information Services Ltd. Silicon & Ferrosilicon: Outlook to 2029, 17th edition. 2020.

[12] Ida Kero, Svend Grådahl, and Gabriella Tranell. Airborne Emissions from Si/FeSi Production. *JOM*, 69(2):365–380, February 2017.

[13] Seshadri Seetharaman. *Treatise on process metallurgy, volume 3: industrial processes*, volume 3. Newnes, 2013.

[14] T Lindstad, S E Olsen, and G Tranell. Greenhouse gas emissions from ferroalloy production. page 10.

[15] B. Ozturk and R. J. Fruehan. The rate of formation of SiO by the reaction of CO or H2 with silica and silicate slags. *Metallurgical Transactions B*, 16(4):801–806, December 1985.

[16] Davy Humphry. XXIII. Electro-chemical researches, on the decomposition of the earths; with observations on the metals obtained from the alkaline earths, and on the amalgam procured from ammonia | Philosophical Transactions of the Royal Society of London. *Royal Society*, 98, January 1808.

[17] Fathi Habashi. Metallothemic reactions - Past, Present and Future. *Research and Reports on Metals*, 2(1):1–16, 2018.

[18] Zhenyu Xing, Jun Lu, and Xiulei (ORCID:0000000246499594) Ji. A Brief Review of Metallothermic Reduction Reactions for Materials Preparation. *Small Methods*, 2(12), August 2018.

[19] Kyoung Hwan Kim, Dong Jin Lee, Kyeong Min Cho, Seon Joon Kim, Jung-Ki Park, and Hee-Tae Jung. Complete magnesiothermic reduction reaction of vertically aligned mesoporous silica channels to form pure silicon nanoparticles. *Scientific Reports*, 5(1):1–7, March 2015. Number: 1 Publisher: Nature Publishing Group.

[20] L. Batchelor, A. Loni, L. T. Canham, M. Hasan, and J. L. Coffer. Manufacture of Mesoporous Silicon from Living Plants and Agricultural Waste: An Environmentally Friendly and Scalable Process. *Silicon*, 4(4):259–266, October 2012.

[21] Kouji Yasuda and Toru H. Okabe. Solar-grade silicon production by metallothermic reduction. *JOM*, 62(12):94–101, December 2010.

[22] J. Dietl and C. Holm. New Aspects in Aluminothermic Reduction of SiO2. *Seventh E.C. Photovoltaic Solar Energy Conference*, pages 726–730, 1987.

[23] Michael V. Glazoff, Vadim S. Zolotorevsky, and Nikolai A. Belov. *Casting Aluminum Alloys*. Elsevier, July 2010.

[24] In-Ho Jung, Sergei A. Decterov, and Arthur D. Pelton. Critical thermodynamic evaluation and optimization of the CaO–MgO–SiO2 system. *Journal of the European Ceramic Society*, 25(4):313–333, April 2005.

[25] Bengt Hallstedl. Assessment of the CaO-Al2O3 System. *Journal of the American Ceramic Society*, 73(1):15–23, January 1990. Publisher: John Wiley & Sons, Ltd.

[26] Huahai Mao, Malin Selleby, and Bo Sundman. A re-evaluation of the liquid phases in the CaO–Al2O3 and MgO–Al2O3 systems. *Calphad*, 28(3):307–312, September 2004.

[27] Murray D. Johnston, Leili Tafaghodi Khajavi, Mark Li, Samira Sokhanvaran, and Mansoor Barati. High-Temperature Refining of Metallurgical-Grade Silicon: A Review. *JOM*, 64(8):935–945, August 2012.

[28] Yoshio Waseda and J. M. Toguri. *The Structure and Properties of Oxide Melts: Application of Basic Science to Metallurgical Processing*. World Scientific, 1998. Google-Books-ID: j626wvLSWSYC.

[29] Huahai Mao, Mats Hillert, Malin Selleby, and Bo Sundman. Thermodynamic Assessment of the CaO–Al2O3–SiO2 System. *Journal of the American Ceramic Society*, 89(1):298–308, 2006. _eprint: https://ceramics.onlinelibrary.wiley.com/doi/pdf/10.1111/j.1551-2916.2005.00698.x.

[30] Young Seok Lee, Dong Joon Min, Sung Mo Jung, and Sang Ho Yi. Influence of Basicity and FeO Content on Viscosity of Blast Furnace Type Slags Containing FeO. *ISIJ International*, 44(8):1283–1290, 2004.

[31] J.-F. Xu, T. Zeng, M.-Q. Sheng, C. Jie, K. Wan, and J.-Y. Zhang. Viscosity of low silica CaO–5MgO–Al2O3–SiO2 slags. *Ironmaking & Steelmaking*, 41(7):486–492, August 2014. Publisher: Taylor & Francis _eprint: https://doi.org/10.1179/1743281213Y.0000000142.

[32] R. Roscoe. The viscosity of suspensions of rigid spheres. *British Journal of Applied Physics*, 3(8):267–269, August 1952.

[33] Lars Klemet Jakobsson. *Distribution of boron between silicon and CaO-SiO2, MgO-SiO2, CaO-MgO-SiO2 and CaO-Al2O3-SiO2 slags at 1600 C.* PhD thesis, Norwegian University of Science and Technology, 2013.

[34] *Schlackenatlas = Slag atlas*. Verlag Stahleisen, Düsseldorf, 1981.

[35] Ethem.T. Turkdogan. *Physiochemical Properties of Slags and Glasses*. Metals Society, 298. London, 1983.

[36] Dimitrios Siafakas, Taishi Matsushita, Anders Eric Wollmar Jarfors, Shinya Hakamada, and Masahito Watanabe. Viscosity of SiO2–CaO–Al2O3 Slag with Low Silica – Influence of CaO/Al2O3, SiO2/Al2O3 Ratio. *ISIJ International*, 58(12):2180–2185, 2018.

[37] T. Matsushita, T. Watanabe, M. Hayashi, and K. Mukai. Thermal, optical and surface/interfacial properties of molten slag systems. *International Materials Reviews*, 56(5-6):287–323, November 2011. Publisher: Taylor & Francis _eprint: https://doi.org/10.1179/1743280411Y.0000000007.

[38] Haiping Sun, Naoya Yoneda, Kunihiko Nakashima, and Katsumi Mori. Interfacial tensions between CaO-SiO2-Al2O3 slag and Fe-O-S, Fe-Si, Fe-Al, Fe-C, Fe-Cr or Fe-Ni alloys. *Tetsu-To-Hagane/Journal of the Iron and Steel Institute of Japan*, 83(1):1–6, 1997. Publisher: .

[39] Tarek El Gammal, Hans-Jörg Schrinner, and Erwin Wosch. Influence of carbon, silicon and molybdenum on the separating and emulsifying behaviour of steel and slag. *Steel Research*, 67(4):138–143, 1996. _eprint: https://onlinelibrary.wiley.com/doi/pdf/10.1002/srin.199605470.

[40] Haiping Sun, Kunihiko Nakashima, and Katsumi Mori. Influence of Slag Composition on Slag–Iron Interfacial Tension. *ISIJ International*, 46(3):407–412, 2006.

[41] Seung Hwan Ahn, Lars Klemet Jakobsson, and Gabriella Tranell. Distribution of Calcium and Aluminum Between Molten Silicon and Silica-Rich CaO-Al2O3-SiO2 Slags at 1823 K (1550 °C). *Metallurgical and Materials Transactions B*, 48(1):308–316, February 2017.

[42] Christophe Dumay and Michel Allibert. Distribution of Al and Ca between ferrosilicons and CaO-Al2O3-SiO2 slags at 1450°C. *Scandinavian Journal of Metallurgy*, 31(2):107–114, April 2002. Publisher: John Wiley & Sons, Ltd.

[43] T. Engh, C. Simensen, and O. Wijk. *Principles of metal refining*. Oxford University Press Inc. 1992.

[44] I.A. Goncharov, E.O. Paton Electric Welding Institute, NASU, V.I. Galinich, E.O. Paton Electric Welding Institute, NASU, D.D. Mishchenko, E.O. Paton Electric Welding Institute, NASU, V.S. Sudavtsova, and I.M. Frantsevich Institute of Problems of Materials Science, NASU. Prediction of thermodynamical properties of melts of the CaO-Al_2O_3 system. *The Paton Welding Journal*, 2014(4):26–29, April 2014.

[45] Mitsuru Tanahashi, Toshiharu Fujisawa, and Chikabumi Yamauchi. Oxidative Removal of Boron from Molten Silicon by CaO-based Flux Treatment with Oxygen Gas Injection. *Metallurgical and Materials Transactions B*, 45(2):629–642, April 2014.

[46] David R. Gaskell. *Introduction to the thermodynamics of materials*. Taylor & Francis, March 2008. Google-Books-ID: cBwoAQAAMAAJ.

[47] Xin Lu, Takahiro Miki, Takehito Hiraki, Hongmin Zhu, and Tetsuya Nagasaka. Thermodynamics of Elements in Dilute Silicon Melts. *JOM*, 71(4):1456–1470, April 2019.

[48] P. D. Desai. Thermodynamic Properties of Selected Binary Aluminum Alloy Systems. *Journal of Physical and Chemical Reference Data*, 16(1):109–124, January 1987. Publisher: American Institute of Physics.

[49] Takahiro Miki, Kazuki Morita, and Nobuo Sano. Thermodynamic properties of aluminum, magnesium, and calcium in molten silicon. *Metallurgical and Materials Transactions B*, 29(5):1043–1049, October 1998.

[50] Takahiro Miki, Kazuki Morita, and Nobuo Sano. Thermodynamic Properties of Si–Al, –Ca, –Mg Binary and Si–Ca–Al, –Ti, –Fe Ternary Alloys. *Materials Transactions, JIM*, 40(10):1108–1116, 1999.

[51] Larry Kaufman. Coupled phase diagrams and thermochemical data for transition metal binary systems-VI. *Calphad*, 3(1):45–76, January 1979.

[52] K. Iwata, T. Matsumiya, H. Sawada, and K. Kawakami. Prediction of thermodynamic properties of solute elements in Si solutions using first-principles calculations. *Acta Materialia*, 51(2):551–559, January 2003.

[53] Kai Liu, Jijun Wu, Kuixian Wei, Wenhui Ma, Keqiang Xie, Shaoyuan Li, Bin Yang, and Yongnian Dai. Application of molecular interaction volume model on removing impurity aluminum from metallurgical grade silicon by vacuum volatilization. *Vacuum*, 114:6–12, April 2015.

[54] Jafar Safarian, Leiv Kolbeinsen, and Merete Tangstad. Thermodynamic activities in silicon binary melts. *Journal of Materials Science*, 47(14):5561–5580, July 2012.

[55] J. C. Anglezio, C. Servant, and I. Ansara. Contribution to the experimental and thermodynamic assessment of the Al-Ca-Fe-Si system—I. Al-Ca-Fe, Al-Ca-Si, Al-Fe-Si and Ca-Fe-Si systems. *Calphad*, 18(3):273–309, July 1994.

[56] J. R. Wynnyckyj and L. M. Pidgeon. Activities in the Ca-Si system. *Metallurgical Transactions*, 2(4):975–978, April 1971.

[57] E. C. de Oliveira Pinto and C. Takano. Activity of calcium in dilute liquid Si-Ca alloy. *Metallurgical and Materials Transactions B*, 31(6):1267–1272, December 2000.

[58] Arthur D. Pelton. The polynomial representation of thermodynamic properties in dilute solutions. *Metallurgical and Materials Transactions B*, 28(5):869–876, October 1997.

[59] Carl Wagner. *Thermodynamics of Alloys*. Number 4 in Addison-Wesley metallurgy series. Addison-Wesley, Cambridge Mass, 1952.

[60] LS. Darken. Thermodynamics of binary metallic solutions. *Trans. Met. Soc. AIME*, 239:80–89, 1967.

[61] Kazuki Morita, Kousuke Kume, and Nobuo Sano. A Newly Developed Method for Determining SiO_2 Activity of the Silicate Slags Equilibrated with Molten Silicon Alloys. *ISIJ International*, 40(6):554–560, 2000.

[62] Torsten Weiss and Klaus Schwerdtfeger. Chemical equilibria between silicon and slag melts. *Metallurgical and Materials Transactions B*, 25(4):497–504, August 1994.

[63] H. Fujiwara, Liang Yin. Yuan, K. Miyata, E. Ichise, and R. Otsuka. Distribution equilibria of the metallic elements and boron between Si based liquid alloys and CaO-Al2O3-SiO2 fluxes. *Distribution equilibria of the metallic elements and boron between Si based liquid alloys and CaO-Al2O3-SiO2 fluxes*, 60(1):65–71, 1996. Place: Sendai Publisher: Nippon Kinzoku Gakkai.

[64] Richard H Rein and John Chipman. Activities in liquid solution SiO2-CaO-Al2O3 at 1600 degrees C. *Transactions of the Metallurgical Society of AIME*, 233(2):415, 1965.

[65] Kazuki Morita, Kousuke Kume, and Nobuo Sano. Activity measurement of silicate slags equilibrated with molten silicon alloys. *Scandinavian Journal of Metallurgy*, 31(3):178–183, 2002. _eprint: https://onlinelibrary.wiley.com/doi/pdf/10.1034/j.1600-0692.2002.310303.x.

[66] YoungJo Kang, Du Sichen, and Kazuki Morita. Activities of SiO_2 in Some $CaO–Al_2O_3–SiO_2$(–10%MgO) Melts with Low SiO_2 Contents at 1873 K. *ISIJ International*, 47(6):805–810, 2007.

[67] C. W. Bale, E. Bélisle, P. Chartrand, S. A. Decterov, G. Eriksson, K. Hack, I. H. Jung, Y. B. Kang, J. Melançon, A. D. Pelton, C. Robelin, and S. Petersen. FactSage thermochemical software and databases — recent developments. *Calphad*, 33(2):295–311, June 2009.

[68] J. C. Anglézio, C. Servant, and F. Dubrous. Characterization of metallurgical grade silicon. *Journal of Materials Research*, 5(9):1894–1899, September 1990. Publisher: Cambridge University Press.

[69] T. Margaria. Intermetallic Compounds in Metallurgical Silicon. *INFACON 6*, pages 209–214, 1992.

[70] Maria Førde Møll. *Solidification of Silicon: Macro- and Microstructure as Functions of Thermal History and Composition*. PhD thesis, Norges teknisk-naturvitenskapelige universitet, Fakultet for naturvitenskap og teknologi, Institutt for materialteknologi, 2014. Accepted: 2014-12-19T13:28:07Z.

[71] Caroline A. Schneider, Wayne S. Rasband, and Kevin W. Eliceiri. NIH Image to ImageJ: 25 years of image analysis. *Nature Methods*, 9(7):671–675, July 2012. Number: 7 Publisher: Nature Publishing Group.

[72] Geoffrey K. Sigworth. Thermodynamics of dilute liquid silicon alloys. *Canadian Metallurgical Quarterly*, 0(0):1–11, May 2020. Publisher: Taylor & Francis _eprint: https://doi.org/10.1080/00084433.2020.1771012.

[73] Weizhong Ding and Sverre E. Olsen. Manganese and Silicon Distribution between Slag and Metal in Silicomanganese Production. *ISIJ International*, 40(9):850–856, 2000.

Appendices

A EPMA-Analysis

Here will all EPMA-results be presented. In the metal samples, one point on three different areas of the sample of each phase was measured. Table 1 shows the composition of the Si metal equilibrated with 35-65 wt% CaO-Al_2O_3 slag. The white phase was determined to be Si_2Al_2Ca, the light-grey phase is the Si-matrix, and the dark-grey phase is fcc Al. Table 2 shows the composition on the Si metal equilibrated with 45-55 wt% CaO-Al_2O_3 slag. The white phase, light-grey phase, and the dark grey phase were determined to be Si_2Ca, Si_2Al_2Ca, and the Si-matrix, respectively. Table 3 and 4 shows the composition of the 35-65 wt% and 45-55 wt% slag, respectively after equilibration with Si metal. One point on each phase at three different areas of the samples was measured. Some of the slag structures were very fine and therefore analyzed with a defocused beam, and then three points at random areas were measured.

Table 1: EPMA-analysis of the Si-metal equilibrated with 35-65 wt% CaO-Al_2O_3 slag. One point on three different areas of the sample of each phase was measured. All values are given in wt%.

Sample	Si	Al	Ca	Comment
35-65-24-1.1	37.757	36.421	26.952	
35-65-24-1.2	37.857	36.241	26.463	White phase
35-65-24-1.3	37.762	36.388	26.843	
35-65-24-1.4	100.075	0.02	0	
35-65-24-1.5	99.827	0.011	0.001	Light-grey phase
35-65-24-1.6	99.962	0.032	0.025	
35-65-24-1.7	1.774	97.881	0.63	
35-65-24-1.8	2.345	97.78	0.308	Dark-grey phase
35-65-24-1.9	1.665	98.162	0.587	
35-65-24-2.1	39.114	36.392	27.308	
35-65-24-2.2	39.406	36.04	27.011	White phase

35-65-24-2.3	39.282	36.09	27.145	
35-65-24-2.4	100.587	0.04	0.026	
35-65-24-2.5	100.183	0.023	0	Light-grey phase
35-65-24-2.6	100.456	0.085	0.01	
35-65-24-2.7	2.031	97.506	0.312	
35-65-24-2.8	2.027	97.393	0.222	Dark-grey phase
35-65-24-2.9	1.883	97.493	0.362	
35-65-60-1.1	37.458	36.33	26.627	
35-65-60-1.2	37.786	36.245	26.534	White phase
35-65-60-1.3	38.093	36.325	26.554	
35-65-60-1.4	99.064	0.054	0.023	
35-65-60-1.5	99.123	0.008	0	Light-grey phase
35-65-60-1.6	99.032	0.009	0	
35-65-60-1.7	2.215	95.086	0.129	
35-65-60-1.8	2.37	95.518	0.126	Dark-grey phase
35-65-60-1.9	3.191	94.832	0.494	
35-65-60-2.1	37.878	36.556	26.603	
35-65-60-2.2	37.79	36.884	26.842	White phase
35-65-60-2.3	37.411	36.581	26.816	
35-65-60-2.4	99.668	0.026	0.02	
35-65-60-2.5	99.406	0.003	0	Light-grey phase
35-65-60-2.6	99.397	0.012	0.024	
35-65-60-2.7	2.982	97.816	0.181	
35-65-60-2.8	2.851	97.993	0.211	Dark-grey phase
35-65-60-2.9	3.131	96.643	0.212	
35-65-120-1.1	38.857	35.912	26.499	
35-65-120-1.2	39.017	35.933	26.367	White phase
35-65-120-1.3	39.305	35.712	26.177	
35-65-120-1.4	99.866	0.025	0.031	
35-65-120-1.5	100.018	0.04	0.037	Light-grey phase
35-65-120-1.6	99.376	0	0	
35-65-120-1.7	3.03	97.673	0.243	
35-65-120-1.8	3.389	97.697	0.236	Dark-grey phase
35-65-120-1.9	1.776	97.953	0.348	

35-65-120-2.1	38.447	36.424	27.029	
35-65-120-2.2	38.646	36.335	26.942	White phase
35-65-120-2.3	38.67	36.066	26.725	
35-65-120-2.4	100.087	0.023	0.059	
35-65-120-2.5	99.838	0.018	0	Light-grey phase
35-65-120-2.6	99.698	0.018	0.006	
35-65-120-2.7	2.527	95.072	0.074	
35-65-120-2.8	2.657	97.391	0.065	Dark-grey phase
35-65-120-2.9	2.397	97.609	0.149	
35-65-180-1.1	37.93	36.462	26.89	
35-65-180-1.2	38.639	36.279	27.163	White phase
35-65-180-1.3	38.233	36.453	26.838	
35-65-180-1.4	99.747	0.045	0.015	
35-65-180-1.5	99.671	0.014	0.031	Light-grey phase
35-65-180-1.6	99.35	0	0	
35-65-180-1.7	2.785	97.08	0.164	
35-65-180-1.8	2.849	97.268	0.155	Dark-grey phase
35-65-180-1.9	2.457	97.311	0.278	
35-65-180-2.1	38.424	36.037	26.598	
35-65-180-2.2	38.737	35.791	26.712	White phase
35-65-180-2.3	38.607	35.422	26.654	
35-65-180-2.4	98.925	0.036	0.058	
35-65-180-2.5	98.602	0	0.002	Light-grey phase
35-65-180-2.6	99.128	0.001	0	
35-65-180-2.7	3.105	96.852	0.079	
35-65-180-2.8	3.899	97.033	0.045	Dark-grey phase
35-65-180-2.9	3.148	96.791	0.132	
35-65-240-1.1	39.044	36.001	26.582	
35-65-240-1.2	39.218	35.72	26.813	White phase
35-65-240-1.3	38.671	36.173	26.747	
35-65-240-1.4	99.694	0.004	0.014	
35-65-240-1.5	99.429	0.022	0.003	Light-grey phase
35-65-240-1.6	99.599	0.022	0.012	
35-65-240-1.7	2.201	98.191	0.22	

35-65-240-1.8	2.11	98.182	0.261	Dark-grey phase
35-65-240-1.9	2.123	98.39	0.207	
35-65-240-2.1	35.144	36.573	26.772	
35-65-240-2.2	34.956	36.614	27.007	White phase
35-65-240-2.3	35.059	36.233	26.371	
35-65-240-2.4	100.094	0.034	0.021	
35-65-240-2.5	100.025	0.077	0.074	Light-grey phase
35-65-240-2.6	99.679	0.031	0.037	
35-65-240-2.7	2.127	98.08	0.129	
35-65-240-2.8	1.886	98.142	0.153	Dark-grey phase
35-65-240-2.9	1.793	98.627	0.198	

Table 2: EPMA-analysis of the Si-metal equilibrated with 45-55 wt% CaO-Al_2O_3 slag. Three points on each phase at different areas of the samples were measured. All values are given in wt%.

Sample	Si	Al	Ca	Comment
45-55-24-1.1	57.544	0.921	41.903	
45-55-24-1.2	58.165	0.766	41.993	White phase
45-55-24-1.3	57.938	0.777	41.494	
45-55-24-1.4	36.339	35.958	26.833	
45-55-24-1.5	35.551	35.697	26.939	Light-grey phase
45-55-24-1.6	34.893	36.358	26.987	
45-55-24-1.7	100.275	0.075	0.048	
45-55-24-1.8	100.14	0.01	0.027	Dark-grey phase
45-55-24-1.9	99.945	0.004	0	
45-55-24-2.1	58.197	0.876	42.063	
45-55-24-2.2	58.254	0.916	42.262	White phase
45-55-24-2.3	57.868	1.024	41.775	
45-55-24-2.4	38.518	35.787	27.106	
45-55-24-2.5	38.731	35.762	26.982	Light-grey phase
45-55-24-2.6	38.426	35.882	27.302	
45-55-24-2.7	100.354	0.022	0.025	
45-55-24-2.8	100.19	0.011	0	Dark-grey phase
45-55-24-2.9	100.135	0.006	0	
45-55-60-1.1	57.062	1.121	41.957	
45-55-60-1.2	57.183	1.004	41.807	White phase
45-55-60-1.3	57.237	0.799	41.947	
45-55-60-1.4	37.835	36.391	26.758	
45-55-60-1.5	37.933	36.37	26.749	Light-grey phase
45-55-60-1.6	37.806	36.446	26.827	
45-55-60-1.7	99.628	0.005	0.036	
45-55-60-1.8	99.847	0.019	0	Dark-grey phase
45-55-60-1.9	99.479	0.056	0.057	
45-55-120-1.1	58.083	0.982	42.137	
45-55-120-1.2	58.314	1.015	42.05	White phase
45-55-120-1.3	58.105	1.095	42.203	
45-55-120-1.4	38.623	35.943	27.334	
45-55-120-1.5	38.564	36.116	27.072	Light-grey phase

45-55-120-1.6	38.799	35.897	27.324	
45-55-120-1.7	100.602	0.061	0.091	
45-55-120-1.8	100.424	0.03	0.03	Dark-grey phase
45-55-120-1.9	100.389	0.048	0.069	
45-55-180-1.1	58.245	1.103	42.198	
45-55-180-1.2	58.491	1.035	41.397	White phase
45-55-180-1.3	58.572	0.977	42.067	
45-55-180-1.4	39.384	35.627	27.052	
45-55-180-1.5	39.174	35.577	27.369	Light-grey phase
45-55-180-1.6	39.13	35.625	27.202	
45-55-180-1.7	100.677	0.075	0.116	
45-55-180-1.8	100.812	0.024	0.019	Dark-grey phase
45-55-180-1.9	100.617	0.003	0.05	
45-55-240-1.1	57.415	1.171	41.315	
45-55-240-1.2	57.743	1.201	41.48	White phase
45-55-240-1.3	57.427	1.641	41.372	
45-55-240-1.4	37.996	36.111	26.903	
45-55-240-1.5	38.24	36.223	26.787	Light-grey phase
45-55-240-1.6	38.699	36.084	27.005	
45-55-240-1.7	100.029	0.02	0.014	
45-55-240-1.8	99.437	0.013	0.017	Dark-grey phase
45-55-240-1.9	99.922	0.083	0.019	
45-55-240-2.1	58.072	1.075	41.715	
45-55-240-2.2	58.367	0.781	41.886	White phase
45-55-240-2.3	57.951	0.913	41.112	
45-55-240-2.4	38.752	35.796	26.761	
45-55-240-2.5	38.925	35.827	26.656	Light-grey phase
45-55-240-2.6	38.402	35.488	26.959	
45-55-240-2.7	100.285	0.063	0.078	
45-55-240-2.8	100.188	0.011	0	Dark-grey phase
45-55-240-2.9	100.291	0.022	0	

Table 3: EPMA-analysis of the 35-65 wt% slag after equilibrated with Si metal. One point on each phase at three different areas of the samples was measured. All values are given in wt%. Some of the structures were very fine and analyzed with a defocused beam, and then only three points at random areas were measured.

Sample	SiO_2	Al_2O_2	CaO	Comment
35-65-24-2.1	15.209	42.573	40.08	
35-65-24-2.2	15.592	42.983	39.953	Light phase
35-65-24-2.3	15.721	41.905	40.986	
35-65-24-2.4	0.957	74.769	22.134	
35-65-24-2.5	0.99	75.045	22.218	Dark phase
35-65-24-2.6	0.808	75.251	22.158	
35-65-60-1.1	22.103	37.753	38.222	
35-65-60-1.2	23.596	37.673	35.763	Light phase
35-65-60-1.3	21.399	36.183	39.985	
35-65-60-1.4	0.917	75.704	21.957	
35-65-60-1.5	0.828	75.74	21.643	Dark phase
35-65-60-1.6	0.881	75.72	21.859	
35-65-60-2.1	15.485	46.407	37.115	
35-65-60-2.2	16.253	45.347	37.198	Light phase
35-65-60-2.3	17.981	41.662	39.295	
35-65-60-2.4	1.206	75.632	22.044	
35-65-60-2.5	1.161	75.972	21.835	Dark phase
35-65-60-2.6	0.913	75.682	22.027	
35-65-120-1.1	21.286	36.649	40.589	
35-65-120-1.2	21.039	36.725	40.859	Light phase
35-65-120-1.3	22.136	36.742	41.103	
35-65-120-1.4	1.007	76.029	21.937	
35-65-120-1.5	1.368	74.974	21.745	Dark phase
35-65-120-1.6	0.884	76.04	21.806	
35-65-120-2.1	17.477	49.348	31.744	
35-65-120-2.2	18.046	49.497	30.971	Defocused beam
35-65-120-2.3	18.109	48.736	31.759	
35-65-180-1.1	19.228	49.158	31.191	Defocused beam
35-65-180-1.2	19.682	48.799	30.519	
35-65-180-1.3	19.076	48.947	30.416	

35-65-180-1.4	19.682	47.867	30.869	Defocused beam
35-65-180-1.5	19.516	47.967	30.676	
35-65-180-1.6	18.596	48.695	30.475	
35-65-180-2.1	20.467	37.293	41.155	
35-65-180-2.2	20.508	37.262	40.925	Light phase
35-65-180-2.3	20.59	37.389	41.186	
35-65-180-2.4	20.428	47.057	30.517	
35-65-180-2.5	20.99	47.589	29.882	Dark phase
35-65-180-2.6	22.036	50.989	24.647	
35-65-240-2.1	22.105	36.327	40.669	
35-65-240-2.2	21.224	36.662	41.391	Light phase
35-65-240-2.3	22.213	37.943	38.884	
35-65-240-2.4	29.89	43.552	25.171	
35-65-240-2.5	29.552	43.682	25.123	Dark phase
35-65-240-2.6	29.368	43.786	25.238	

Table 4: EPMA-analysis of the 45-55 wt% after equilibrated with Si metal. One point on each phase at three different areas of the samples was measured. All values are given in wt%. Some of the structures were very fine and analyzed with a defocused beam, and then only three points at random areas were measured.

Sample	SiO_2	Al_2O_2	CaO	Comment
45-55-24-1.1	13.87	45.989	38.906	
45-55-24-1.2	13.66	45.922	39.428	Defocused beam
45-55-24-1.3	13.891	45.461	39.472	
45-55-24-2.1	13.198	46.731	39.723	
45-55-24-2.2	13.231	45.789	39.579	Defocused beam
45-55-24-2.3	13.294	46.495	40.037	
45-55-60-1.1	17.172	44.423	39.595	
45-55-60-1.2	17.489	45.132	38.456	Defocused beam
45-55-60-1.3	16.988	45.846	38.786	
45-55-120-1.1	22.073	35.821	41.175	
45-55-120-1.2	21.848	35.861	41.197	Light phase
45-55-120-1.3	21.473	35.807	41.15	
45-55-120-1.4	30.367	43.15	24.22	
45-55-120-1.5	30.137	43.526	23.784	Dark phase
45-55-120-1.6	29.659	43.901	23.634	
45-55-180-1.1	20.582	42.895	37.282	
45-55-180-1.2	20.346	42.818	37.388	Defocused beam
45-55-180-1.3	20.506	42.88	37.641	
45-55-240-1.1	29.056	32.139	36.765	
45-55-240-1.2	27.915	32.657	36.991	Defocused beam
45-55-240-1.3	28.678	32.475	36.328	
45-55-240-2.1	22.68	37.663	41.379	
45-55-240-2.2	22.883	37.448	41.538	Light phase
45-55-240-2.3	23.224	37.513	40.721	
45-55-240-2.4	32.878	44.501	24.092	
45-55-240-2.5	32.899	43.993	23.927	Dark phase
45-55-240-2.6	32.995	44.184	23.872	

B BSE-Images

All metal samples were imaged with BSE. Here, all all images taken will be shown.

B.1 BSE-Images: Si-metal equilibrated with 35-65 wt% CaO-Al_2O_3 Slag

The white, light-grey and dark-grey phases is Si_2Al_2Ca, the Si-matrix and fcc Al, respectively.

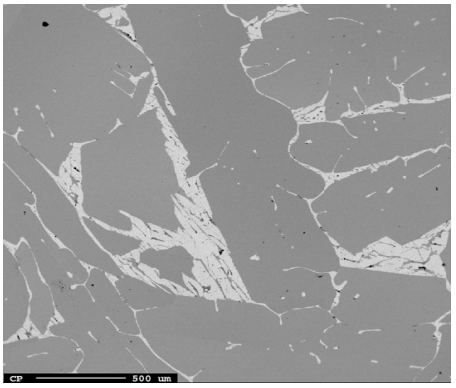

(a) BSE-Image of sample 35-65-24-1 taken at 40x.

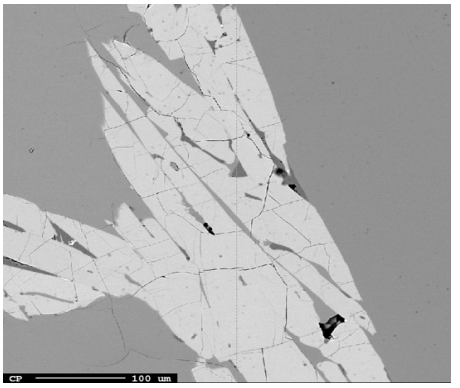

(b) BSE-Image of sample 35-65-24-1 taken at 200x.

Figure 1: BSE-images of sample 35-65-24-1 taken at (a) 40 x and (b) 200x.

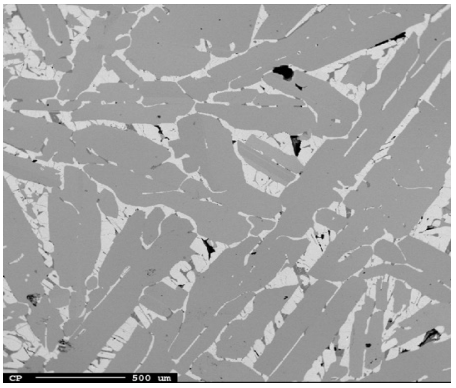

(a) BSE-Image of sample 35-65-24-2 taken at 40x.

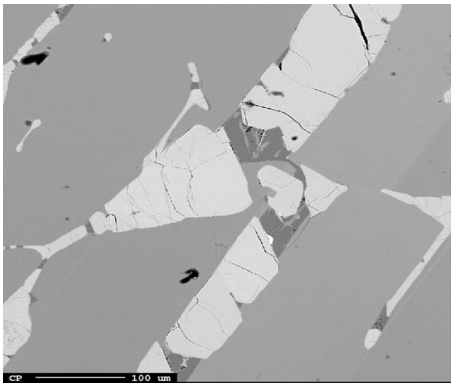

(b) BSE-Image of sample 35-65-24-2 taken at 200x.

Figure 2: BSE-images of sample 35-65-24-2 taken at (a) 40 x and (b) 200x.

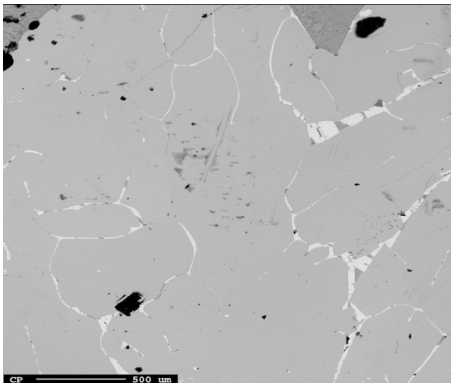

(a) BSE-Image of sample 35-65-60-1 taken at 40x.

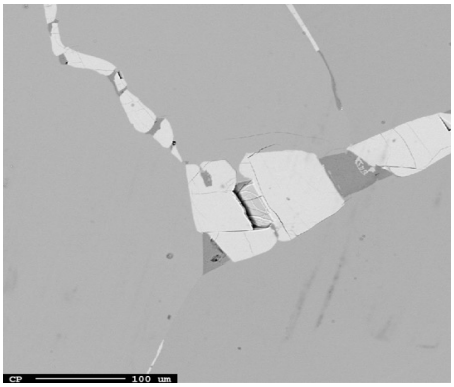

(b) BSE-Image of sample 35-65-60-1 taken at 200x.

Figure 3: BSE-images of sample 35-65-60-1 taken at (a) 40 x and (b) 200x.

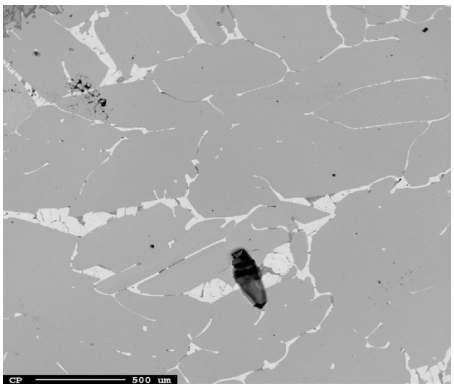

(a) BSE-Image of sample 35-65-60-2 taken at 40x.

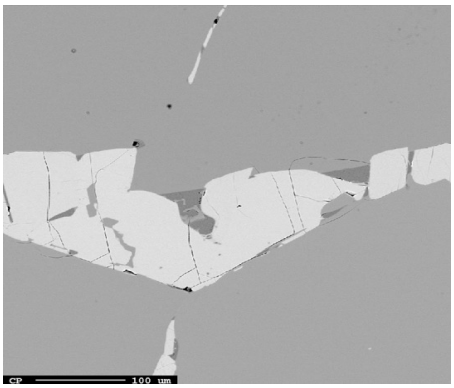

(b) BSE-Image of sample 35-65-60-2 taken at 200x.

Figure 4: BSE-images of sample 35-65-60-2 taken at (a) 40 x and (b) 200x.

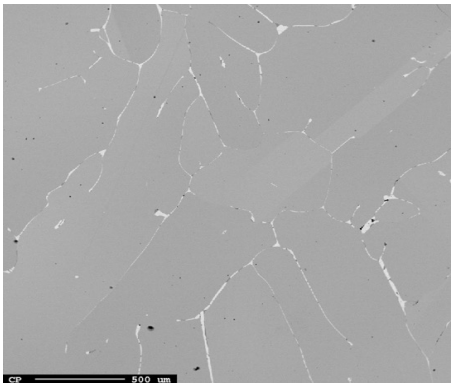

(a) BSE-Image of sample 35-65-120-1 taken at 40x.

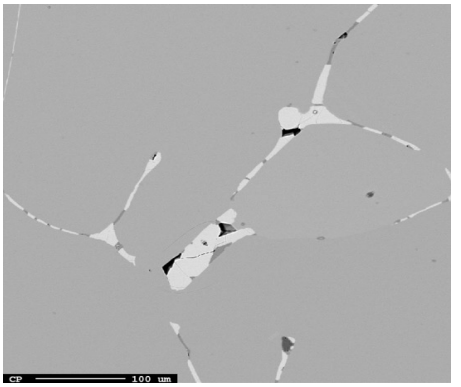

(b) BSE-Image of sample 35-65-120-1 taken at 200x.

Figure 5: BSE-images of sample 35-65-120-1 taken at (a) 40 x and (b) 200x.

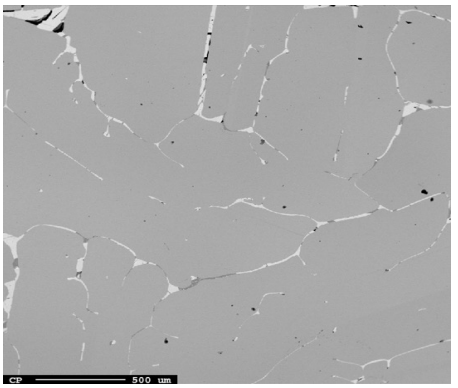

(a) BSE-Image of sample 35-65-120-2 taken at 40x.

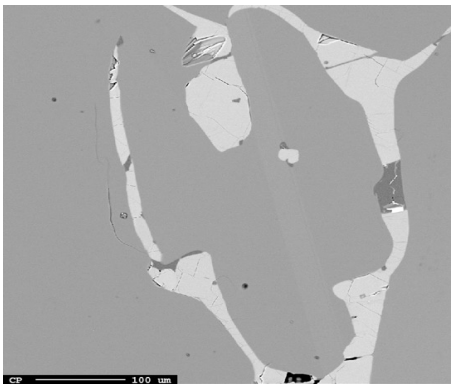

(b) BSE-Image of sample 35-65-120-2 taken at 200x.

Figure 6: BSE-images of sample 35-65-120-2 taken at (a) 40 x and (b) 200x.

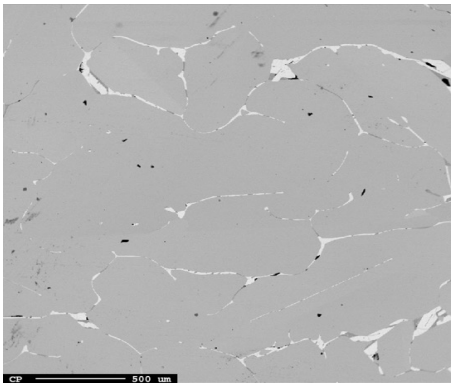

(a) BSE-Image of sample 35-65-180-1 taken at 40x.

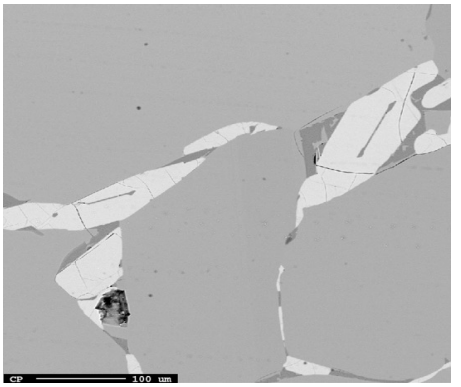

(b) BSE-Image of sample 35-65-180-1 taken at 200x.

Figure 7: BSE-images of sample 35-65-180-1 taken at (a) 40 x and (b) 200x.

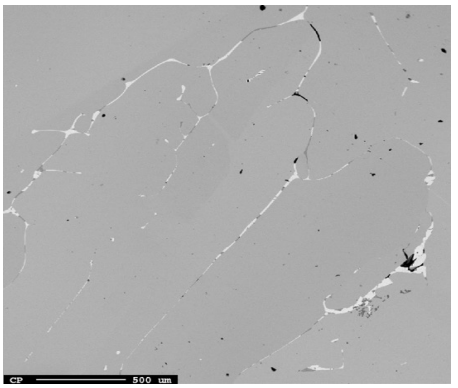

(a) BSE-Image of sample 35-65-180-2 taken at 40x.

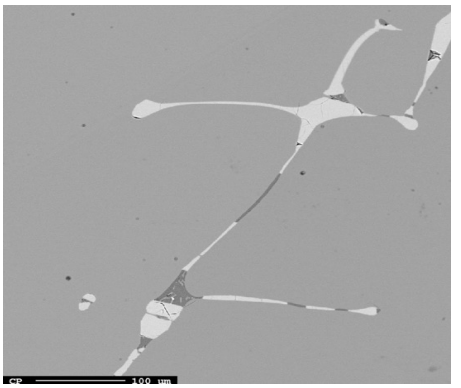

(b) BSE-Image of sample 35-65-180-2 taken at 200x.

Figure 8: BSE-images of sample 35-65-180-2 taken at (a) 40 x and (b) 200x.

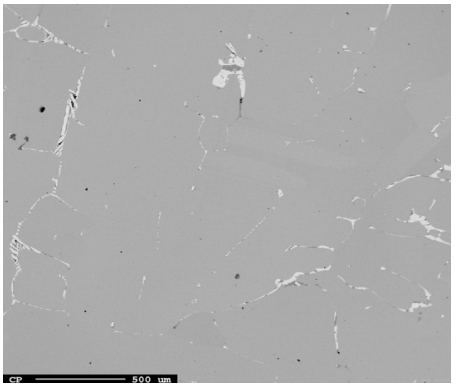

(a) BSE-Image of sample 35-65-240-1 taken at 40x.

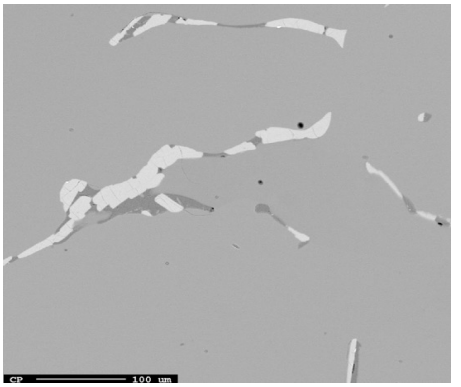

(b) BSE-Image of sample 35-65-240-1 taken at 200x.

Figure 9: BSE-images of sample 35-65-240-1 taken at (a) 40 x and (b) 200x.

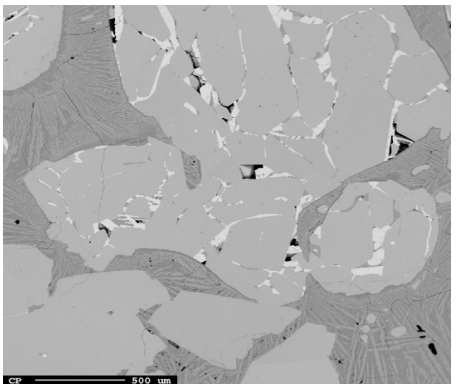

(a) BSE-Image of sample 35-65-240-2 taken at 40x.

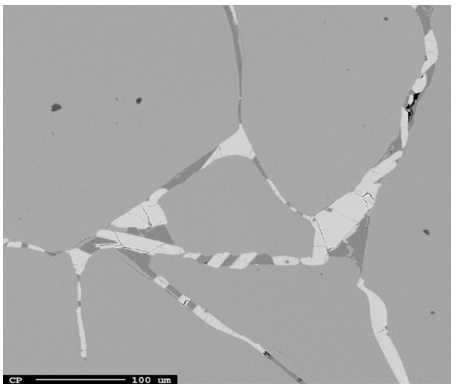

(b) BSE-Image of sample 35-65-240-2 taken at 200x.

Figure 10: BSE-images of sample 35-65-240-2 taken at (a) 40 x and (b) 200x.

B.2 BSE-Images: Si-metal equilibrated with 45-55 wt% CaO-Al_2O_3 slag

The white, light-grey and dark-grey phase is Si_2Ca, Si_2Al_2Ca, and the Si-matrix, respectively.

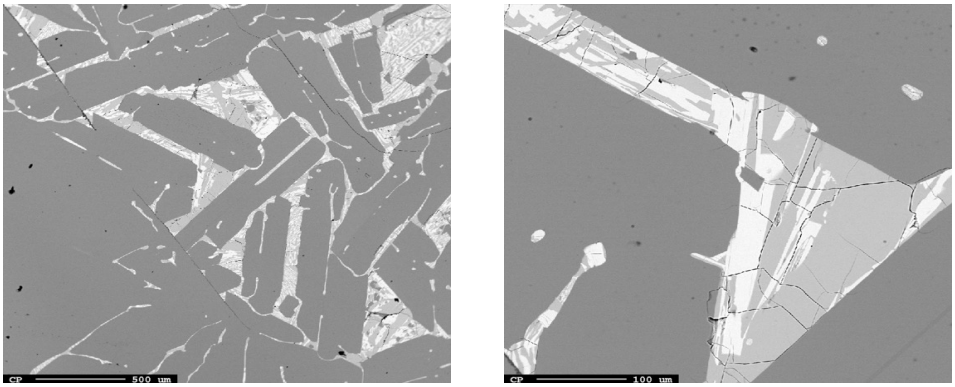

(a) BSE-Image of sample 45-55-24-1 taken at 40x. **(b)** BSE-Image of sample 45-55-24-1 taken at 200x.

Figure 11: BSE-images of sample 45-55-24-1 taken at (a) 40 x and (b) 200x.

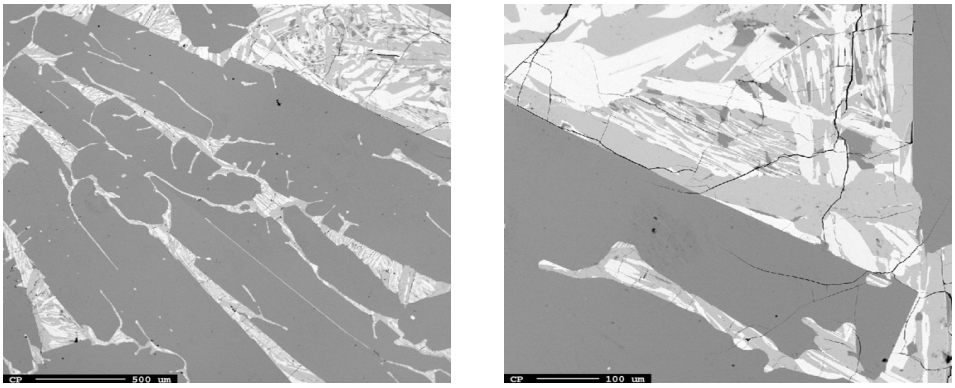

(a) BSE-Image of sample 45-55-24-2 taken at 40x. **(b)** BSE-Image of sample 45-55-24-2 taken at 200x.

Figure 12: BSE-images of sample 45-55-24-2 taken at (a) 40 x and (b) 200x.

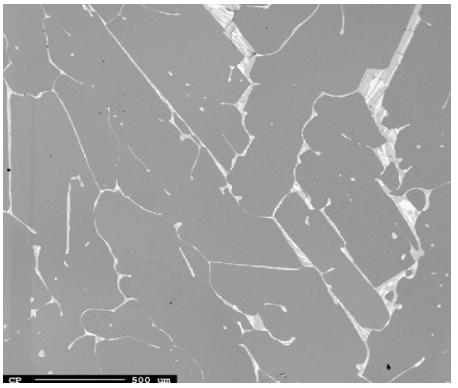

(a) BSE-Image of sample 45-55-60-1 taken at 40x.

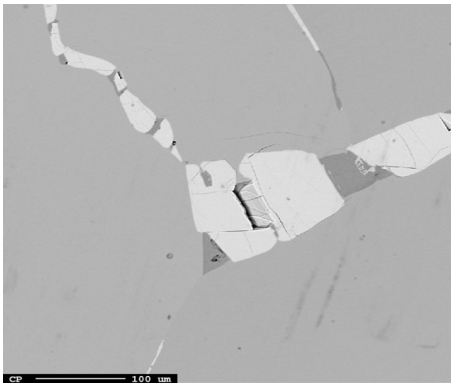

(b) BSE-Image of sample 45-55-60-1 taken at 200x.

Figure 13: BSE-images of sample 45-55-60-1 taken at (a) 40 x and (b) 200x.

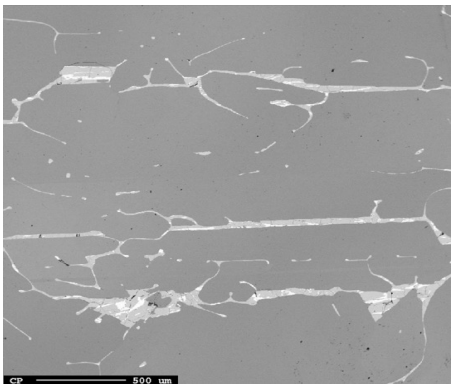

(a) BSE-Image of sample 45-55-120-1 taken at 40x.

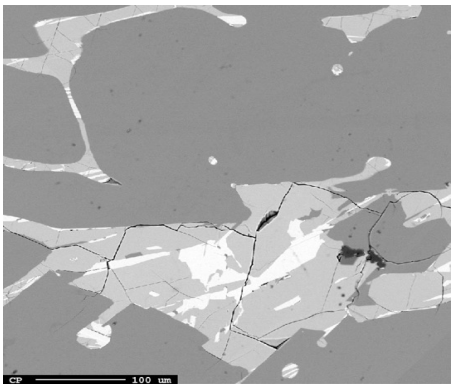

(b) BSE-Image of sample 45-55-120-1 taken at 200x.

Figure 14: BSE-images of sample 45-55-120-1 taken at (a) 40 x and (b) 200x.

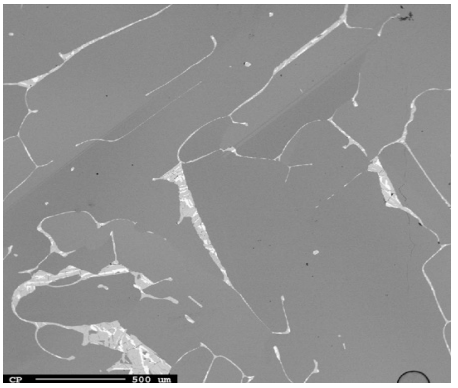

(a) BSE-Image of sample 45-55-180-1 taken at 40x.

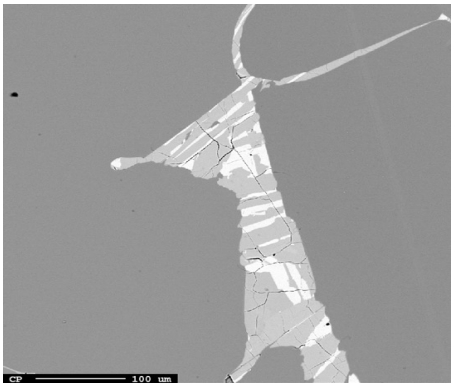

(b) BSE-Image of sample 45-55-180-1 taken at 200x.

Figure 15: BSE-images of sample 45-55-180-1 taken at (a) 40 x and (b) 200x.

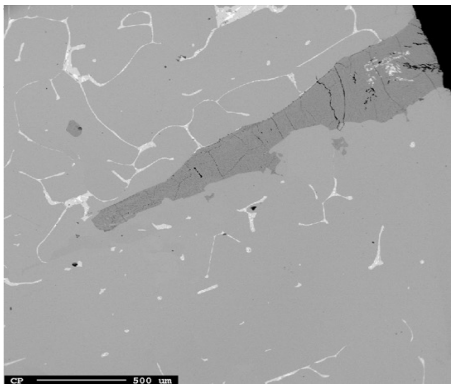

(a) BSE-Image of sample 45-55-240-1 taken at 40x.

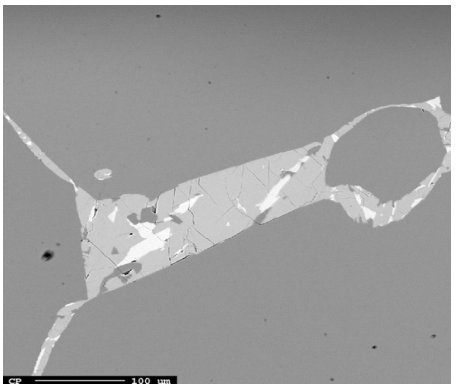

(b) BSE-Image of sample 45-55-240-1 taken at 200x.

Figure 16: BSE-images of sample 45-55-240-1 taken at (a) 40 x and (b) 200x.

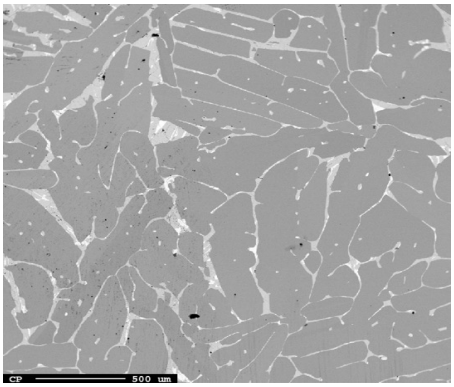

(a) BSE-Image of sample 45-55-240-2 taken at 40x.

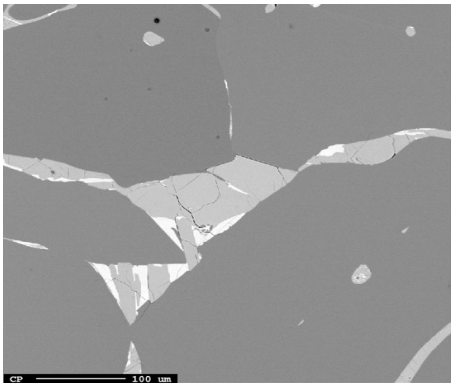

(b) BSE-Image of sample 45-55-240-2 taken at 200x.

Figure 17: BSE-images of sample 45-55-240-2 taken at (a) 40 x and (b) 200x.

C Binary Images from ImageJ

Area fractions of all phases were done with the threshold function in ImageJ. [71] It was assumed that the area fraction was equal to the volume fraction of the phase. The measured area is the white area in the pictures.

C.1 Binary images: Si-metal equilibrated with 35-65 wt% $CaO\text{-}Al_2O_3$ slag

The white phase is the Si_2Al_2Ca phase and the black phase is the Si-matrix.

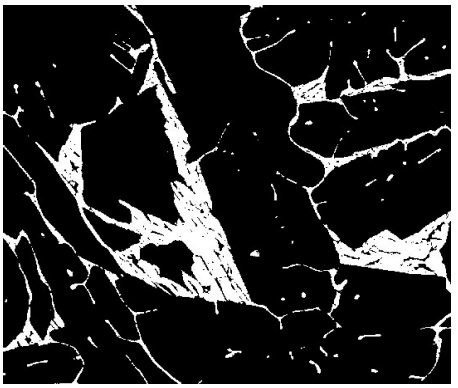

(a) Binary image of sample 35-65-24-1 analyzed at 40x.

(b) Binary image of sample 35-65-24-2 analyzed at 40x.

Figure 18: Binary images of samples 35-65-24-1 and 35-65-24-2 (1/1 metal/slag ratio).

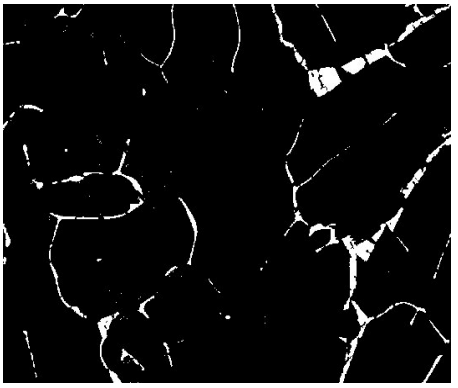

(a) Binary image of sample 35-65-60-1 analyzed at 40x.

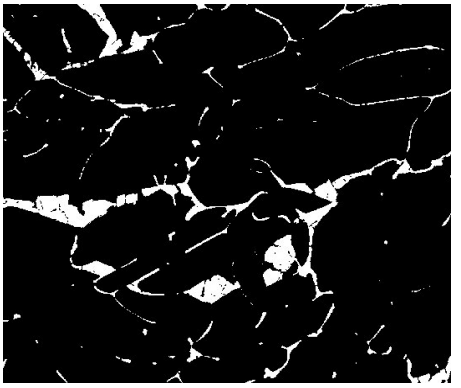

(b) Binary image of sample 35-65-60-2 analyzed at 40x.

Figure 19: Binary images of samples 35-65-60-1 and 35-65-60-2 (2.5/1 metal/slag ratio).

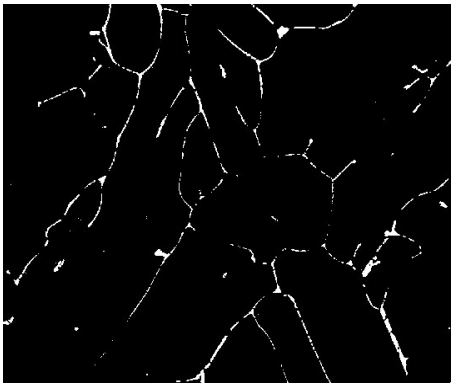

(a) Binary image of sample 35-65-120-1 analyzed at 40x.

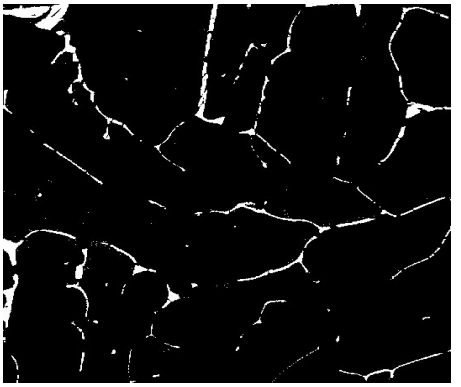

(b) Binary image of sample 35-65-120-2 analyzed at 40x.

Figure 20: Binary images of samples 35-65-120-1 and 35-65-120-2 (5/1 metal/slag ratio).

(a) Binary image of sample 35-65-180-1 analyzed at 40x.

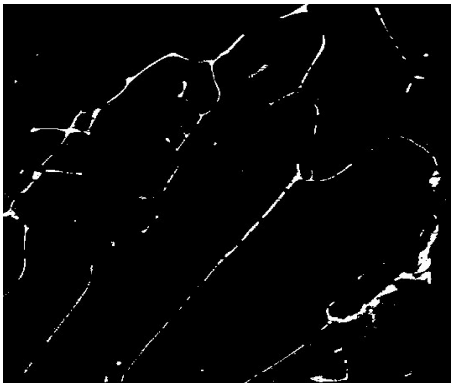

(b) Binary image of sample 35-65-180-2 analyzed at 40x.

Figure 21: Binary images of samples 35-65-180-1 and 35-65-180-2 (7.5/1 metal/slag ratio).

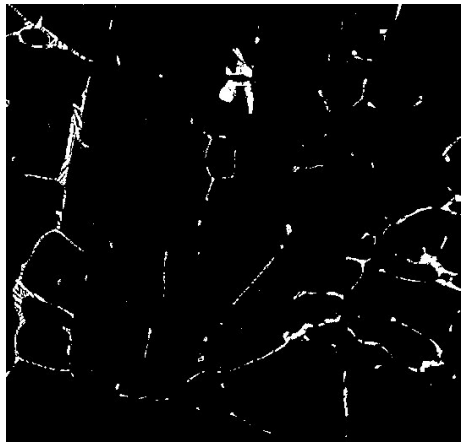

Figure 22: Binary image of sample 35-65-240-1 (metal/slag ratio 10/1).

The area fraction on the was only calculated for one parallel for the samples 35-65-240, since sample 35-65-240-2 was imaged both with slag and metal.

C.2 Binary images: Si-metal equilibrated with 45-55 wt% $CaO\text{-}Al_2O_3$ slag

The area fraction of the phases in the Si metal equilibrated with 45-55 wt% $CaO\text{-}Al_2O_3$ slag were calculated by first, calculating the total area of the white and light-grey phase, and then calculating the area fraction for only the white phase. Where the white phase is Si_2Ca+Si_2Al_2Ca and the black phase is the Si-matrix. To find the total area fraction of the light-grey phase, the area of the white phase was subtracted from the area of the light-grey phase + the white phase.

(a) Total area of the white and light-grey phase in sample 45-55-24-1. Analyzed at 40x.

(b) Total area of the white phase in sample 45-55-24-1. Analyzed at 40x.

Figure 23: Binary images of sample 35-65-24-1 (1/1 metal/slag ratio).

(a) Total area of the white and light-grey phase in sample 45-55-24-2. Analyzed at 40x.

(b) Total area of the white phase in sample 45-55-24-2. Analyzed at 40x.

Figure 24: Binary images of sample 35-65-24-1 (1/1 metal/slag ratio).

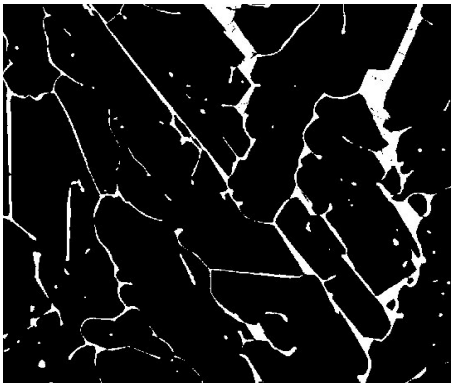

(a) Total area of the white and light-grey phase in sample 45-55-60-1. Analyzed at 40x.

(b) Total area of the white phase in sample 45-55-60-1. Analyzed at 40x.

Figure 25: Binary images of sample 45-55-60-1 (2.5/1 metal/slag ratio).

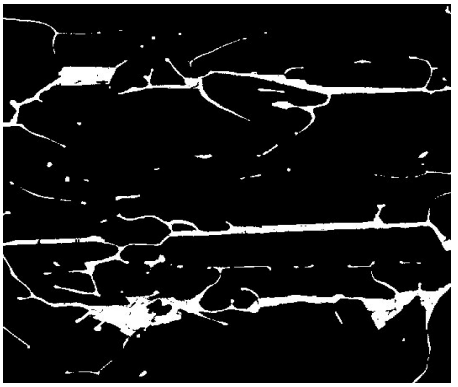

(a) Total area of the white and light-grey phase in sample 45-55-120-1. Analyzed at 40x.

(b) Total area of the white phase in sample 45-55-120-1. Analyzed at 40x.

Figure 26: Binary images of sample 45-55-120-1 (5/1 metal/slag ratio).

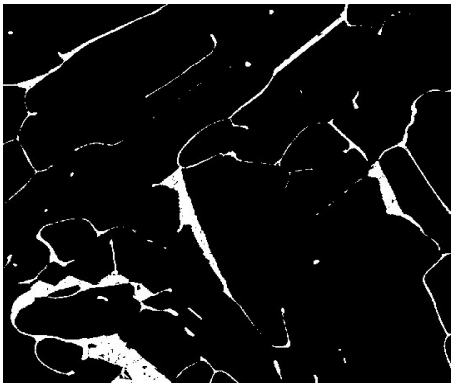

(a) Total area of the white and light-grey phase in sample 45-55-180-1. Analyzed at 40x.

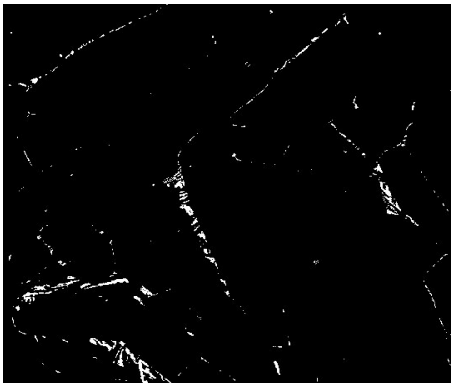

(b) Total area of the white phase in sample 45-55-180-1. Analyzed at 40x.

Figure 27: Binary images of sample 45-55-180-1 (7.5/1 metal/slag ratio).

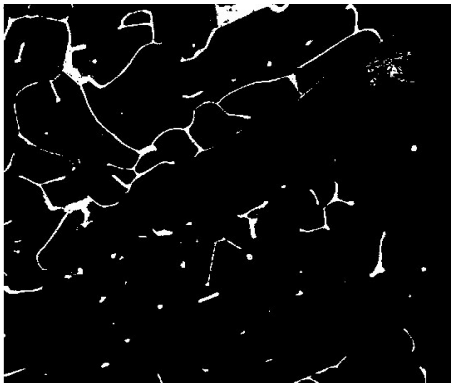

(a) Total area of the white and light-grey phase in sample 45-55-240-1. Analyzed at 40x.

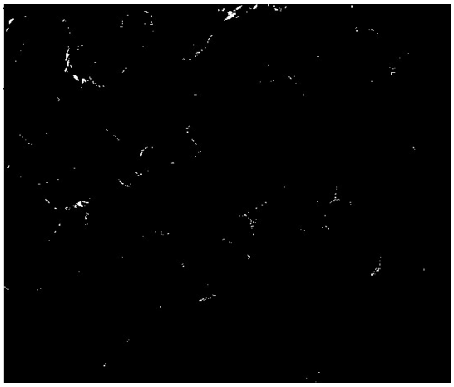

(b) Total area of the white phase in sample 45-55-240-1. Analyzed at 40x.

Figure 28: Binary images of sample 45-55-240-1 (10/1 metal/slag ratio).

(a) Total area of the white and light-grey phase in sample 45-55-240-2. Analyzed at 40x.

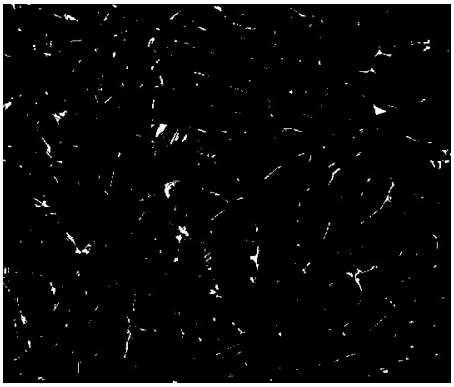

(b) Total area of the white phase in sample 45-55-240-2. Analyzed at 40x.

Figure 29: Binary images of sample 45-55-240-2 (10/1 metal/slag ratio).

D Statistical Analysis

Statistical analysis on the EPMA- and area fractions were performed. A confidence interval of 95 % was used, with a student t-distribution. All deviations are based on the average from two replicate splits, and the results were 95 % confidence interval are calculated, the results are written as the averaged values plus/minus the deviation. When assuming a normal distribution of the data, the upper and lower confidence limits (UCL and LCL) can be written as:

$$UCL_{1-\alpha} = \bar{X}_n + t_{n-1,\frac{\alpha}{2}} \times \frac{S_n}{\sqrt{n}} \tag{1}$$

$$LCL_{1-\alpha} = \bar{X}_n - t_{n-1,\frac{\alpha}{2}} \times \frac{S_n}{\sqrt{n}} \tag{2}$$

Where, $\bar{X}_n$ is the average value of between to replicate splits, t is found from the t-distribution table, n is the number of observations, α is the chosen confidence interval (0.05), and S_n is the standard deviation between the two averaged values.

D.1 Example Calculation

Here, an example calculation of how the 95 % confidence interval was calculated will be shown here. The parameters are for the Si concentration measured by EPMA in the white, mixed phase (Si_2Al_2Ca) in the Si metal equilibrated with 35-65 wt% CaO-Al_2O_3 slag for samples 35-65-24-1 and 35-65-24-2. One point was analyzed on three random areas of the same phase for each sample.

Table 5: Parameters for calculating a 95 % confidence interval of the amount of Si in the mixed, white phase (Si_2Al_2Ca) in the Si metal equilibrated with 35-65 wt% CaO-Al_2O_3 slag for samples 35-65-24-1 and 35-65-24-2.

Analysis number	X_1	$\bar{X}_1$	S_1	X_2	$\bar{X}_2$	S_2
1	37.757	37.792	0.046	39.114	39.267	0.120
2	37.857			39.406		
3	37.762			39.282		

Since there was two parallels analyzed, n=2. The average between the two parallels are 38.53, while the averaged standard deviation is 0.0967. From the t-distribution table, when

n=2 and $\alpha = 0.05$, the t-value is 12.706. Inserting these values into equation (1) and (2), the concentration of Si in the Si_2Al_2Ca phase after equilibration with 35-65 wt% CaO-Al_2O_3 slag is 38.53 ± 0.13.

E Solidification Calculations with FactSage

Solidification calculations were performed in FactSage for all experiments. Here, only the metal/slag ratios 1/1 and 10/1 will be presented from each series as much of it looks similar.

E.1 Si metal after equilibration with 35-65 wt% CaO-Al_2O_3 Slag

Metal slag ratio of 1/1:

```
EQUILIBRIUM COOLING

COMPONENTS:
[35_65_1_to_1_liq]          AMOUNT/gram =  2.5101E+01

CONSTITUENTS AND PHASES AT 917.29 C
(temperature of final disappearance of LIQUID)

CONS. PHASE                    TOTAL AMT/g.atom TOTAL AMT/gram
  1   1 Slag-liq                  2.2223E-15     -4.4553E-14
TOTAL:                          2.2223E-15     -4.4553E-14

  2   1 CaAl4O7_solid(s)         -1.6806E-15      6.6250E-15
TOTAL:                          -1.6806E-15      6.6250E-15

  2A  1 CaAl4O7_solid(s)         -2.1464E-14      8.4612E-14
TOTAL:                          -2.1464E-14      8.4612E-14

  3   1 Si_diamond_A4(s)          6.4103E-01      1.8004E+01
  3   2 CaAl4O7_solid(s)         -1.6955E-15      6.6838E-15
TOTAL:                          6.4103E-01      1.8004E+01

  4   1 Si_diamond_A4(s)          1.0195E-04      2.8633E-03
  4   2 CaAl2O4_solid(s)          2.8054E-04      6.3338E-03
TOTAL:                          3.8249E-04      9.1971E-03

  4A  1 Si_diamond_A4(s)          6.7503E-02      1.8959E+00
  4A  2 CaAl2O4_solid(s)          6.6025E-07      1.4907E-05
TOTAL:                          6.7504E-02      1.8959E+00

  5   1 Si_diamond_A4(s)          3.0702E-04      8.6228E-03
  5   2 CaSi2_C12_hR18_R-3m(s)    1.4398E-03      4.6192E-02
  5   3 CaAl2O4_solid(s)          5.1286E-10      1.1579E-08
TOTAL:                          1.7468E-03      5.4814E-02

  6   1 Si_diamond_A4(s)          3.2897E-02      9.2393E-01
  6   2 CaSi2_C12_hR18_R-3m(s)    3.4210E-02      1.0976E+00
  6   3 CaAl2Si2_P3m1(s)          1.0374E-01      3.1165E+00
  6   4 CaAl2O4_solid(s)          1.3602E-07      3.0709E-06
TOTAL:                          1.7084E-01      5.1380E+00

                               TOTAL AMT/g.atom TOTAL AMT/gram
Slag-liq                        2.2223E-15     -4.4553E-14
Si_diamond_A4(s)                7.4184E-01      2.0835E+01
CaSi2_C12_hR18_R-3m(s)          3.5650E-02      1.1437E+00
CaAl2Si2_P3m1(s)                1.0374E-01      3.1165E+00
CaAl2O4_solid(s)                2.8134E-04      6.3518E-03
CaAl4O7_solid(s)               -2.4841E-14      9.7921E-14

('Double-Click' on any phase listed above to recycle it through EQUILIB)

SUMMARY OF REACTIONS

Cooling
1650 to 1650.00 C      (DELTA H = -5.6942E-07 J)
LIQUID cooling

Constituent 1
1650.00 to 1640.68 C   (DELTA H = -2.3039E+02 J)
LIQUID -> Slag-liq
```

```
Constituent 2
1640.67 C (isothermal) (DELTA H = -4.4879E-01 J)
LIQUID + Slag-liq -> CaAl4O7_solid(s)

Constituent 2A
1640.67 to 1367.59 C   (DELTA H = -6.7105E+03 J)
LIQUID -> CaAl4O7_solid(s)

Constituent 3
1367.59 to 1131.75 C   (DELTA H = -3.7789E+04 J)
LIQUID -> Si_diamond_A4(s) + CaAl4O7_solid(s)

Constituent 4
1131.75 to 1131.63 C   (DELTA H = -7.7186E+00 J)
LIQUID + CaAl4O7_solid(s) -> Si_diamond_A4(s) + CaAl2O4_solid(s)

Constituent 4A
1131.63 to 918.41 C    (DELTA H = -8.3525E+03 J)
LIQUID -> Si_diamond_A4(s) + CaAl2O4_solid(s)

Constituent 5
918.41 to 917.29 C     (DELTA H = -8.2721E+01 J)
LIQUID -> Si_diamond_A4(s) + CaSi2_C12_hR18_R-3m(s) + CaAl2O4_solid(s)

Constituent 6
917.29 C (isothermal)  (DELTA H = -5.0921E+03 J)
LIQUID -> Si_diamond_A4(s) + CaSi2_C12_hR18_R-3m(s) + CaAl2Si2_P3m1(s) + CaAl2O4_solid(s)

COMPOSITION OF PHASES IN CONSTITUENTS AT 917.29 C
(temperature of final disappearance of LIQUID)

Constituent 1
Slag-liq
                                MOLE FRACTION   MASS FRACTION
Ca                                1.6110E-01      2.8249E-01
Si                                1.1508E-06      1.4141E-06
Al                                2.7112E-01      3.2005E-01
O                                 5.6778E-01      3.9745E-01
                                TOTAL AMT/g.atom TOTAL AMT/gram
                                   2.2223E-15     -4.4553E-14
Constituent 2
CaAl4O7_solid(s)
                                MOLE FRACTION   MASS FRACTION
Ca                                1.7056E-01      6.5789E-01
Al                                6.8222E-01      1.7716E+00
O                                 1.1939E+00      1.8384E+00
                                TOTAL AMT/g.atom TOTAL AMT/gram
                                  -1.6806E-15      6.6250E-15
Constituent 2A
CaAl4O7_solid(s)
                                MOLE FRACTION   MASS FRACTION
Ca                                1.7056E-01      6.5789E-01
Al                                6.8222E-01      1.7716E+00
O                                 1.1939E+00      1.8384E+00
                                TOTAL AMT/g.atom TOTAL AMT/gram
                                  -2.1464E-14      8.4612E-14
Constituent 3
Si_diamond_A4(s)
                                MOLE FRACTION   MASS FRACTION
Si                                1.0000E+00      1.0000E+00
```

```
                                MOLE FRACTION   MASS FRACTION
Si                                1.0000E+00      1.0000E+00
                               TOTAL AMT/g.atom TOTAL AMT/gram
                                  6.4103E-01      1.8004E+01

CaAl4O7_solid(s)
                                MOLE FRACTION   MASS FRACTION
Ca                                1.7056E-01      6.5788E-01
Al                                6.8223E-01      1.7716E+00
O                                 1.1939E+00      1.8384E+00
                               TOTAL AMT/g.atom TOTAL AMT/gram
                                 -1.6955E-15      6.6838E-15

Constituent 4
Si_diamond_A4(s)
                                MOLE FRACTION   MASS FRACTION
Si                                1.0000E+00      1.0000E+00
                               TOTAL AMT/g.atom TOTAL AMT/gram
                                  1.0195E-04      2.8633E-03

CaAl2O4_solid(s)
                                MOLE FRACTION   MASS FRACTION
Ca                                1.4286E-01      2.5360E-01
Al                                2.8571E-01      3.4145E-01
O                                 5.7143E-01      4.0495E-01
                               TOTAL AMT/g.atom TOTAL AMT/gram
                                  2.8054E-04      6.3338E-03

Constituent 4A
Si_diamond_A4(s)
                                MOLE FRACTION   MASS FRACTION
Si                                1.0000E+00      1.0000E+00
                               TOTAL AMT/g.atom TOTAL AMT/gram
                                  6.7503E-02      1.8959E+00

CaAl2O4_solid(s)
                                MOLE FRACTION   MASS FRACTION
Ca                                1.4286E-01      2.5360E-01
Al                                2.8571E-01      3.4145E-01
O                                 5.7143E-01      4.0495E-01
                               TOTAL AMT/g.atom TOTAL AMT/gram
                                  6.6025E-07      1.4907E-05

Constituent 5
Si_diamond_A4(s)
                                MOLE FRACTION   MASS FRACTION
Si                                1.0000E+00      1.0000E+00
                               TOTAL AMT/g.atom TOTAL AMT/gram
                                  3.0702E-04      8.6228E-03

CaSi2_C12_hR18_R-3m(s)
                                MOLE FRACTION   MASS FRACTION
Ca                                3.3333E-01      4.1640E-01
Si                                6.6667E-01      5.8360E-01
                               TOTAL AMT/g.atom TOTAL AMT/gram
                                  1.4398E-03      4.6192E-02

CaAl2O4_solid(s)
                                MOLE FRACTION   MASS FRACTION
Ca                                1.4286E-01      2.5360E-01
Al                                2.8571E-01      3.4145E-01
O                                 5.7143E-01      4.0495E-01
                               TOTAL AMT/g.atom TOTAL AMT/gram
                                  5.1286E-10      1.1579E-08
```

```
Constituent 6
Si_diamond_A4(s)
                                MOLE FRACTION   MASS FRACTION
Si                                1.0000E+00      1.0000E+00
                                TOTAL AMT/g.atom TOTAL AMT/gram
                                   3.2897E-02      9.2393E-01
CaSi2_C12_hR18_R-3m(s)
                                MOLE FRACTION   MASS FRACTION
Ca                                3.3333E-01      4.1640E-01
Si                                6.6667E-01      5.8360E-01
                                TOTAL AMT/g.atom TOTAL AMT/gram
                                   3.4210E-02      1.0976E+00
CaAl2Si2_P3m1(s)
                                MOLE FRACTION   MASS FRACTION
Ca                                2.0000E-01      2.6681E-01
Si                                4.0000E-01      3.7394E-01
Al                                4.0000E-01      3.5925E-01
                                TOTAL AMT/g.atom TOTAL AMT/gram
                                   1.0374E-01      3.1165E+00
CaAl2O4_solid(s)
                                MOLE FRACTION   MASS FRACTION
Ca                                1.4286E-01      2.5360E-01
Al                                2.8571E-01      3.4145E-01
O                                 5.7143E-01      4.0495E-01
                                TOTAL AMT/g.atom TOTAL AMT/gram
                                   1.3602E-07      3.0709E-06
```

Metal slag ratio of 10/1:

```
EQUILIBRIUM COOLING

COMPONENTS:
[35_65_10_to_1_liq]          AMOUNT/gram =  2.4197E+02

CONSTITUENTS AND PHASES AT 578.19 C
(temperature of final disappearance of LIQUID)

CONS. PHASE                    TOTAL AMT/g.atom TOTAL AMT/gram
  1   1 Slag-liq                 -1.2595E-13     -4.8168E-13
TOTAL:                           -1.2595E-13     -4.8168E-13

  2   1 CaAl12O19_solid(s)        2.3076E-13      1.8635E-12
TOTAL:                           2.3076E-13      1.8635E-12

  2A  1 CaAl12O19_solid(s)        1.1714E-13      9.4597E-13
TOTAL:                           1.1714E-13      9.4597E-13

  3   1 Si_diamond_A4(s)          6.0202E+00      1.6908E+02
  3   2 CaAl12O19_solid(s)        3.4168E-14      2.7593E-13
TOTAL:                           6.0202E+00      1.6908E+02

  4   1 Si_diamond_A4(s)          4.4083E-02      1.2381E+00
  4   2 CaAl4O7_solid(s)          1.5130E-23      3.4587E-21
TOTAL:                           4.4083E-02      1.2381E+00

  4A  1 Si_diamond_A4(s)          2.1519E+00      6.0437E+01
  4A  2 CaAl4O7_solid(s)          1.8592E-25      4.2502E-23
TOTAL:                           2.1519E+00      6.0437E+01

  5   1 Si_diamond_A4(s)          1.8916E-03      5.3126E-02
  5   2 CaAl2O4_solid(s)          2.4912E-13      3.4537E-11
TOTAL:                           1.8916E-03      5.3126E-02

  5A  1 Si_diamond_A4(s)          4.6534E-02      1.3069E+00
  5A  2 CaAl2O4_solid(s)          2.5142E-17      3.4856E-15
TOTAL:                           4.6534E-02      1.3069E+00

  6   1 Si_diamond_A4(s)          5.6494E-02      1.5867E+00
  6   2 CaAl2Si2_P3m1(s)          1.8052E-01      5.4231E+00
  6   3 CaAl4O7_solid(s)          3.3069E-13     -4.0963E-11
TOTAL:                           2.3701E-01      7.0098E+00

  7   1 Si_diamond_A4(s)          2.0870E-02      5.8616E-01
  7   2 CaAl2Si2_P3m1(s)          4.2579E-02      1.2792E+00
  7   3 CaAl12O19_solid(s)        6.2776E-03      1.3101E-01
TOTAL:                           6.9727E-02      1.9964E+00

  7A  1 Si_diamond_A4(s)          2.1984E-03      6.1742E-02
  7A  2 CaAl2Si2_P3m1(s)          5.3852E-04      1.6179E-02
  7A  3 CaAl12O19_solid(s)        1.3542E-08      2.8263E-07
TOTAL:                           2.7369E-03      7.7921E-02

  8   1 FCC_A1                    2.5234E-02      6.8128E-01
  8   2 Si_diamond_A4(s)          3.0590E-03      8.5914E-02
  8   3 CaAl2Si2_P3m1(s)          1.8322E-04      5.5044E-03
  8   4 CaAl12O19_solid(s)        5.4662E-09      1.1408E-07
TOTAL:                           2.8476E-02      7.7269E-01
```

```
                                TOTAL AMT/g.atom TOTAL AMT/gram
FCC_A1                             2.5234E-02      6.8128E-01
Si_diamond_A4(s)                   8.3473E+00      2.3444E+02
CaAl2Si2_P3m1(s)                   2.2382E-01      6.7240E+00
CaAl2O4_solid(s)                   2.4915E-13      3.4540E-11
CaAl4O7_solid(s)                   3.3069E-13     -4.0963E-11
CaAl12O19_solid(s)                 6.2776E-03      1.3101E-01

('Double-Click' on any phase listed above to recycle it through EQUILIB)

SUMMARY OF REACTIONS

Cooling
1650 to 1650.00 C      (DELTA H =  7.0157E-06 J)
LIQUID cooling

Constituent 1
1650.00 to 1537.39 C   (DELTA H = -2.6961E+04 J)
LIQUID -> Slag-liq

Constituent 2
1537.39 to 1535.81 C   (DELTA H = -4.6283E+02 J)
LIQUID + Slag-liq -> CaAl12O19_solid(s)

Constituent 2A
1535.81 to 1405.39 C   (DELTA H = -3.0933E+04 J)
LIQUID -> CaAl12O19_solid(s)

Constituent 3
1405.39 to 1382.64 C   (DELTA H = -3.0789E+05 J)
LIQUID -> Si_diamond_A4(s) + CaAl12O19_solid(s)

Constituent 4
1382.64 to 1382.07 C   (DELTA H = -2.3484E+03 J)
LIQUID + CaAl12O19_solid(s) -> Si_diamond_A4(s) + CaAl4O7_solid(s)

Constituent 4A
1382.07 to 1018.78 C   (DELTA H = -1.9592E+05 J)
LIQUID -> Si_diamond_A4(s) + CaAl4O7_solid(s)

Constituent 5
1018.78 to 1016.89 C   (DELTA H = -5.3437E+02 J)
LIQUID + CaAl4O7_solid(s) -> Si_diamond_A4(s) + CaAl2O4_solid(s)

Constituent 5A
1016.89 to 920.13 C    (DELTA H = -2.4966E+04 J)
LIQUID -> Si_diamond_A4(s) + CaAl2O4_solid(s)

Constituent 6
920.13 to 903.14 C     (DELTA H = -1.1077E+04 J)
LIQUID + CaAl2O4_solid(s) -> Si_diamond_A4(s) + CaAl2Si2_P3m1(s) + CaAl4O7_solid(s)

Constituent 7
903.14 to 667.27 C     (DELTA H = -5.6337E+04 J)
LIQUID + CaAl4O7_solid(s) -> Si_diamond_A4(s) + CaAl2Si2_P3m1(s) + CaAl12O19_solid(s)

Constituent 7A
667.27 to 578.19 C     (DELTA H = -2.0051E+04 J)
LIQUID -> Si_diamond_A4(s) + CaAl2Si2_P3m1(s) + CaAl12O19_solid(s)
```

```
Constituent 8
578.19 C (isothermal)  (DELTA H = -3.9846E+02 J)
LIQUID -> FCC_A1 + Si_diamond_A4(s) + CaAl2Si2_P3m1(s) + CaAl12O19_solid(s)

COMPOSITION OF PHASES IN CONSTITUENTS AT 578.19 C
(temperature of final disappearance of LIQUID)

Constituent 1
Slag-liq
                                MOLE FRACTION   MASS FRACTION
Ca                                1.0642E-01      1.9369E-01
Si                                1.7872E-11      2.2795E-11
Al                                3.1487E-01      3.8582E-01
O                                 5.7872E-01      4.2049E-01
                                TOTAL AMT/g.atom TOTAL AMT/gram
                                 -1.2595E-13     -4.8168E-13
Constituent 2
CaAl12O19_solid(s)
                                MOLE FRACTION   MASS FRACTION
Ca                                2.4707E-02      1.7220E-02
Al                                2.9648E-01      1.3912E-01
O                                 4.6943E-01      1.3062E-01
                                TOTAL AMT/g.atom TOTAL AMT/gram
                                  2.3076E-13      1.8635E-12
Constituent 2A
CaAl12O19_solid(s)
                                MOLE FRACTION   MASS FRACTION
Ca                                2.4707E-02      1.7221E-02
Al                                2.9648E-01      1.3912E-01
O                                 4.6943E-01      1.3062E-01
                                TOTAL AMT/g.atom TOTAL AMT/gram
                                  1.1714E-13      9.4597E-13
Constituent 3
Si_diamond_A4(s)
                                MOLE FRACTION   MASS FRACTION
Si                                1.0000E+00      1.0000E+00
                                TOTAL AMT/g.atom TOTAL AMT/gram
                                  6.0202E+00      1.6908E+02
CaAl12O19_solid(s)
                                MOLE FRACTION   MASS FRACTION
Ca                                2.4707E-02      1.7221E-02
Al                                2.9648E-01      1.3912E-01
O                                 4.6943E-01      1.3062E-01
                                TOTAL AMT/g.atom TOTAL AMT/gram
                                  3.4168E-14      2.7593E-13
Constituent 4
Si_diamond_A4(s)
                                MOLE FRACTION   MASS FRACTION
Si                                1.0000E+00      1.0000E+00
                                TOTAL AMT/g.atom TOTAL AMT/gram
                                  4.4083E-02      1.2381E+00
CaAl4O7_solid(s)
                                MOLE FRACTION   MASS FRACTION
Ca                               -4.1869E-02     -5.0347E-03
Al                               -1.6748E-01     -1.3558E-02
O                                -2.9308E-01     -1.4069E-02
                                TOTAL AMT/g.atom TOTAL AMT/gram
                                  1.5130E-23      3.4587E-21
```

```
Constituent 4A
Si_diamond_A4(s)
                                MOLE FRACTION   MASS FRACTION
Si                                1.0000E+00      1.0000E+00
                               TOTAL AMT/g.atom TOTAL AMT/gram
                                  2.1519E+00      6.0437E+01
CaAl4O7_solid(s)
                                MOLE FRACTION   MASS FRACTION
Ca                               -4.1869E-02     -5.0346E-03
Al                               -1.6748E-01     -1.3558E-02
O                                -2.9308E-01     -1.4069E-02
                               TOTAL AMT/g.atom TOTAL AMT/gram
                                  1.8592E-25      4.2502E-23
Constituent 5
Si_diamond_A4(s)
                                MOLE FRACTION   MASS FRACTION
Si                                1.0000E+00      1.0000E+00
                               TOTAL AMT/g.atom TOTAL AMT/gram
                                  1.8916E-03      5.3126E-02
CaAl2O4_solid(s)
                                MOLE FRACTION   MASS FRACTION
Ca                               -3.7317E-01     -4.0098E-02
Al                               -7.4634E-01     -5.3990E-02
O                                -1.4927E+00     -6.4030E-02
                               TOTAL AMT/g.atom TOTAL AMT/gram
                                  2.4912E-13      3.4537E-11
Constituent 5A
Si_diamond_A4(s)
                                MOLE FRACTION   MASS FRACTION
Si                                1.0000E+00      1.0000E+00
                               TOTAL AMT/g.atom TOTAL AMT/gram
                                  4.6534E-02      1.3069E+00
CaAl2O4_solid(s)
                                MOLE FRACTION   MASS FRACTION
Ca                               -3.7317E-01     -4.0098E-02
Al                               -7.4634E-01     -5.3990E-02
O                                -1.4927E+00     -6.4030E-02
                               TOTAL AMT/g.atom TOTAL AMT/gram
                                  2.5142E-17      3.4856E-15
Constituent 6
Si_diamond_A4(s)
                                MOLE FRACTION   MASS FRACTION
Si                                1.0000E+00      1.0000E+00
                               TOTAL AMT/g.atom TOTAL AMT/gram
                                  5.6494E-02      1.5867E+00
CaAl2Si2_P3m1(s)
                                MOLE FRACTION   MASS FRACTION
Ca                                2.0000E-01      2.6681E-01
Si                                4.0000E-01      3.7394E-01
Al                                4.0000E-01      3.5925E-01
                               TOTAL AMT/g.atom TOTAL AMT/gram
                                  1.8052E-01      5.4231E+00
CaAl4O7_solid(s)
                                MOLE FRACTION   MASS FRACTION
Ca                               -4.0901E-02     -3.4383E-02
Al                               -1.6361E-01     -9.2590E-02
O                                -2.8631E-01     -9.6081E-02
                               TOTAL AMT/g.atom TOTAL AMT/gram
                                  3.3069E-13     -4.0963E-11
```

```
Constituent 7
Si_diamond_A4(s)
                                MOLE FRACTION   MASS FRACTION
Si                                1.0000E+00      1.0000E+00
                                TOTAL AMT/g.atom TOTAL AMT/gram
                                  2.0870E-02      5.8616E-01

CaAl2Si2_P3m1(s)
                                MOLE FRACTION   MASS FRACTION
Ca                                2.0000E-01      2.6681E-01
Si                                4.0000E-01      3.7394E-01
Al                                4.0000E-01      3.5925E-01
                                TOTAL AMT/g.atom TOTAL AMT/gram
                                  4.2579E-02      1.2792E+00

CaAl12O19_solid(s)
                                MOLE FRACTION   MASS FRACTION
Ca                                3.1250E-02      6.0011E-02
Al                                3.7500E-01      4.8481E-01
O                                 5.9375E-01      4.5518E-01
                                TOTAL AMT/g.atom TOTAL AMT/gram
                                  6.2776E-03      1.3101E-01

Constituent 7A
Si_diamond_A4(s)
                                MOLE FRACTION   MASS FRACTION
Si                                1.0000E+00      1.0000E+00
                                TOTAL AMT/g.atom TOTAL AMT/gram
                                  2.1984E-03      6.1742E-02

CaAl2Si2_P3m1(s)
                                MOLE FRACTION   MASS FRACTION
Ca                                2.0000E-01      2.6681E-01
Si                                4.0000E-01      3.7394E-01
Al                                4.0000E-01      3.5925E-01
                                TOTAL AMT/g.atom TOTAL AMT/gram
                                  5.3852E-04      1.6179E-02

CaAl12O19_solid(s)
                                MOLE FRACTION   MASS FRACTION
Ca                                3.1250E-02      6.0011E-02
Al                                3.7500E-01      4.8481E-01
O                                 5.9375E-01      4.5518E-01
                                TOTAL AMT/g.atom TOTAL AMT/gram
                                  1.3542E-08      2.8263E-07

Constituent 8
FCC_A1
                                MOLE FRACTION   MASS FRACTION
Ca                                1.7837E-10      2.6479E-10
Si                                1.5016E-02      1.5621E-02
Al                                9.8498E-01      9.8438E-01
O                                 2.1967E-31      1.3018E-31
                                TOTAL AMT/g.atom TOTAL AMT/gram
                                  2.5234E-02      6.8128E-01

Si_diamond_A4(s)
                                MOLE FRACTION   MASS FRACTION
Si                                1.0000E+00      1.0000E+00
                                TOTAL AMT/g.atom TOTAL AMT/gram
                                  3.0590E-03      8.5914E-02
```

```
CaAl2Si2_P3m1(s)
                                 MOLE FRACTION   MASS FRACTION
Ca                                 2.0000E-01      2.6681E-01
Si                                 4.0000E-01      3.7394E-01
Al                                 4.0000E-01      3.5925E-01
                                TOTAL AMT/g.atom TOTAL AMT/gram
                                   1.8322E-04      5.5044E-03

CaAl12O19_solid(s)
                                 MOLE FRACTION   MASS FRACTION
Ca                                 3.1250E-02      6.0011E-02
Al                                 3.7500E-01      4.8481E-01
O                                  5.9375E-01      4.5518E-01
                                TOTAL AMT/g.atom TOTAL AMT/gram
                                   5.4662E-09      1.1408E-07
```

E.2 Si metal after equilibration with 45-55 wt% CaO-Al_2O_3 Slag

Metal/slag ratio of 1/1:

```
 EQUILIBRIUM COOLING

COMPONENTS:
[_1to1_liq_11]              AMOUNT/gram =  2.5747E+01

CONSTITUENTS AND PHASES AT 917.29 C
(temperature of final disappearance of LIQUID)

CONS. PHASE                    TOTAL AMT/g.atom TOTAL AMT/gram
  1   1 Slag-liq                  4.5943E-15      4.4014E-13
TOTAL:                          4.5943E-15      4.4014E-13

  2   1 CaAl4O7_solid(s)          9.7995E-15     -1.3120E-13
TOTAL:                          9.7995E-15     -1.3120E-13

  2A  1 CaAl4O7_solid(s)          1.6241E-14     -2.1745E-13
TOTAL:                          1.6241E-14     -2.1745E-13

  3   1 Si_diamond_A4(s)          4.6728E-01      1.3124E+01
  3   2 CaAl4O7_solid(s)          1.4515E-15     -1.9434E-14
TOTAL:                          4.6728E-01      1.3124E+01

  4   1 Si_diamond_A4(s)          1.1847E-04      3.3273E-03
  4   2 CaAl2O4_solid(s)          2.2394E-04      5.0559E-03
TOTAL:                          3.4241E-04      8.3831E-03

  4A  1 Si_diamond_A4(s)          1.6431E-01      4.6146E+00
  4A  2 CaAl2O4_solid(s)          1.3866E-06      3.1305E-05
TOTAL:                          1.6431E-01      4.6146E+00

  5   1 Si_diamond_A4(s)          1.6067E-02      4.5125E-01
  5   2 CaSi2_C12_hR18_R-3m(s)    7.9008E-02      2.5348E+00
  5   3 CaAl2O4_solid(s)          1.2226E-08      2.7602E-07
TOTAL:                          9.5075E-02      2.9860E+00

  6   1 Si_diamond_A4(s)          3.2105E-02      9.0168E-01
  6   2 CaSi2_C12_hR18_R-3m(s)    3.3386E-02      1.0711E+00
  6   3 CaAl2Si2_P3m1(s)          1.0124E-01      3.0415E+00
  6   4 CaAl2O4_solid(s)          1.3274E-07      2.9970E-06
TOTAL:                          1.6673E-01      5.0143E+00

                               TOTAL AMT/g.atom TOTAL AMT/gram
Slag-liq                       4.5943E-15      4.4014E-13
Si_diamond_A4(s)               6.7988E-01      1.9095E+01
CaSi2_C12_hR18_R-3m(s)         1.1239E-01      3.6059E+00
CaAl2Si2_P3m1(s)               1.0124E-01      3.0415E+00
CaAl2O4_solid(s)               2.2547E-04      5.0905E-03
CaAl4O7_solid(s)               2.7492E-14     -3.6808E-13

('Double-Click' on any phase listed above to recycle it through EQUILIB)

SUMMARY OF REACTIONS

Cooling
1650 to 1592.58 C      (DELTA H = -1.4452E+03 J)
LIQUID cooling
```

```
Constituent 1
1650 to 1592.58 C       (DELTA H = -1.4452E+03 J)
LIQUID -> Slag-liq

Constituent 2
1592.58 to 1592.55 C    (DELTA H = -2.2214E+00 J)
Slag-liq -> LIQUID + CaAl4O7_solid(s)

Constituent 2A
1592.55 to 1345.58 C    (DELTA H = -6.1940E+03 J)
LIQUID -> CaAl4O7_solid(s)

Constituent 3
1345.58 to 1215.39 C    (DELTA H = -2.6472E+04 J)
LIQUID -> Si_diamond_A4(s) + CaAl4O7_solid(s)

Constituent 4
1215.39 to 1215.33 C    (DELTA H = -7.1142E+00 J)
LIQUID + CaAl4O7_solid(s) -> Si_diamond_A4(s) + CaAl2O4_solid(s)

Constituent 4A
1215.33 to 956.99 C     (DELTA H = -1.4224E+04 J)
LIQUID -> Si_diamond_A4(s) + CaAl2O4_solid(s)

Constituent 5
956.99 to 917.29 C      (DELTA H = -4.0186E+03 J)
LIQUID -> Si_diamond_A4(s) + CaSi2_C12_hR18_R-3m(s) + CaAl2O4_solid(s)

Constituent 6
917.29 C (isothermal)   (DELTA H = -4.9695E+03 J)
LIQUID -> Si_diamond_A4(s) + CaSi2_C12_hR18_R-3m(s) + CaAl2Si2_P3m1(s) + CaAl2O4_solid(s)

COMPOSITION OF PHASES IN CONSTITUENTS AT 917.29 C
(temperature of final disappearance of LIQUID)

Constituent 1
Slag-liq
                                MOLE FRACTION   MASS FRACTION
Ca                                1.6110E-01      2.8249E-01
Si                                1.1508E-06      1.4141E-06
Al                                2.7112E-01      3.2005E-01
O                                 5.6778E-01      3.9745E-01
                               TOTAL AMT/g.atom TOTAL AMT/gram
                                  4.5943E-15      4.4014E-13
Constituent 2
CaAl4O7_solid(s)
                                MOLE FRACTION   MASS FRACTION
Ca                               -2.9123E-02     -1.8088E-01
Al                               -1.1649E-01     -4.8709E-01
O                                -2.0386E-01     -5.0546E-01
                               TOTAL AMT/g.atom TOTAL AMT/gram
                                  9.7995E-15     -1.3120E-13
Constituent 2A
CaAl4O7_solid(s)
                                MOLE FRACTION   MASS FRACTION
Ca                               -2.9123E-02     -1.8088E-01
Al                               -1.1649E-01     -4.8709E-01
O                                -2.0386E-01     -5.0546E-01
                               TOTAL AMT/g.atom TOTAL AMT/gram
                                  1.6241E-14     -2.1745E-13
```

```
Constituent 3
Si_diamond_A4(s)
                                MOLE FRACTION   MASS FRACTION
Si                                1.0000E+00      1.0000E+00
                               TOTAL AMT/g.atom TOTAL AMT/gram
                                  4.6728E-01      1.3124E+01

CaAl4O7_solid(s)
                                MOLE FRACTION   MASS FRACTION
Ca                               -2.9123E-02     -1.8088E-01
Al                               -1.1649E-01     -4.8709E-01
O                                -2.0386E-01     -5.0546E-01
                               TOTAL AMT/g.atom TOTAL AMT/gram
                                  1.4515E-15     -1.9434E-14

Constituent 4
Si_diamond_A4(s)
                                MOLE FRACTION   MASS FRACTION
Si                                1.0000E+00      1.0000E+00
                               TOTAL AMT/g.atom TOTAL AMT/gram
                                  1.1847E-04      3.3273E-03

CaAl2O4_solid(s)
                                MOLE FRACTION   MASS FRACTION
Ca                                1.4286E-01      2.5360E-01
Al                                2.8571E-01      3.4145E-01
O                                 5.7143E-01      4.0495E-01
                               TOTAL AMT/g.atom TOTAL AMT/gram
                                  2.2394E-04      5.0559E-03

Constituent 4A
Si_diamond_A4(s)
                                MOLE FRACTION   MASS FRACTION
Si                                1.0000E+00      1.0000E+00
                               TOTAL AMT/g.atom TOTAL AMT/gram
                                  1.6431E-01      4.6146E+00

CaAl2O4_solid(s)
                                MOLE FRACTION   MASS FRACTION
Ca                                1.4286E-01      2.5360E-01
Al                                2.8571E-01      3.4145E-01
O                                 5.7143E-01      4.0495E-01
                               TOTAL AMT/g.atom TOTAL AMT/gram
                                  1.3866E-06      3.1305E-05

Constituent 5
Si_diamond_A4(s)
                                MOLE FRACTION   MASS FRACTION
Si                                1.0000E+00      1.0000E+00
                               TOTAL AMT/g.atom TOTAL AMT/gram
                                  1.6067E-02      4.5125E-01

CaSi2_C12_hR18_R-3m(s)
                                MOLE FRACTION   MASS FRACTION
Ca                                3.3333E-01      4.1640E-01
Si                                6.6667E-01      5.8360E-01
                               TOTAL AMT/g.atom TOTAL AMT/gram
                                  7.9008E-02      2.5348E+00

CaAl2O4_solid(s)
                                MOLE FRACTION   MASS FRACTION
Ca                                1.4286E-01      2.5360E-01
Al                                2.8571E-01      3.4145E-01
O                                 5.7143E-01      4.0495E-01
                               TOTAL AMT/g.atom TOTAL AMT/gram
                                  1.2226E-08      2.7602E-07
```

```
Constituent 6
Si_diamond_A4(s)
                                  MOLE FRACTION   MASS FRACTION
Si                                  1.0000E+00      1.0000E+00
                                TOTAL AMT/g.atom TOTAL AMT/gram
                                    3.2105E-02      9.0168E-01
CaSi2_C12_hR18_R-3m(s)
                                  MOLE FRACTION   MASS FRACTION
Ca                                  3.3333E-01      4.1640E-01
Si                                  6.6667E-01      5.8360E-01
                                TOTAL AMT/g.atom TOTAL AMT/gram
                                    3.3386E-02      1.0711E+00
CaAl2Si2_P3m1(s)
                                  MOLE FRACTION   MASS FRACTION
Ca                                  2.0000E-01      2.6681E-01
Si                                  4.0000E-01      3.7394E-01
Al                                  4.0000E-01      3.5925E-01
                                TOTAL AMT/g.atom TOTAL AMT/gram
                                    1.0124E-01      3.0415E+00
CaAl2O4_solid(s)
                                  MOLE FRACTION   MASS FRACTION
Ca                                  1.4286E-01      2.5360E-01
Al                                  2.8571E-01      3.4145E-01
O                                   5.7143E-01      4.0495E-01
                                TOTAL AMT/g.atom TOTAL AMT/gram
                                    1.3274E-07      2.9970E-06
```

Metal/slag ratio of 10/1:

```
 EQUILIBRIUM COOLING

COMPONENTS:
[_10to1_liq_11]              AMOUNT/gram =  2.4273E+02

CONSTITUENTS AND PHASES AT 917.29 C
(temperature of final disappearance of LIQUID)

CONS. PHASE                      TOTAL AMT/g.atom TOTAL AMT/gram
  1   1 Slag-liq                   -7.9965E-14      1.5517E-12
TOTAL:                             -7.9965E-14      1.5517E-12

  2   1 CaAl4O7_solid(s)           -1.8691E-13     -4.1917E-12
TOTAL:                             -1.8691E-13     -4.1917E-12

  2A  1 CaAl4O7_solid(s)           -2.6632E-14     -5.9727E-13
TOTAL:                             -2.6632E-14     -5.9727E-13

  3   1 Si_diamond_A4(s)            8.0404E+00      2.2582E+02
  3   2 CaAl4O7_solid(s)           -2.6432E-14     -5.9279E-13
TOTAL:                             8.0404E+00      2.2582E+02

  4   1 Si_diamond_A4(s)            2.1611E-03      6.0695E-02
  4   2 CaAl2O4_solid(s)            6.0211E-03      1.3594E-01
TOTAL:                             8.1822E-03      1.9663E-01

  4A  1 Si_diamond_A4(s)            1.5591E-01      4.3789E+00
  4A  2 CaAl2O4_solid(s)            1.5462E-06      3.4908E-05
TOTAL:                             1.5592E-01      4.3790E+00

  5   1 Si_diamond_A4(s)            3.2794E-03      9.2104E-02
  5   2 CaAl2Si2_P3m1(s)            1.0432E-02      3.1340E-01
  5   3 CaAl2O4_solid(s)            1.6758E-08      3.7834E-07
TOTAL:                             1.3711E-02      4.0551E-01

  6   1 Si_diamond_A4(s)            7.6368E-02      2.1448E+00
  6   2 CaSi2_C12_hR18_R-3m(s)      7.9415E-02      2.5479E+00
  6   3 CaAl2Si2_P3m1(s)            2.4082E-01      7.2347E+00
  6   4 CaAl2O4_solid(s)            3.1576E-07      7.1289E-06
TOTAL:                             3.9660E-01      1.1927E+01

                                 TOTAL AMT/g.atom TOTAL AMT/gram
Slag-liq                           -7.9965E-14      1.5517E-12
Si_diamond_A4(s)                    8.2782E+00      2.3250E+02
CaSi2_C12_hR18_R-3m(s)              7.9415E-02      2.5479E+00
CaAl2Si2_P3m1(s)                    2.5125E-01      7.5481E+00
CaAl2O4_solid(s)                    6.0230E-03      1.3598E-01
```

```
SUMMARY OF REACTIONS

Cooling
1650 to 1650.00 C      (DELTA H = -4.8243E-06 J)
LIQUID cooling

Constituent 1
1650.00 to 1468.69 C   (DELTA H = -4.3298E+04 J)
LIQUID -> Slag-liq

Constituent 2
1468.69 to 1467.39 C   (DELTA H = -4.1038E+02 J)
LIQUID + Slag-liq -> CaAl4O7_solid(s)

Constituent 2A
1467.39 to 1404.24 C   (DELTA H = -1.4966E+04 J)
LIQUID -> CaAl4O7_solid(s)

Constituent 3
1404.24 to 1128.24 C   (DELTA H = -4.7081E+05 J)
LIQUID -> Si_diamond_A4(s) + CaAl4O7_solid(s)

Constituent 4
1128.24 to 1127.14 C   (DELTA H = -3.6575E+02 J)
LIQUID + CaAl4O7_solid(s) -> Si_diamond_A4(s) + CaAl2O4_solid(s)

Constituent 4A
1127.14 to 917.59 C    (DELTA H = -5.7175E+04 J)
LIQUID -> Si_diamond_A4(s) + CaAl2O4_solid(s)

Constituent 5
917.59 to 917.29 C     (DELTA H = -4.7951E+02 J)
LIQUID -> Si_diamond_A4(s) + CaAl2Si2_P3m1(s) + CaAl2O4_solid(s)

Constituent 6
917.29 C (isothermal)  (DELTA H = -1.1821E+04 J)
LIQUID -> Si_diamond_A4(s) + CaSi2_C12_hR18_R-3m(s) + CaAl2Si2_P3m1(s) + CaAl2O4_solid(s)

COMPOSITION OF PHASES IN CONSTITUENTS AT 917.29 C
(temperature of final disappearance of LIQUID)

Constituent 1
Slag-liq
                                MOLE FRACTION   MASS FRACTION
Ca                                1.6110E-01      2.8249E-01
Si                                1.1508E-06      1.4141E-06
Al                                2.7112E-01      3.2005E-01
O                                 5.6778E-01      3.9745E-01
                               TOTAL AMT/g.atom TOTAL AMT/gram
                                 -7.9965E-14      1.5517E-12
Constituent 2
CaAl4O7_solid(s)
                                MOLE FRACTION   MASS FRACTION
Ca                                6.9351E-03      9.6862E-02
Al                                2.7740E-02      2.6084E-01
O                                 4.8548E-02      2.7068E-01
                               TOTAL AMT/g.atom TOTAL AMT/gram
                                 -1.8691E-13     -4.1917E-12
```

```
Constituent 2A
CaAl4O7_solid(s)
                              MOLE FRACTION   MASS FRACTION
Ca                              6.9353E-03      9.6862E-02
Al                              2.7741E-02      2.6084E-01
O                               4.8547E-02      2.7068E-01
                             TOTAL AMT/g.atom TOTAL AMT/gram
                               -2.6632E-14     -5.9727E-13

Constituent 3
Si_diamond_A4(s)
                              MOLE FRACTION   MASS FRACTION
Si                              1.0000E+00      1.0000E+00
                             TOTAL AMT/g.atom TOTAL AMT/gram
                                8.0404E+00      2.2582E+02
CaAl4O7_solid(s)
                              MOLE FRACTION   MASS FRACTION
Ca                              6.9354E-03      9.6862E-02
Al                              2.7740E-02      2.6084E-01
O                               4.8547E-02      2.7067E-01
                             TOTAL AMT/g.atom TOTAL AMT/gram
                               -2.6432E-14     -5.9279E-13

Constituent 4
Si_diamond_A4(s)
                              MOLE FRACTION   MASS FRACTION
Si                              1.0000E+00      1.0000E+00
                             TOTAL AMT/g.atom TOTAL AMT/gram
                                2.1611E-03      6.0695E-02
CaAl2O4_solid(s)
                              MOLE FRACTION   MASS FRACTION
Ca                              1.4286E-01      2.5360E-01
Al                              2.8571E-01      3.4145E-01
O                               5.7143E-01      4.0495E-01
                             TOTAL AMT/g.atom TOTAL AMT/gram
                                6.0211E-03      1.3594E-01

Constituent 4A
Si_diamond_A4(s)
                              MOLE FRACTION   MASS FRACTION
Si                              1.0000E+00      1.0000E+00
                             TOTAL AMT/g.atom TOTAL AMT/gram
                                1.5591E-01      4.3789E+00
CaAl2O4_solid(s)
                              MOLE FRACTION   MASS FRACTION
Ca                              1.4286E-01      2.5360E-01
Al                              2.8571E-01      3.4145E-01
O                               5.7143E-01      4.0495E-01
                             TOTAL AMT/g.atom TOTAL AMT/gram
                                1.5462E-06      3.4908E-05

Constituent 5
Si_diamond_A4(s)
                              MOLE FRACTION   MASS FRACTION
Si                              1.0000E+00      1.0000E+00
                             TOTAL AMT/g.atom TOTAL AMT/gram
                                3.2794E-03      9.2104E-02
CaAl2Si2_P3m1(s)
                              MOLE FRACTION   MASS FRACTION
Ca                              2.0000E-01      2.6681E-01
Si                              4.0000E-01      3.7394E-01
Al                              4.0000E-01      3.5925E-01
                             TOTAL AMT/g.atom TOTAL AMT/gram
                                1.0432E-02      3.1340E-01
```

```
CaAl2O4_solid(s)
                                MOLE FRACTION   MASS FRACTION
Ca                                1.4286E-01      2.5360E-01
Al                                2.8571E-01      3.4145E-01
O                                 5.7143E-01      4.0495E-01
                                TOTAL AMT/g.atom TOTAL AMT/gram
                                  1.6758E-08      3.7834E-07

Constituent 6
Si_diamond_A4(s)
                                MOLE FRACTION   MASS FRACTION
Si                                1.0000E+00      1.0000E+00
                                TOTAL AMT/g.atom TOTAL AMT/gram
                                  7.6368E-02      2.1448E+00

CaSi2_C12_hR18_R-3m(s)
                                MOLE FRACTION   MASS FRACTION
Ca                                3.3333E-01      4.1640E-01
Si                                6.6667E-01      5.8360E-01
                                TOTAL AMT/g.atom TOTAL AMT/gram
                                  7.9415E-02      2.5479E+00

CaAl2Si2_P3m1(s)
                                MOLE FRACTION   MASS FRACTION
Ca                                2.0000E-01      2.6681E-01
Si                                4.0000E-01      3.7394E-01
Al                                4.0000E-01      3.5925E-01
                                TOTAL AMT/g.atom TOTAL AMT/gram
                                  2.4082E-01      7.2347E+00

CaAl2O4_solid(s)
                                MOLE FRACTION   MASS FRACTION
Ca                                1.4286E-01      2.5360E-01
Al                                2.8571E-01      3.4145E-01
O                                 5.7143E-01      4.0495E-01
                                TOTAL AMT/g.atom TOTAL AMT/gram
                                  3.1576E-07      7.1289E-06
```

F Calculation of Activity Coefficients

The activity coefficients of Al and Ca were calculated based on their respective concentrations. These calculations are based on:

- The activity of Si is the same as the mole fraction, $a_{Si} = X_{Si}$
- The activity of CaO, Al_2O_3 and SiO_2 were found by plotting the equilibrium slag compositions in the isoactivity diagram by Rein and Chipman [64], which is valid for a 1600 °temperature. The plotted diagrams are shown in figure 30-33.
- The activity of Al_2O_3 was converted from $AlO_{1.5}$, with the relation $a^2_{Al_2O_3} = a^4_{AlO_{1.5}}$
- Interaction coefficients are not considered.

Table 6: Mole fractions of the species Si, Al and Ca from the 35-65 and 45-55 wt% slag series, converted from their respective concentrations in Si at equilibrium.

	35-65 wt%			**45-55 wt%**		
	Si	**Al**	**Ca**	**Si**	**Al**	**Ca**
1	0.8625	0.0966	0.0409	0.8766	0.0773	0.0461
2.5	0.9434	0.0423	0.0143	0.9543	0.0318	0.0139
5	0.9630	0.0293	0.0077	0.9600	0.0294	0.0106
7.5	0.9716	0.0213	0.0071	0.9682	0.0258	0.0059
10	0.9509	0.0350	0.0141	0.9821	0.0155	0.0025

Table 7: Activities of CaO, SiO_2 and $AlO_{1.5}$, obtained from isoactivity diagrams from Rein and Chipman.

Metal/slag ratio	**35-65 wt%**			**45-55 wt%**		
	a_{CaO}	a_{SiO_2}	$a_{AlO_{1.5}}$	a_{CaO}	a_{SiO_2}	$a_{AlO_{1.5}}$
1	0.09	0.004	0.49	0.07	0.003	0.656
2.5	0.06	0.0075	0.5625	0.12	0.0001	0.5
5	0.275	0.025	0.49	0.049	0.009	0.7
7.5	0.05	0.01	0.5625	0.275	0.02	0.68
10	0.02	0.05	0.85	0.02	0.1	0.656

Table 6 shows the mole fractions used for the calculations, and table 7 shows the obtained activities of CaO, SiO_2 and $AlO_{1.5}$ from isoactivity diagrams from Rein and Chipman.

Here, an example calculation of the activity coefficient of of Al in Si from the 1/1 metal/slag ratio in the 35-65 wt% slag series.

The activity coefficient of Al in Si was calculated by the equilibrium:

$$3\,\mathrm{Si} + 2\,\mathrm{Al_2O_3} \rightleftharpoons 3\,\mathrm{SiO_2} + 4\,\mathrm{Al}$$

With the equilibrium constant:

$$K = \frac{a_{Al}^4 \cdot a_{SiO_2}^3}{a_{Si}^3 \cdot a_{AlO_{1.5}}^4}$$

With the equilibrium constant: K = 4.12×10^{-12} at 1923 K. [4]

We have that:

$$a_{Al} = X_{Al} \cdot \gamma_{Al}^0$$

Which gives:

$$\gamma_{Al}^4 = \frac{K \cdot a_{Si}^3 \cdot a_{AlO_{1.5}}^4}{X_{Al}^4 \cdot a_{SiO_2}^3}$$

$$\frac{4.12 \times 10^{-12} \cdot (0.8625)^3 \cdot (0.49)^4}{(0.0966)^4 \cdot (0.004)^3}$$

$$\Rightarrow \gamma_{Al}^4 = 0.0273$$

$$\Rightarrow \gamma_{Al} = \sqrt[4]{0.0273} = \underline{\underline{0.407}}$$

Here, an example calculation of the activity coefficient of of Ca in Si from the 1/1 metal/slag ratio in the 35-65 wt% slag series.

The activity coefficient of Ca was calculated from the equilibrium:

$$\mathrm{Si} + 2\,\mathrm{CaO} \rightleftharpoons \mathrm{SiO_2} + 2\,\mathrm{Ca}$$

With the equilibrium constant:

$$K = \frac{a_{SiO_2} \cdot a_{Ca}^2}{a_{Si} \cdot a_{CaO}^2}$$

With the equilibrium constant: K = 6.33 $\times$ 10^{-8} at 1923 K. [4]

We have that:

$$a_{Ca} = X_{Ca} \cdot \gamma_{Ca}^0$$

Which gives:

$$\gamma_{Ca}^2 = \frac{K \cdot a_{CaO}^2 \cdot a_{Si}}{X_{Ca}^2 \cdot a_{SiO_2}}$$

$$\gamma_{Ca}^2 = \frac{6.33 \times 10^{-8} \cdot 0.07^2 \cdot 0.8766}{0.0773^2 \cdot 0.003}$$

$$\Rightarrow \gamma_{Ca}^2 = 1.52 \times 10^{-5}$$

$$\Rightarrow \gamma_{Ca} = \sqrt{1.52 \times 10^{-5}} = \underline{\underline{0.00389}}$$

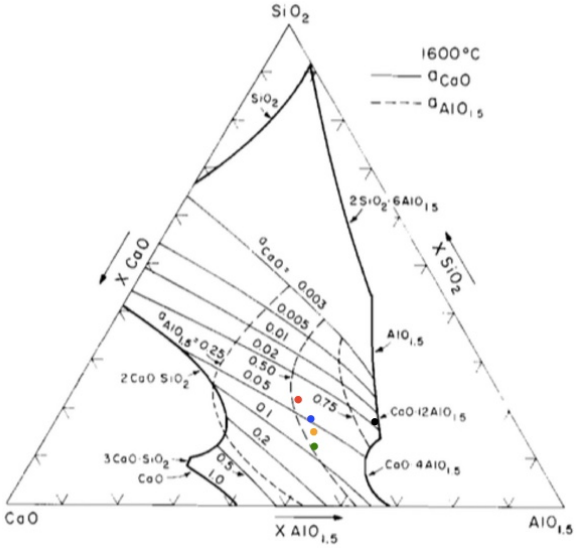

Figure 30: Plotted points of the obtained mole fractions based on concentrations in the 35-65 wt% slag series after equilibrium in the CaO-$AlO_{1.5}$ isoactivity diagram by Rein and Chipman [64] at 1600 °C. Where the green point are for the metal/slag ratio of 1/1, yellow: 2.5/1, red: 5/1, blue: 7.5/1 and black: 10/1.

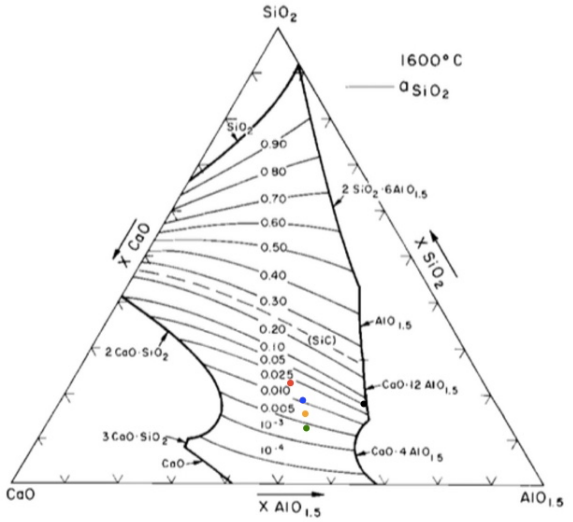

Figure 31: Plotted points of the mole fractions based on concentrations in the 35-65 wt% slag series after equilibrium in the CaO-$AlO_{1.5}$ isoactivity diagram by Rein and Chipman [64] at 1600 °C. Where the green point are for the metal/slag ratio of 1/1, yellow: 2.5/1, red: 5/1, blue: 7.5/1 and black: 10/1.

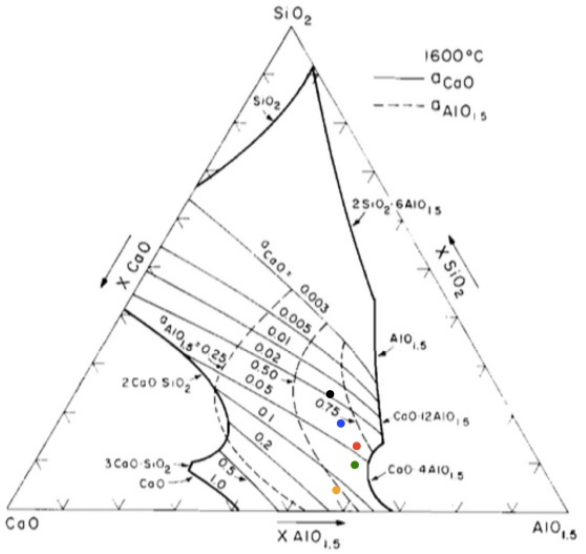

Figure 32: Plotted points of the obtained mole fractions based on concentrations in the 45-55 wt% slag series after equilibrium in the CaO-$AlO_{1.5}$ isoactivity diagram by Rein and Chipman [64] at 1600 °C. Where the green point are for the metal/slag ratio of 1/1, yellow: 2.5/1, red: 5/1, blue: 7.5/1 and black: 10/1.

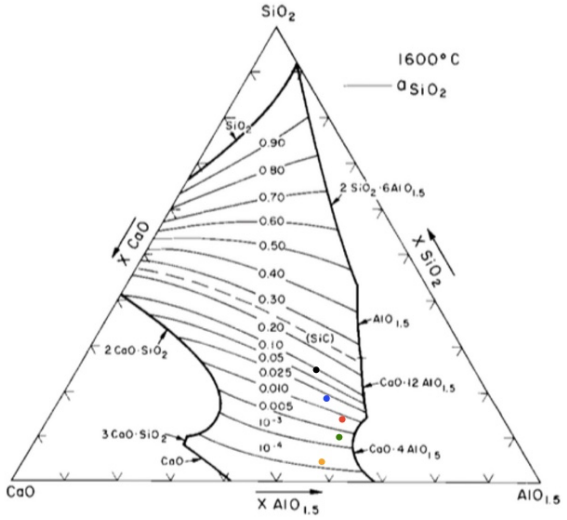

Figure 33: Plotted points of the obtained mole fractions based on concentrations in the 45-55 wt% slag series after equilibrium in the SiO_2 isoactivity diagram by Rein and Chipman [64] at 1600 °C. Where the green point are for the metal/slag ratio of 1/1, yellow: 2.5/1, red: 5/1, blue: 7.5/1 and black: 10/1.

Safia Hassan

Distribution of Aluminum and Calcium between Silicon and CaO-Al_2O_3-SiO_2 Slags at 1650 °C

NTNU
Norwegian University of
Science and Technology